CHARGED PARTICLE PAIR PRODUCTION ASSOCIATED WITH A LEPTON PAIR IN Z DECAYS: INDICATION FOR AN EXCESS IN THE TAU CHANNEL

by

YIBIN PAN

A thesis submitted in partial fulfillment of the requirements for the degree of

Doctor of Philosophy

(Physics)

at the

UNIVERSITY OF WISCONSIN-MADISON

1991

CHARGED PARTICLE PAIR PRODUCTION ASSOCIATED WITH A LEPTON PAIR IN Z DECAYS: INDICATION FOR AN EXCESS IN THE TAU CHANNEL

Yibin Pan

Under the supervision of Professor Sau Lan Wu
at the University of Wisconsin-Madison

ABSTRACT

In a sample of 200000 Z decays, events with two leptons and an additional pair of opposite charged particles are studied. The 35 events found show a possible excess in the tau channel compared with the expectation from electroweak processes. Other features of the events are studied and are not found to be in contradiction to the electroweak prediction for the radiation of virtual photons.

Acknowledgements

The achievement of this degree is really the result of many people's efforts. It is impossible to simply use words to express my thanks to those who have helped and encouraged me in this process, nor can I list all of them here.

I would like to thank my parents for the unmatched love and support they gave me. It is them who showed me the importance of the knowledge of the science and it is them who supported me throughout my whole education in China and eventually made possible my trip to the United States for my graduate studies. I would also like to thank all the teachers who have taught me, both in China and in the States. I would especially like to mention the teachers in the No13 High School in Handan, China, who first introduced me to the wonderful world of physics.

I would like to thank my advisor, Prof. Sau Lan Wu, who has guided and generously supported me throughout the entire course of my graduate studies. Her insight into physics and her persistence in the pursuit of the truths of the universe have been the best sources of my learnings as a physics student. The active and cooperative environment she creates in her Wisconsin group makes our research work both enjoyable and fruitful.

I would like to thank Prof. T.T. Wu for his valuable suggestions and comments on many of the vital aspects of the analysis presented here. It is always educational and pleasant to discuss with him.

I would like to give my special thanks to Dr. John Conway. Not only did he collaborate on the l^+l^-V searches, but he also kindly read over the draft of this thesis and corrected enormous errors concerning the grammar and spelling. I appreciate his scientific acuity and constant willingness to help.

I would also like to thank my friends, Yongsheng Gao and Zhaohui Shi, who have helped me greatly both in the process of the analysis and in the preparation of this thesis. I am lucky to have friends like them who are always available when needed.

I am indebted to Dr. Joe Boudreau and Dr. John Hilgart who kindly let me use their images of the LEP machine and of the ALEPH detector and its subcomponents in my thesis. John Hilgart and Youssef Saadi have also helped this analysis by providing a lot of thoughtful inputs and by helping to port the four-lepton Monte Carlo generators to the computer system we were working on. Many other Wisconsin group members have also lent their support to this analysis.

I benefited a lot from the useful discussions with many people in the ALEPH Collaboration. Among them are Prof. J. Steinberger, Prof. J. LeFrancǫis, Prof. L. Foà, Prof. L. Rolandi. Many, many others have helped and I would like to thank all of them.

Yibin Pan , 27 July 1991

Contents

Chapter 1

The experiment

1.1 Introduction

Since its introduction twenty years ago, the Standard Model [1,2,3,4], which describes the fundamental constituents of the matter and their interactions, has been extensively checked by a large variety of experiments worldwide. Although some of its vitally important predictions, such as the the existence of the Higgs boson [5] and top quark, have not been confirmed, this simple and elegant model has not been found to be in contradiction with any of the experimental results thus far, and in many cases the agreements are quite remarkable.

However, it is always interesting to search for some possible new phenomena outside the predictions of such a successful theory. The large Z machines like SLC and LEP, while having produced many new results in good agreement with the model, have also opened new opportunities for such searches.

This dissertation, in an attempt to search for the possible deviations from the Standard Model, presents a study of a special class of events, the so called l^+l^-V events.

l^+l^-V denotes a simple configuration: a pair of oppositely charged leptons of the same type ("l^+l^- ") associated with another charged particle-antiparticle pair of stable particles(the "V"). Here, l^+l^- can be e^+e^- , $\mu^+\mu^-$, or $\tau^+\tau^-$, and "V" can be e^+e^- , $\mu^+\mu^-$, or $\pi^+\pi^-$. All the particles are expected to be "prompt", i.e., to be coming from point-like e^+e^- interactions.

In the following sections and chapters, a brief description of the experiment is given first, then the event selection procedure is described in detail. At the end, the results and some discussion are presented.

Limited by the size of the data sample, the results are subject to statistical fluctuations. To be conservative and objective, no theories as for possible explanations of the results will be discussed.

1.2 LEP accelerator and ALEPH detector

The Large Electron Positron (LEP) accelerator is a 27 kilometer circumference circular electron-positron storage ring designed and constructed to be able to accelerate, store, and collide electrons and positrons at up to 110 GeV (55 GeV per beam) of the centre-of-mass (c.m.s.) energy at its first stage (LEP-I), and at up to 200 GeV c.m.s. energy with a future upgrade. An overall view of LEP, with its injector chain, the storage ring, and the interaction sites, is shown in figure 1.1.

Before entering into the main LEP ring, the electrons and positrons are produced, accumulated, and accelerated to about 22 GeV in the injector complex consisting of LIL (LEP Injector Linac), EPA (Electron Positron Accumulator), and two synchrotrons PS and SPS. The beams are then further accelerated by the 256 superconducting RF cavities in the main LEP ring. After reaching the desired energy, the beams are squeezed and focused into collisions. Four bunches of counterrotating electron and positron beams are provided simultaneously by the machine for the collisions at four interaction points, which are surrounded by the detectors of the four experiments operating at LEP. Among these four detectors is the one used for this analysis, the ALEPH (A LEP PHysics) detector.

The ALEPH detector is a general purpose, finely segmented hermetic detector. Nearly 3000 tons in weight and over 2000 cubic meters in volume, it is built to collect large amounts of detailed information from complex events. Among others, one of its design purposes is to search for new phenomena.

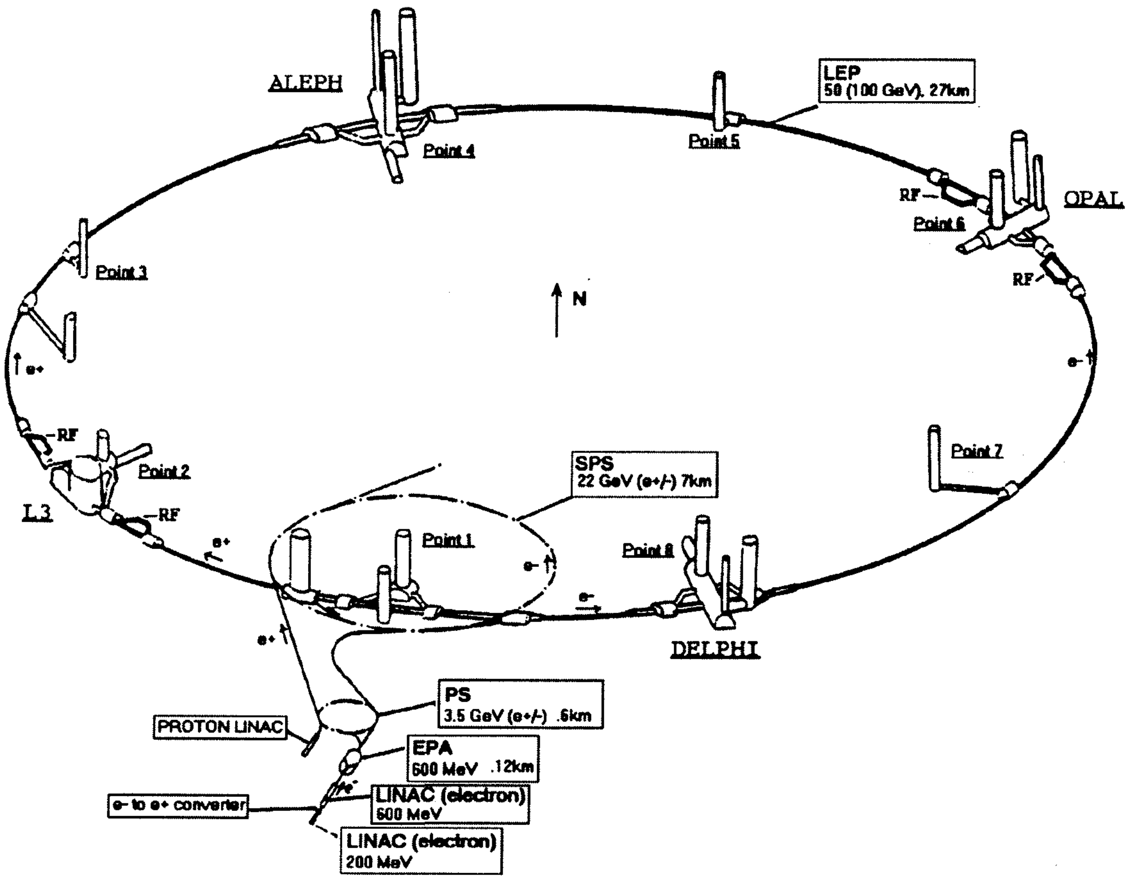

Figure 1.1: An overall view of LEP, its injector chain, the storage ring, and the interaction sites.

The detector is composed of three major subsystems, the tracking detectors, the superconducting magnet which provides a homogeneous high magnetic field of 15000 Gauss for the tracking, and the calorimeters. They work together to produce complete pictures for events.

The section below describes some of the main components related to this analysis. More detailed information, including the descriptions of the magnet, the electronics, the triggering system, the luminosity measurements and the performance of the detector can be found in [6].

1.2.1 The anatomy of the ALEPH detector

A cut-away view of the detector is shown in figure 1.2.1. The electrons and positrons travel through the beam pipe and collide in the center of the detector. The silicon strip microvertex detector (not shown) which immediately surrounds the collision point was installed but not used in this analysis.

Outside the beam pipe and the microvertex detector is the inner track chamber (ITC), a multilayer axial-wire drift chamber which provides up to 8 coordinates per track, with an resolution of 100 μm, in the plane perpendicular to the beam line. The ITC is one of the two tracking device in the detector, and is also used as a triggering device.

The TPC

Surrounding the ITC is the other tracking device, a large cylindrical time projection chamber (TPC). Measuring 4.4 meters in length and 3.6 meters in diameter,

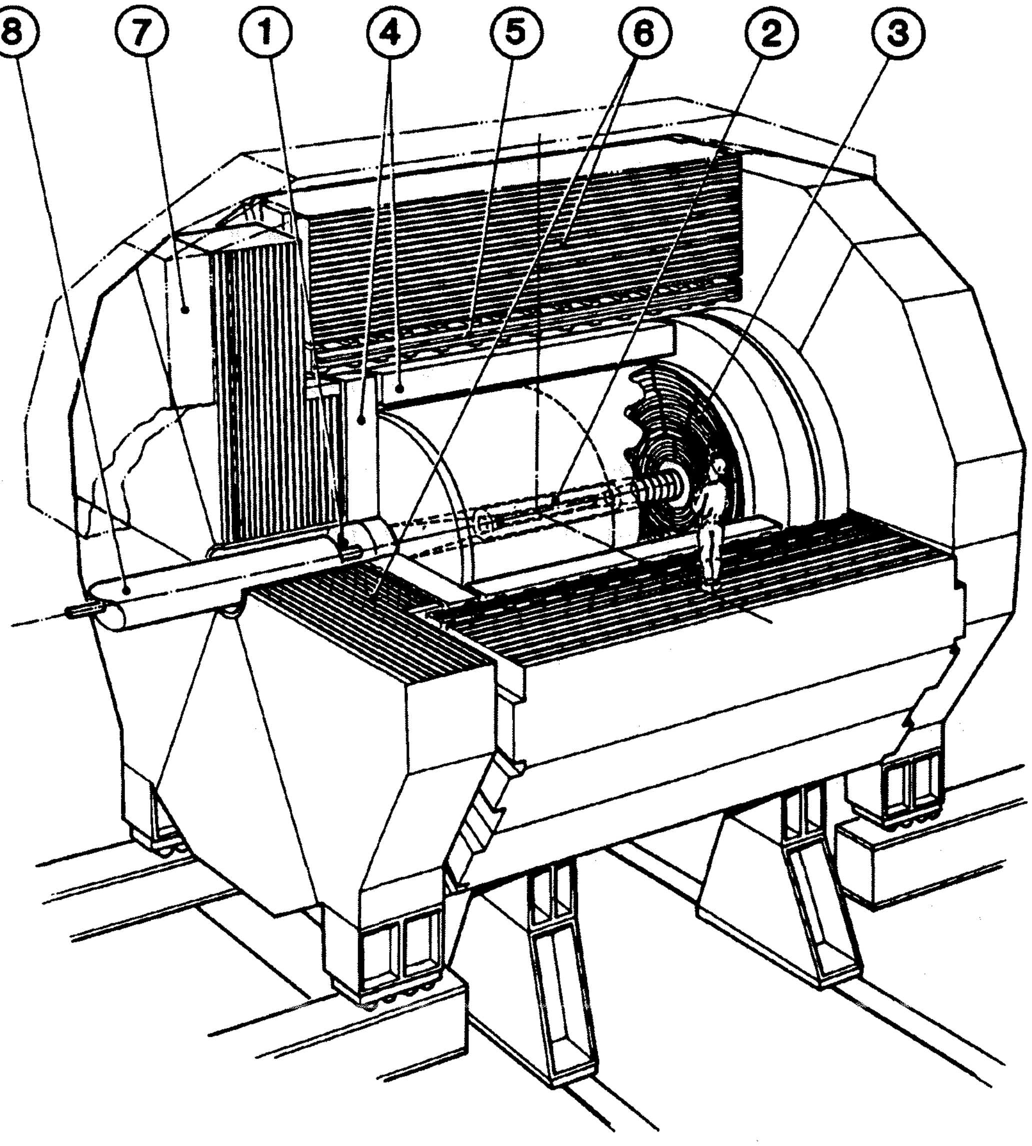

Figure 1.2: The ALEPH detector. 1) Luminosity monitor 2) Inner tracking chamber. 3) Time projection chamber 4) Electromagnetic calorimeter. 5) Superconducting coil 6) Hadronic calorimeter. 7) Muon chamber. 8) Low-beta superconducting quadrupoles.

the TPC records up to 21 three-dimensional coordinates for each charged particle. This yields precise measurements of the momenta of the tracks, and also provides an excellent two track separation capability. With the magnetic field provided, a track momenta measurement accuracy of $\Delta p/p^2 = 1.5\times10^{-3}$ is made possible by the TPC itself. A higher accuracy ($\simeq 10^{-3}$) is achieved by combining the TPC and ITC together. A schematic picture of the TPC is shown in figure 1.3. In figure 1.4, a typical Z decay event as seen by the TPC and the ITC is also shown.

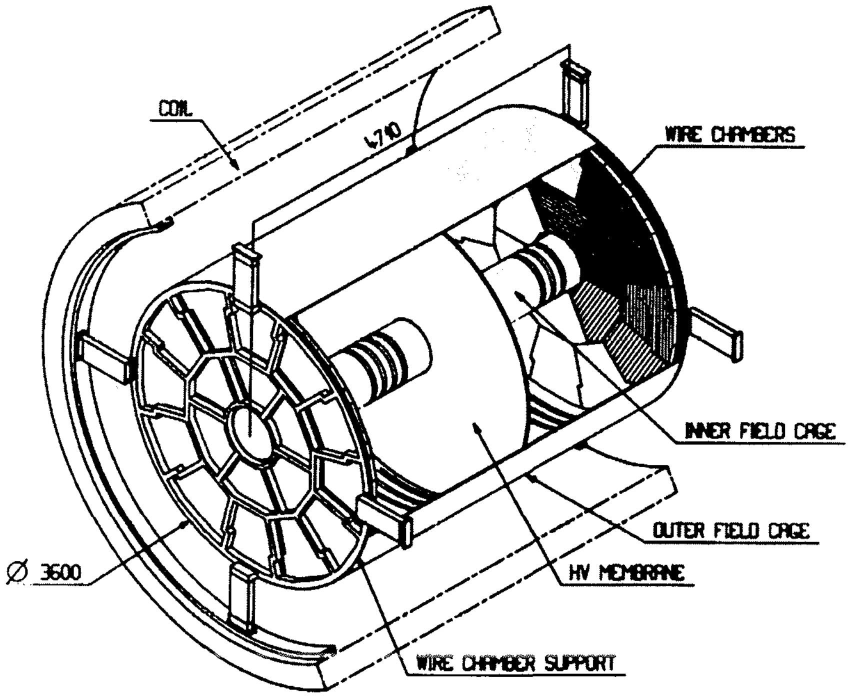

Figure 1.3: The ALEPH TPC

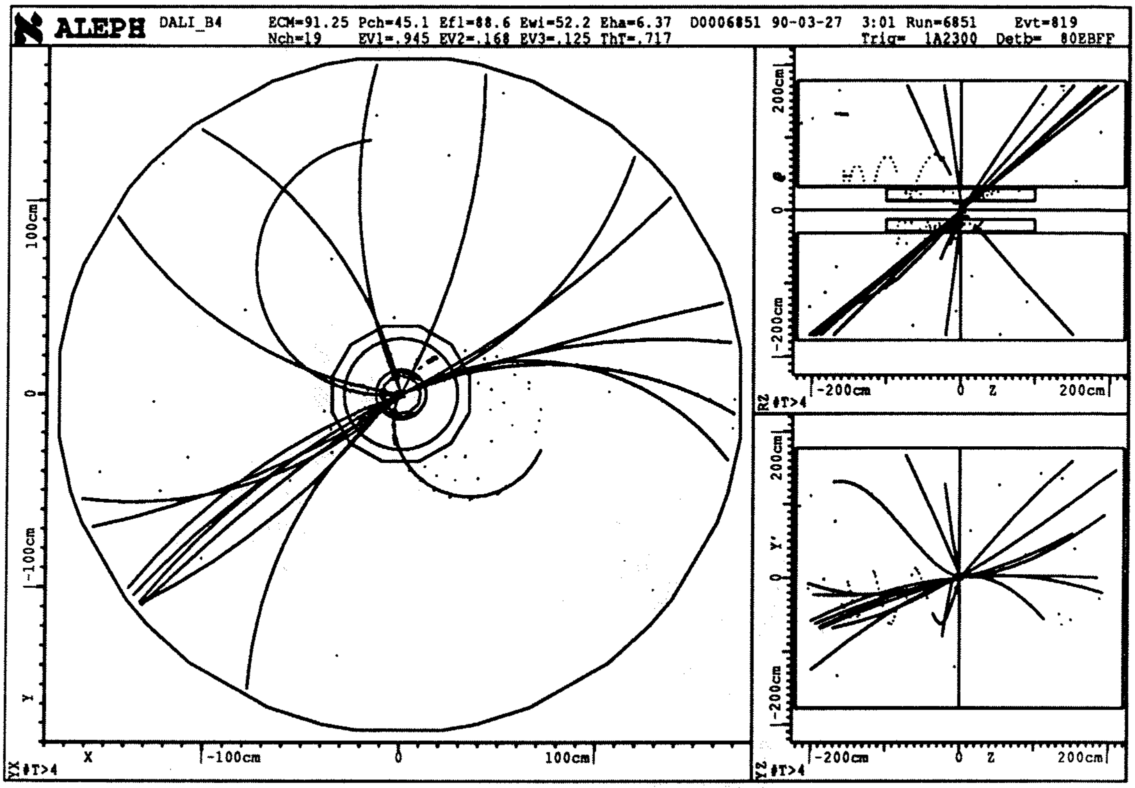

Figure 1.4: A typical hadronic Z as seen by the TPC and the ITC.

The TPC also records the energy loss (dE/dx) information of the tracks through its measurements of up to 340 samples of the ionization for each track. This provides a powerful technique for the particle identification, especially in separating electrons from the pions. Figure 1.2.1 (a) shows the dE/dx of the tracks from Z decays plotted against the momentum p in GeV, lines are those expected for electrons, pions, kaons, and protons. In the low energy (< 10 GeV) the pions and the electrons are well separated. This is also illustrated in figure 1.2.1 (b), where the dE/dx distributions for pions and electrons from hadronic Z decays are plotted. The TPC dE/dx resolution is about 4.5%.

Combining the dE/dx measurements with the information from the calorimeters, one can obtain a π/e separation at about 10^{-3}/(GeV/c) in a typical hadronic jet.

The ECAL

Outside the TPC, but inside the magnet coil, is the electromagnetic calorimeter (ECAL) (figure 1.6). The thirty six ECAL modules, mounted both in the barrel and endcap regions surrounding the TPC and covering 3.9π of solid angle, are each made up of 45 alternative layers of lead and wire proportional chambers (figure 1.7). In depth, this represents 22 radiation lengths (X_0), large enough to absorb almost all the electromagnetic energies as carried by photons and the electrons.

To measure the energy and the positions of the electromagnetic showers, small cathode readout pads are placed throughout each layer of wire chambers. In readout, the pads are internally connected to form the so called "towers" pointing towards the interaction point. Each tower is about $1^0 \times 1^0$ in size and produces three readouts for the first 10 layers (the first "stack", corresponding to $4X_0$), the next 23 layers (the second stack, $9X_0$), and the last 12 layers (the third stack, $9X_0$). This arrangement, yielding $18\%/\sqrt{E}$ (GeV) for the energy

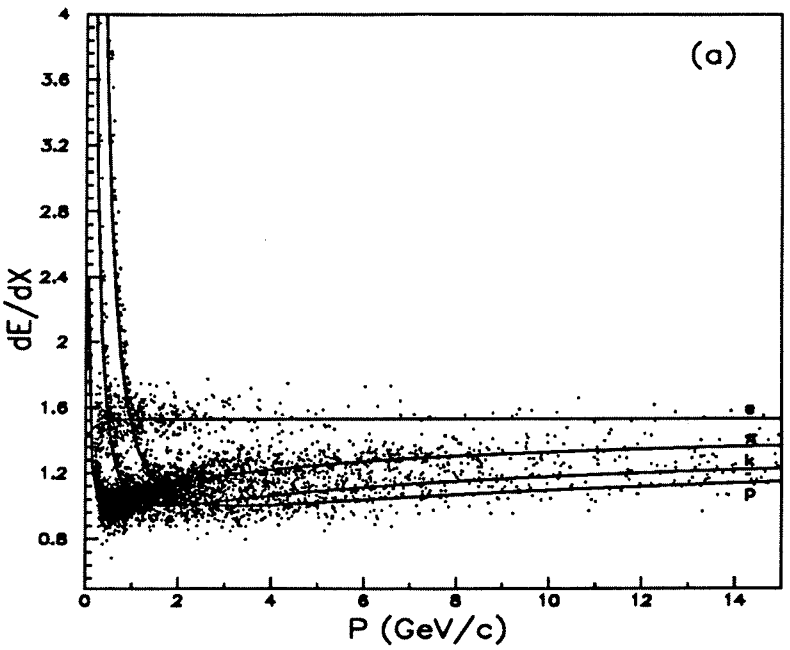

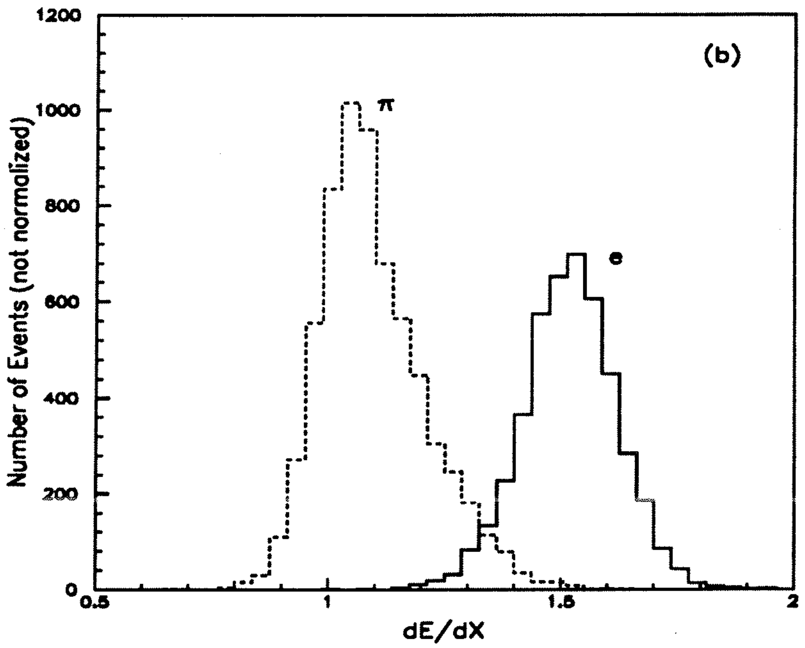

Figure 1.5: dE/dx measurement in the TPC. a) dE/dx versus momentum p for the tracks in a sample of Monte Carlo Z decays. Tracks are required to have at least 80 wire hits. The values of dE/dx are normalized to 1 at minimum ionization. Solid lines are the expected values for electrons, pions, kaons, and protons. b) The dE/dx distribution for electrons and pions in the same sample.

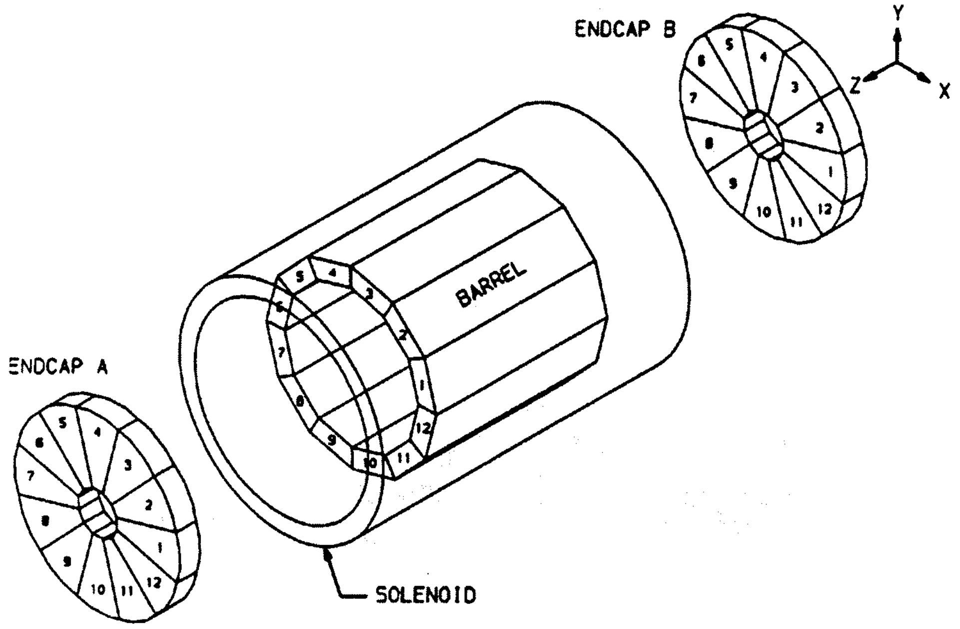

Figure 1.6: The Electromagnetic Calorimeter, barrel and endcaps

resolution, also provides a highly granular means to determine the shower positions and to do the pattern recognition. In addition, each wire chamber is read out separately in every module. These wire signals have very high sensitivities and are used as part of trigger signals. The wire signals are also used to calibrate the pad readout due to their low noise. Most interestingly, they can be used in a unique way to identify the particles in low multiplicity events. The last point can be illustrated by the cases shown in figure 1.8, where only one track hits a single module. The profile of the forty five layer readout reflects exactly the way the shower develops and hence provides some information about the nature of that shower.

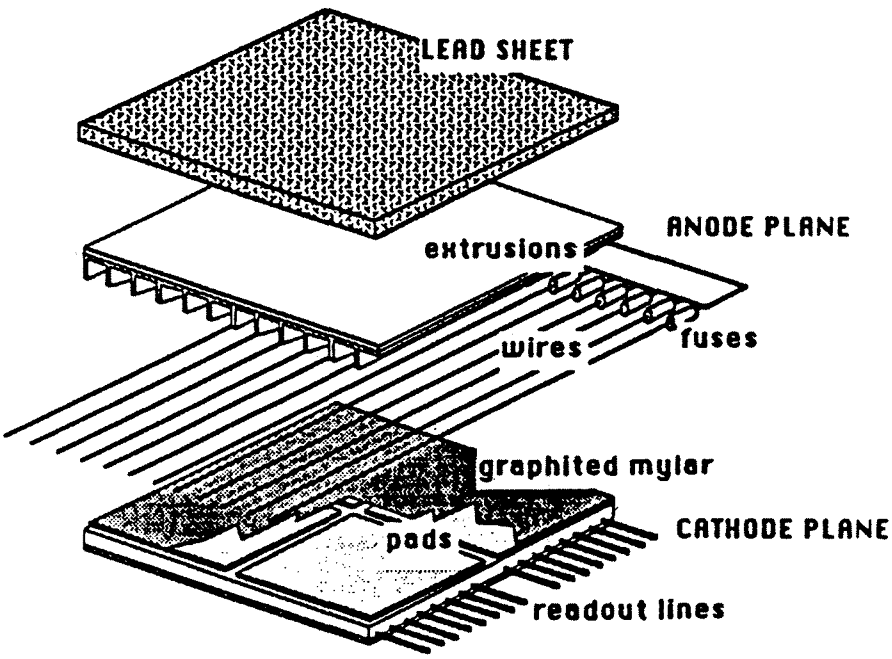

Figure 1.7: Structure of the ECAL layer

In more general cases, several quantities (called "estimators") are extracted from the ECAL signals to help in the particle identification.

One of them is called R_T, a shower compactness estimator defined as :

$$R_T = \frac{X_{measured} - X_{expected}}{\sigma(X)},$$

where $X = E_0/p$ and p is the momentum of the particle measured by the tracking devices. E_0 is the sum of shower energy deposited in three stacks of the four towers immediately surrounding the extrapolated trajectory of the track in the ECAL. If E_i is the shower energy deposited in the ith stack of these four towers, $E_0 = \sum_{i=1}^{3} E_i$. The $X_{expected}$ is determined by test-beam to be 0.83, independent of the angle and the momentum for electrons with $p > 2GeV/c$. The variance of

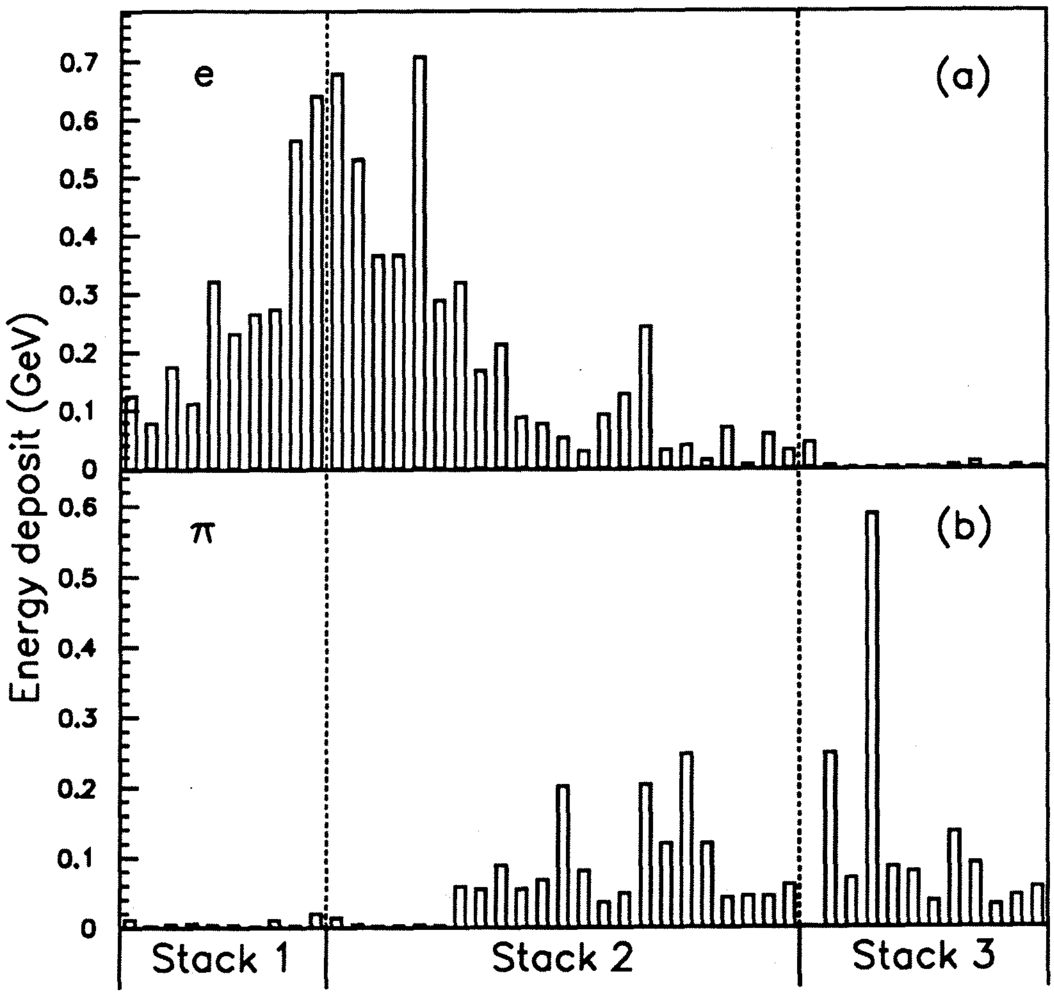

Figure 1.8: Typical ECAL wire profile of a) electron and b) pion. Each bar represents one layer of energy deposit. Electrons usually deposit most of their energy in the first two stacks, while pions start shower much later, often in the second and the third stack.

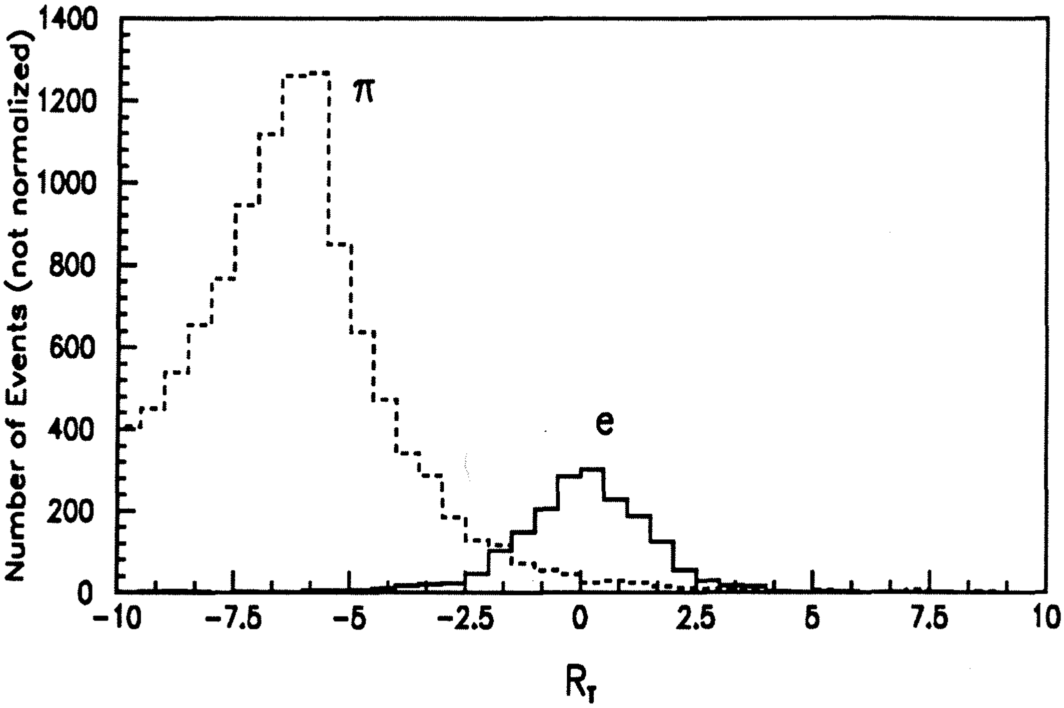

Figure 1.9: The R_T distribution for the electrons(solid line) and the pions (dashed line) in the Monte Carlo hadronic Z decays. The two distributions are not normalized.

X, $\sigma^2(X)$, is also obtained from the test-beam measurements and parametrized with respected to the momentum. For electrons, R_T is close to zero with a unit variance, and for pions, R_T tends to be different. The R_T distributions for electrons and pions are shown in figure 1.9.

Another estimator called R_L is based on the longitudinal information of the shower associated to the track. Let S_i be the mean longitudinal position of the shower in stack i. A variable A is then defined as:

$$A = \frac{E_0}{\sum_{i=1}^{3} E_i S_i},$$

where E_0 and E_i are the same as defined before.

R_L is defined with respect to A just as R_T is to X:

$$R_L = \frac{A_{measured} - A_{expected}}{\sigma(A)}$$

Likewise, $A_{expected}$ and $\sigma^2(A)$ are obtained and parametrized by the test-beams. The R_L distributions are shown in figure 1.10.

The R_T and R_L prove to be very powerful in separating electrons and pions, especially in the high momentum ($>$ 5 GeV) range, thanks to the high precision and fine granularity of the ECAL.

As mentioned before, the dE/dx method is very effective in separating the low momentum electrons and pions. Thus it is complementary to the ECAL method.

The ECAL can also be used together with the tracking devices to identify the charged ρ's from the tau decays. A ρ decays into a charged and a neutral pion. The charged pion is measured by the TPC and the ITC, and the neutral pion which itself decays into two photons can be detected by the ECAL. If the neutral pion is soft, as is the case for many tau decays, these two photons are separated in the ECAL. Hence their invariant mass is measurable. If this invariant mass is consistent with the π^0 mass, the two photons are assumed to be from the neutral pion. The invariant mass of this reconstructed π^0 and the charged pion is then calculated and compared with the charged ρ mass. If these two masses match again, the $\pi^0\pi^\pm$ system is most likely to be a ρ in origin.

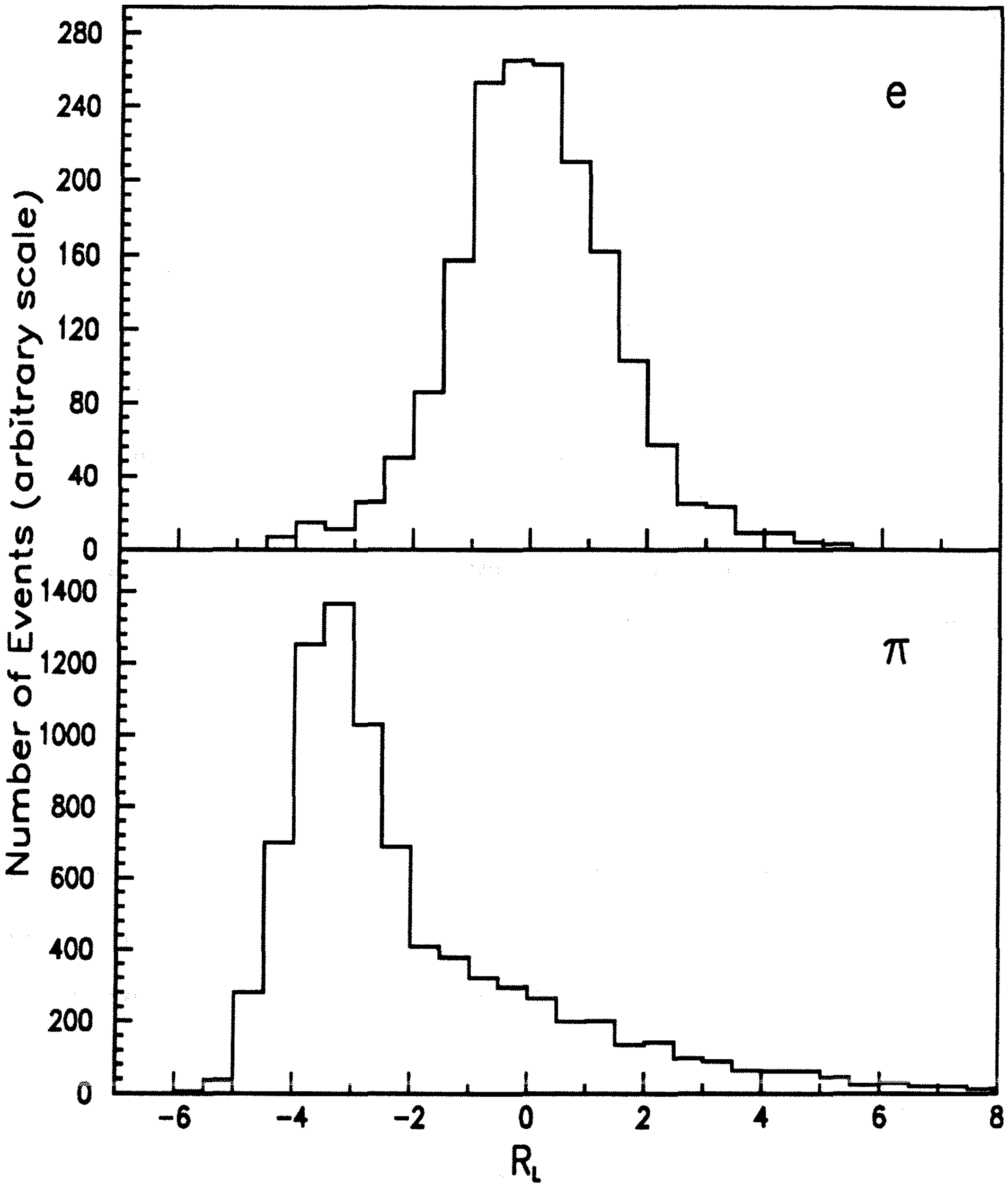

Figure 1.10: The R_L distribution for the electrons and the pions in the Monte Carlo hadronic Z decays. The two distributions are not normalized.

The HCAL and the muon detector

The other calorimeter, the hadron calorimeter (HCAL) measures the hadronic shower in the events (figure 1.11). Like the ECAL, the HCAL also has a layered sandwich structure, in which iron sheets and limited streamer tubes are placed

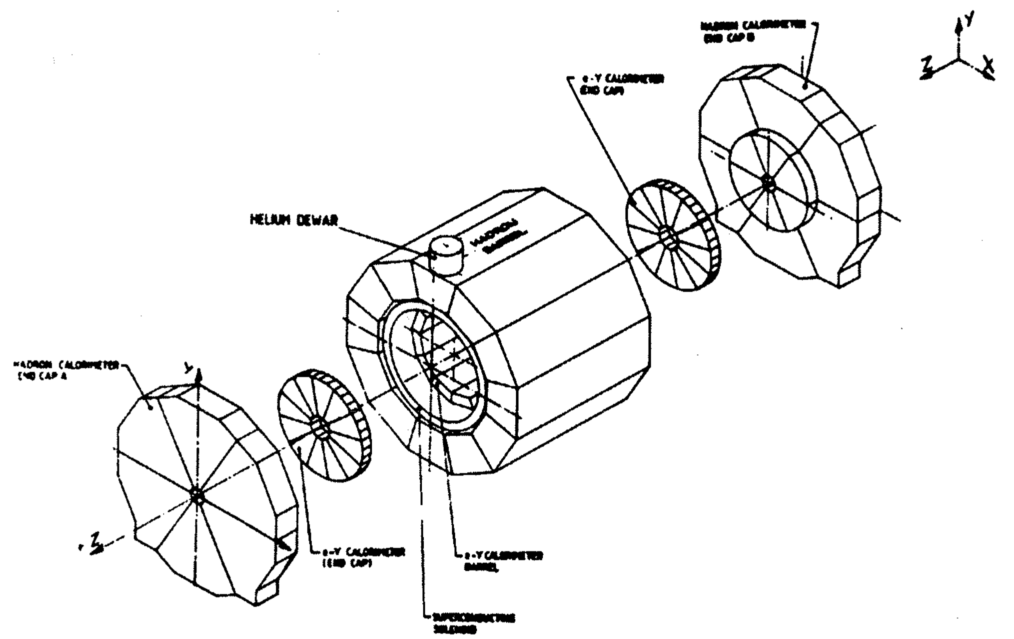

Figure 1.11: The Hadronic Calorimeter

in each of the twenty three layers. The whole structure has more than seven interaction lengths and is located just outside the magnet. It also serves as the return yoke of the magnetic coil. As an extension to the HCAL, a structure of two additional double layers of streamer tubes are separately mounted outside it to measure the muons penetrating the iron sheets. These layers are then called the muon detector.

As with the ECAL, the HCAL is divided into modules. Each module has readouts from the wires and the localized pads, which are also connected in towers. In addition, aluminum strips are placed parallel to the wires on one side of each streamer tube. These strips are coupled capacitively to the wires to provide a third source of signals.

In all, there are three types of signals serving different purposes; the pad readouts give the measurement of the energy deposited in the calorimeter with a resolution of about $84\%/\sqrt{E}$ (GeV); the wire readouts are used for triggering; and readout from each strip provides a digital signal that indicates whether or not the corresponding tube is hit. The tube hit patterns caused by pions and the muons are quite different, as shown in figure 1.12, and hence can be used for π/μ separation.

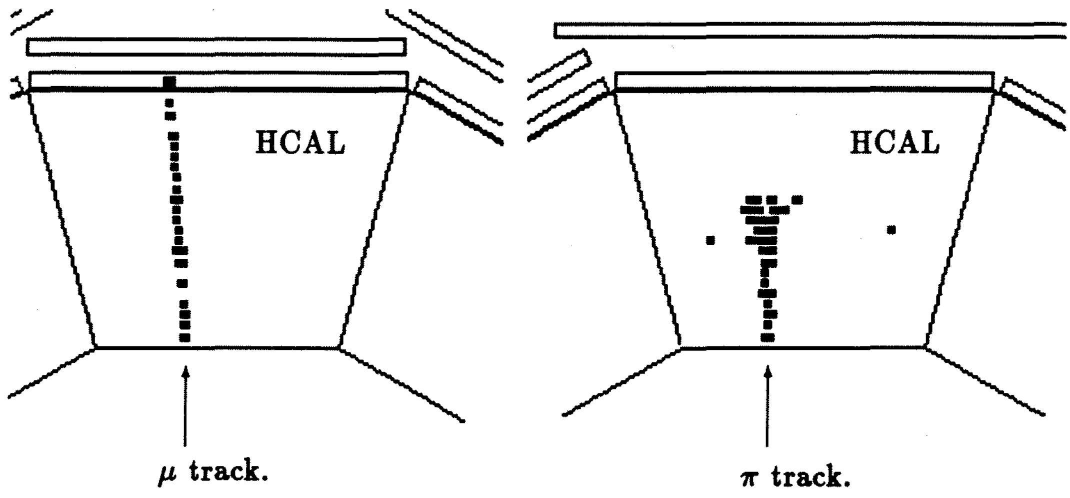

Figure 1.12: Typical HCAL hit pattern for the muon(left) and the pion(right). Muons usually penetrate the HCAL with a clean narrow path. In contrast, pions often shower in the HCAL, leaving a wider hit pattern.

1.3 The data and the simulated events

The LEP machine was commissioned in the summer of 1989, and in August of that year all the four detectors recorded their first hadronic Z decays. The 1989 data taking ended in December and the running restarted in March of 1990. Both the accelerator and the ALEPH detector ran smoothly till the end of August, when the 1990 running finished.

As the first accelerator ever being able to produce large amount of Z's, LEP, in the initial stage, gives its highest priority to the high precision measurements of the electroweak parameters. This results in the "scanning" strategy LEP took for the 1989 and 1990 runs. Under this strategy, electrons and positrons were colliding not only at the Z resonance peak of about 91 GeV but also at several centre of mass energy points around the peak. The percentage of events collected on the peak is about 70%. This scan method made possible detailed studies of the Z line shape which is very important in the determination of the electroweak parameters. However, as the cross section for Z production is much smaller when the c.m. energy is not at the peak, the effective luminosity is reduced. The integrated luminosity corresponding to the 1989 and 1990 data is 8.5 pb^{-1}. This is equivalent to about 6.2 pb^{-1} of on-peak luminosity.

All the data ALEPH took in both 1989 and 1990 are used in this analysis. There are more than 4 million events in the sample, of which about 200,000 are visible Z decays. The events are all reconstructed by the ALEPH reconstruction program, JULIA [7] , and stored on disks for analysis.

Throughout the analysis, simulated events are used for many purposes such as studying the backgrounds, justifying the selection procedure, determining the efficiency etc.

Events are first generated by various Monte Carlo event generators. In the generating processes, the coordinates of the decay vertices and the four-momenta vectors of all the particles in an event are simulated using the Monte Carlo method, under the guidance of the suitable theoretical calculations. These generated vectors and coordinates, along with the "true" identities of the particle types, are then processed by the ALEPH detector simulation program GALEPH.

GALEPH, which is based on GEANT3 [8], takes care of the detail detector informations such as the geometry and material, the working mechanisms of all the subcomponents, the electronics and the triggering system, and simulates the machine responses to the events. Other physics aspects, for example, the particle-media interactions (multiple scattering, hadronic interaction, photon conversion, energy loss, etc.) and the decays of the long lifetime particles in the detector volume, are also simulated by the program. At the end of the detector simulation, the simulated signals are written in the same form as the ALEPH on-line data acquisition system produces for the real data. These signals are assembled by JULIA the same way as it does for the data into more recognizable forms such as the tracks, the energy clusters, the vertices, etc. And afterwards the analysis-ready simulated events are made.

Neither GALEPH nor JULIA make use of the physics nature of the events and thus are considered to be unbiased. However, the generators heavily depend on the theoretical understandings of the physics processes. Some of the processes are well understood but some others are calculated only under certain assumptions. While approximations are unavoidable in most of the generators, we try to use only those we think to have been best understood and tuned to the data.

Chapter 2

The l^+l^-V Event Selection

The goal of our analysis is to select only those with the $l^+l^- V$ signature from a large amount of data collected by the detector. After the selection, the properties of the selected events will be studied, especially the production rates associated with each of the lepton channels of $e^+e^- V$, $\mu^+\mu^-V$ and $\tau^+\tau^-V$. Predictably, the initial data sample is dominated by various unwanted background sources. These backgrounds have to be kept out of the final sample while maintaining the selection efficiency for the interesting events at a reasonable level.

In an event counting experiment such as this, it is most critical to make sure the identity of every selected event is clearly understood. This means our analysis must not only be able to select out the $e^+e^- V$, $\mu^+\mu^-V$ and $\tau^+\tau^-V$ events we are looking for, but also be able to make a clean separation of the three types. The crosstalk among them must be reduced to a minimum.

Although the ALEPH particle identification is quite good, it is not perfect. To minimize the inefficiency introduced by the particle identification algorithm and to avoid the possible biasing of different particle channels due to the particle identification algorithm, our analysis is designed to rely more on the excellent precise tracking capability of the ALEPH detector. The kinematic features of our signals are investigated and used in our analysis whenever possible.

2.1 Signal signatures

The events we are looking for are expected to be simple and clean, given the straightforward l^+l^-V configuration. The e^+e^-V and $\mu^+\mu^-V$ events simply show up in the detector as four-prong events (i.e. events with four charged tracks) with no energy losses. But as the τ 's in the $\tau^+\tau^-V$ events are not directly measured, what we expect to see there are the "V" along with the τ decay products. When both τ 's in a $\tau^+\tau^-V$ event decay into one charged track (1-prong decay) the event will have four charged tracks in its final state, and if one of the two τ 's makes a 3-prong decay while the other still has a 1-prong decay, the event has six charged tracks. Though both τ 's can make 3-prong decays, the rate is too low and the backgrounds are too high. Therefore this case is not considered. Other τ decay configurations are also neglected.

In summary, the interesting events will have either four or six charged tracks in the final states. Needless to say, not all four- or six-track events are signal events, they have to satisfy many other requirements before can be called l^+l^-V events.

2.2 Selection procedure

As with many "typical" event selection procedures, the one we choose to select the l^+l^-V signals is based on a series of "cuts" . These cuts work together in a complementary way to define the event signatures, to eliminate various backgrounds, to classify the selected events into different channels. In the following sections, these cuts are listed one by one as they are applied.

2.2.1 Preliminary requirements

To begin with, events are required to have either 4 or 6 "good" charged tracks with total charge zero. Here, a "good" track is a track with the following properties:

- It is reconstructed by the tracking devices ITC and TPC with at least 4 TPC hits.
- It satisfies the conditions of $|d_0| < 2\ cm$ and $|z_0| < 5\ cm$ where, d_0 and z_0 are the coordinates of the closest approach of a reconstructed track to the collision point in $r - \phi$ and z direction, respectively.
- It makes an angle of least 18.2° with the beam axis.

These track quality requirements ensure that the tracks are most likely coming from the Z decay and are well measured.

In addition, at most two extra tracks are allowed in the 4-good-track events and the allowance is zero in the 6-track case. (Any track fails above good track definition but has at least three TPC hits is called an extra track). The extra track allowance is meant to save the events with tracks from back scattering or tracks kicked out from the detector material by the "good" tracks.

From now on, we ignore the extra tracks and when we say tracks we refer to the good tracks.

The data sample we start with corresponds to about 189k hadronic events and contains a total of about several million events, including hadronic, di-lepton, two-photon, cosmic ray, beam gas and noise triggered events. After the above requirements, there are 3346 events left.

2.2.2 Charged energy requirement

The sum of the energy of the charged tracks in an event must be more than 16 GeV. The main purpose of this requirement is to remove two-photon events. The charged energy distribution for the events with four or six tracks is shown in figure 2.1.

One can see that there is data excess at low charged energy; study reveals that this peak is mostly due to the two-photon process and hence this 16 GeV cut is made to eliminate it. After this requirement, there are 2699 events left.

2.2.3 Tau triplet mass cut

Most of the events surviving so far are $Z^0 \longrightarrow \tau^+\tau^-$ events with at least one τ in each event decays into three charged tracks. This kind of $\tau^+\tau^-$ events fakes the $\tau^+\tau^-V$ topology. For example, in the four track case, if one takes a pair of opposite charged tracks from the 3-prong side as a V, and takes the other two tracks as the products of a $\tau^+\tau^-$ pair both decaying into one charged track, one ends up with a four prong $\tau^+\tau^-V$. Similarly, a six track $\tau^+\tau^-$ event fakes a 6-prong $\tau^+\tau^-V$ with a 3-on-1 $\tau^+\tau^-$ decay.

On the other hand, if a τ decays into three charged tracks, the invariant mass of these tracks should be less than the τ mass (1.784 GeV) as long as the

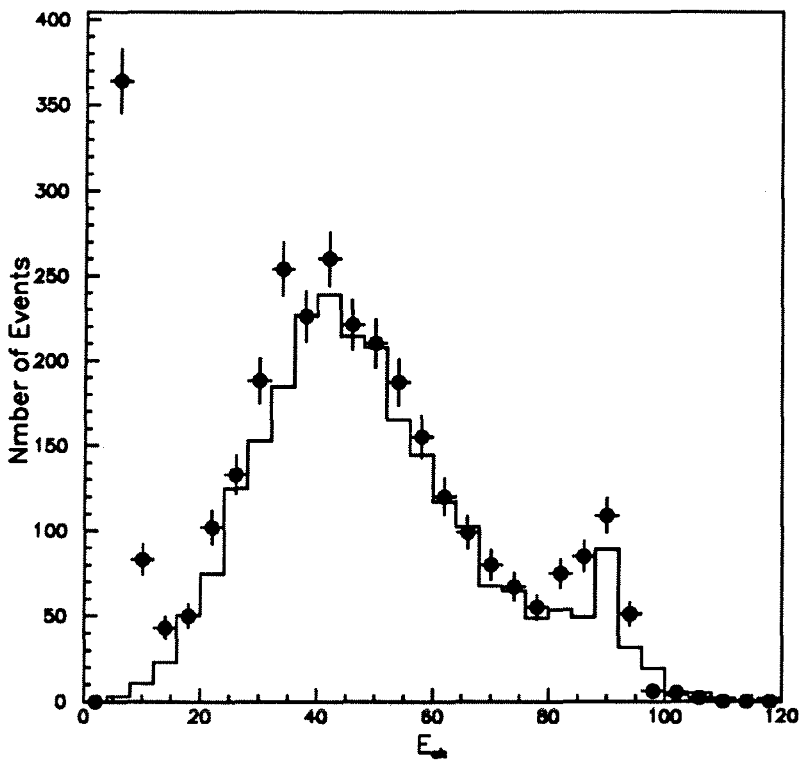

Figure 2.1: The charged energy distribution. Dots are the data and solid line are the lepton pair and hadronic Z decay Monte Carlo events.

tracks are well measured. Figure 2.2 shows the Monte Carlo simulated mass distribution of such triplets of charged tracks. Because of the uncounted neutral particle including one or two neutrinos, most of the masses are actually below the τ mass. Only in very few cases the triplet masses are above 1.7 GeV due to the measurement errors or photon conversion.

This means that in most of the cases it is quite safe to expect at least one triplet combination of the charged tracks with mass less than 1.7 GeV in a four track $\tau^+\tau^-$ event, and in a six track $\tau^+\tau^-$ event, at least two. In order to get

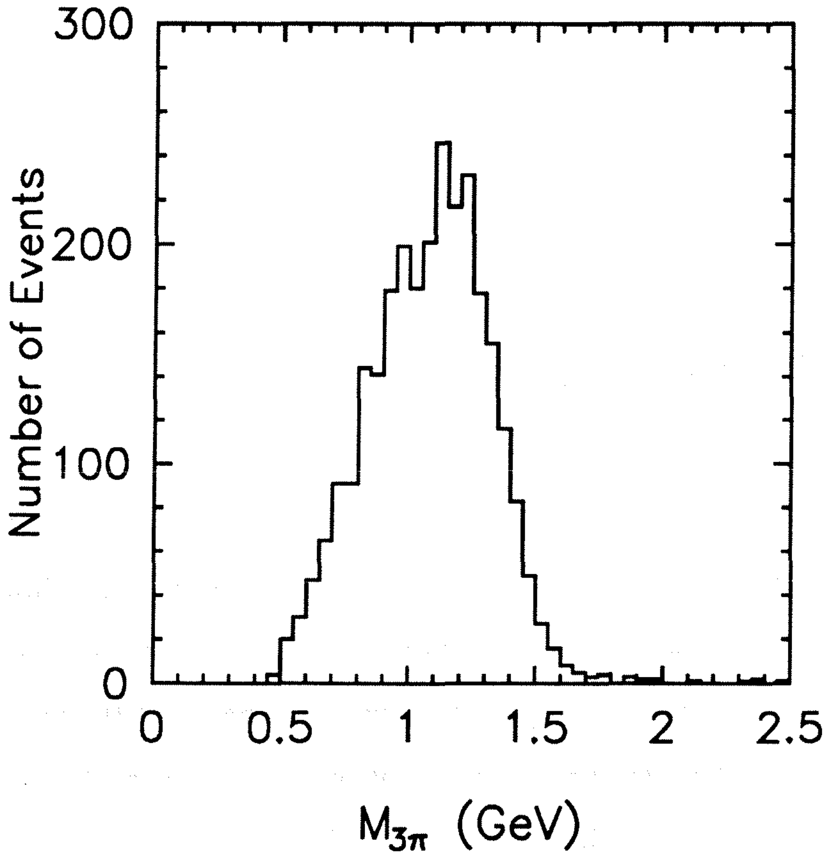

Figure 2.2: The tau triplet mass distribution.

rid of the $\tau^+\tau^-$ events, a cut is set to require that in a four track event there be no triplets of charged tracks with total charge to be $\pm$ 1 and invariant mass less than 1.7 GeV, and in a 6-track events there be one and only one such low mass triplet which is one of the τ decay product. After this cut 248 events remain.

The fact that we are able to cut the triplet mass at so low a value is made possible by the precise three dimensional tracking capability of our detector. However, as having been shown in figure 2.2, there are a very small portion of τ triplets having measured mass above 1.7 GeV. Hence, it is expected that some $\tau^+\tau^-$ events may pass this cut, the cuts introduced later further eliminate those events.

2.2.4 Pair conversion cut

Events with photons which convert into electron pairs in the material of the detector may also contaminate the l^+l^-V signal. This is because the converted pair often fakes the V. To take care of this case, a special algorithm is used to find out the converted pairs, and the events with conversions are rejected. This algorithm is similar to the one originally used by the Mark II collaboration [9] and is based on the fact that when a real photon converts, the resulting two tracks will have near zero invariant mass and hence are parallel to each other at the converting point. More specifically, for each pair of tracks suspected to be coming from a conversion, the algorithm works as follows: In the plane perpendicular to the beam direction, the point where the tracks are parallel to each other is determined from the track parameters. In the same plane, the distance δ_{xy} between the two tracks at this point is also calculated. In 3-D space,

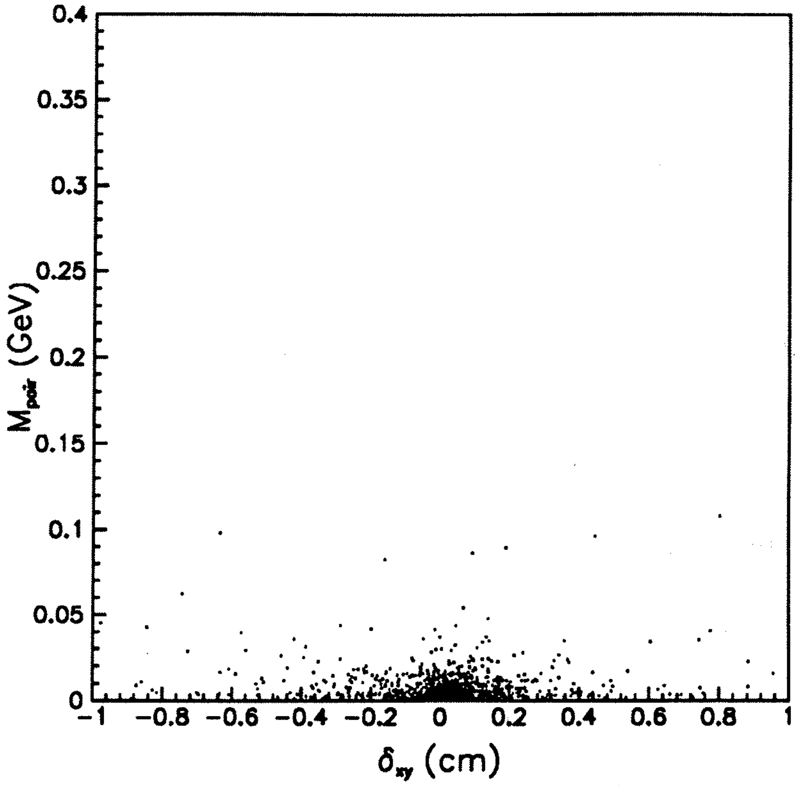

Figure 2.3: M_{pair} vs. δ_{xy} plot for the simulated pair conversions in the Monte Carlo lepton pair events.

the point corresponding to the one just calculated is taken to be the place where the possible conversion occurs and the invariant mass, M_{pair}, of these two tracks is then evaluated there. For real converted pairs, both M_{pair} and δ_{xy} are very small. This is not the case for normal massive pairs. So a converted pair can be identified from these two quantities.

Figure 2.3 shows a M_{pair} vs. δ_{xy} scattering plot for the Monte Carlo simulated converted pairs. The distribution is just as predicted.

Now for each of the 248 remaining events, the above algorithm is used to examine all opposite charged track pairs in the event. Particle identifications are not considered, and the τ triplet in 6 track events is excluded. If any pair examined in an event gives $M_{pair} < 50$ MeV and $\delta_{xy} < 4mm$, the event is rejected. This procedure leaves 83 events.

Since particle identification is not applied, there is no check on whether the tracks under question are actually electrons. In order to keep the low mass $\mu^+\mu^-$ or $\pi^+\pi^-$ pairs from being called converted pairs, the cuts on M_{pair} and δ_{xy} have to be set rather loose, as it is done here. This way, some conversions still have a chance to "leak in". Later, after we have applied the particle identifications, we will tighten the cuts to eliminate the remain conversions.

2.2.5 Forming the V

From this point on, the τ triplet in a six track event will be treated just as a single charged track (called "triplet track") . The four-momentum of this track is just the sum of the momenta of the three charged tracks, assumed to be pions.

Also, for each track in the event, the energy of an associated ECAL cluster is used in place of the track momentum as measured by the tracking devices if the cluster energy is larger. The direction of the track is not changed. This energy re-scaling recipe is meant to compensate for the bremsstrahlung of the electrons.

Now we are in the position to see whether the events actually contain the V's as the $l^+l^- V$ events are supposed to do. Any pair of oppositely charged tracks (excluding the triplet track in the six-track event case) can be the potential V in an event. However, only the pairs satisfying the following requirements are considered:

- The opening angle of the two tracks forming the pair $< 120°$.

- The angle between the remaining two tracks $> 90°$.

For each V assumption, the pair is called a V candidate and the other two tracks are called lepton tracks.

Sixty one events are found to contain at least one such V candidate. All the V assumptions will be tested later.

Although not all the "V"s in the l^+l^-V events satisfy the above angular requirements, this cut helps to reject low multiplicity hadronic Z decays. Also it reduces the false V assumptions in the l^+l^-V events, especially before any particle identifications are considered.

2.2.6 Verifying the V assumptions

The cuts in this section, together with those in the next three sections, are designed to test each V assumption made in an event. In other words, these cuts will be repeated until all the assumed V's in the event are checked. An event is kept if it contains at least one V satisfying all these cuts.

In an l^+l^-V event, if the V is correctly chosen, the recoil frame against the V, namely the frame with energy $E_{frame} = E_{cms} - E_V$ and momentum $P_{frame} = -P_V$, is expected to be the same as the rest frame of the remaining two leptons.

In such a frame, the leptons have the following general features:

- The total momentum of the two leptons is close to zero. The two leptons tend to be collinear (back to back).

- Each of the leptons will usually have the same energy which should equal to half the system available energy of $\sqrt{(E_{cms} - E_V)^2 - (-P_V)^2}$.

- The existence of initial and final state radiation (ISR and FSR) may shift the above total momentum away from zero and hence the two leptons may not be strictly collinear. The same ISR and FSR may also offset the lepton energy away from the expectation.

- For $\tau^+\tau^-$ pairs, what we measure are the decay products of the τ 's, so the collinear rule is further violated and the measured track energy will be substantially less than E, due to the missing neutrinos.

- The measurement error will also smear the energies and the directions of the tracks.

The above features are familiar since they are also the features of the leptons in the normal di-lepton events from the e^+e^- colliders, only there the laboratory frame *is* the rest frame. These di-lepton events are well understood so they can be used as a gauge for the l^+l^-V cuts. For example, $Z^0 \longrightarrow l^+l^-$ events are used here for this purpose.

With these guidelines in mind, we set up our cuts as follows:

For each candidate V, the V=e^+e^- , $\mu^+\mu^-$, and $\pi^+\pi^-$ particle hypotheses are made in turn to calculate the V four-momentum. (This reflects our philosophy to use the particle identification as late as possible. However, we found that since the V energy is usually very large compared to the π mass, the different particle hypotheses actually have little effect on the results as far as variables in this section are concerned). In each case, the lepton tracks are then boosted into the above mentioned recoil frame. Requirements on the collinearity and energy of the leptons are made in the boosted system.

- Collinearity: In the $\tau^+\tau^-$ system (see figure 2.4), if θ_1 is the maximum angle between the τ lepton and the measured τ track (recall that a triplet, if there, is treated as as a single track!), then θ_1 is a direct function of the energy and momentum of the τ lepton and also the energy , the momentum and the particle type of the its decay products. More specifically, θ_1 is determined by the formula:

$$\theta_1 = \sin^{-1} \frac{\sqrt{(E-E_1)(M_T{}^2 E_1 - M_1{}^2 E_T\ ) - \frac{1}{4}(M_T{}^2 - M_1{}^2)^2}}{P_T\ P_1}$$

where E is the expected τ lepton energy, $E = \frac{1}{2}\sqrt{(E_{cms} - E_V)^2 - (-P_V)^2}$, and P_T is the τ lepton momenta, $P_T = \sqrt{E^2 - M_T{}^2}$, the variables E_1, P_1, and M_1 are, respectively, the energy, momentum, and mass of the τ track. In one prong τ decay case, M_1 is taken to be zero, and in triplet τ decay case, M_1 is the triplet invariant mass assuming all three tracks in the triplet to be pions.

A typical relation between θ_1 and E_1, as calculated by the above formula, is shown in figure 2.5.

The same formula exists on the other τ side. Namely if θ_2 is the max angle between the τ^+ lepton and its decayed track, we have:

$$\theta_2 = \sin^{-1} \frac{\sqrt{(E-E_2)(M_T{}^2 E_2 - M_2{}^2 E_T\ ) - \frac{1}{4}(M_T{}^2 - M_2{}^2)^2}}{P_T\ P_2}$$

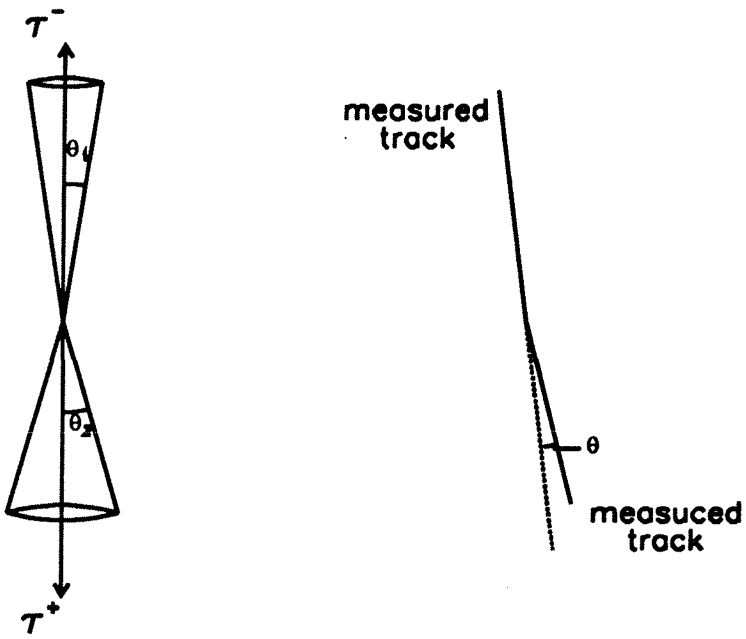

Figure 2.4: Defination of the angles θ_1, θ_2, and θ. Track from the tau decay is expected to be within a cone with a half angle of θ_1 (or θ_2) around the original tau. θ is the collinear angle between the two tracks from the τ^- and the τ^+ decays. The triplet from the tau decay is treated as a single track.

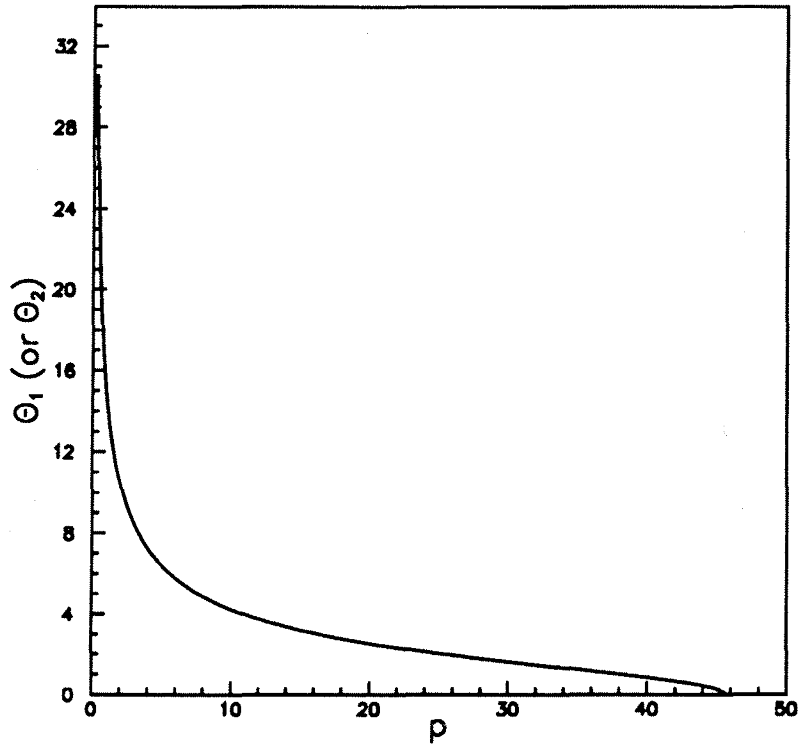

Figure 2.5: Maxmum angle between the tau decay product and the tau lepton as the function of the momentum of the tau decay product. The momentum of the tau lepton is set to be 45.6 GeV. The mass of the tau decay product is set to be the electron mass.

(E_2, P_2, and M_2 the energy, momentum, and mass of the measured track from τ^+).

Now let θ be the collinear angle between the two measured τ tracks, we will have $\theta < \theta_1 + \theta_2$.

For the e^+e^- (or $\mu^+\mu^-$) system , if one uses the above formulas to calculate θ_1 and θ_2 as they are (even though they are not τ 's!) and define θ the same way, the relation $\theta < \theta_1 + \theta_2$ still holds in most of the case. This is because θ in the e^+e^- or $\mu^+\mu^-$ cases should equal to zero if there is no ISR and FSR.

A 2° allowance is made to cover the effects of radiation and the measurement errors. Hence the collinear cut is loosened to:

$$\theta - \theta_1 - \theta_2 \ < 2^\circ$$

The $\theta - \theta_1 - \theta_2$ distributions for the e^+e^- , $\mu^+\mu^-$, and $\tau^+\tau^-$ system are shown in figure 2.6. They are calculated using the corresponding $Z^0 \longrightarrow l^+l^-$ Monte Carlo events.

- Energy : Still in the boosted frame, let E_1 and E_2 be the energies of the measured lepton track, and E, as before, be the calculated lepton energy. The ratio E_1/E or E_2/E represents the fraction of the visible energy in the tau decays. It is required $E_1/E > 0.05$ and $E_2/E > 0.05$. This is mainly to cut further the $\tau^+\tau^-$ background events which are not eliminated by the cut in section 2.2.3. Plots in figure 2.7 show the distributions of E_1/E (or the same, E_2/E). These distributions are also calculated from the simulated $Z^0 \longrightarrow l^+l^-$ events.

If we require there be at least one V assumption in an event satisfying both the above collinear and the energy cuts, we have 56 events left.

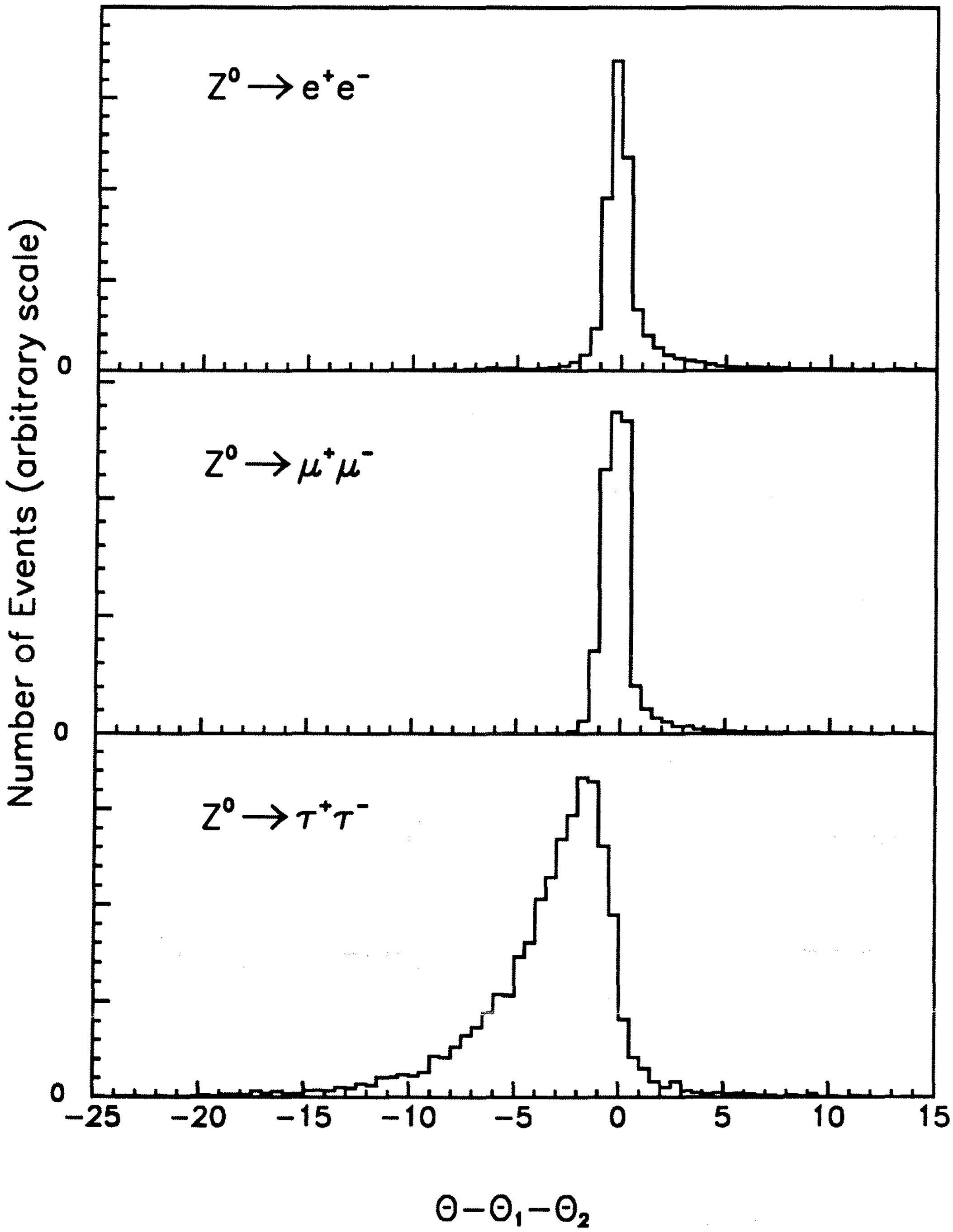

Figure 2.6: The $\theta - \theta_1 - \theta_2$ distribution as calculated from the $Z \longrightarrow e^+e^-$, $\mu^+\mu^-$, $\tau^+\tau^-$ Monte Carlo.

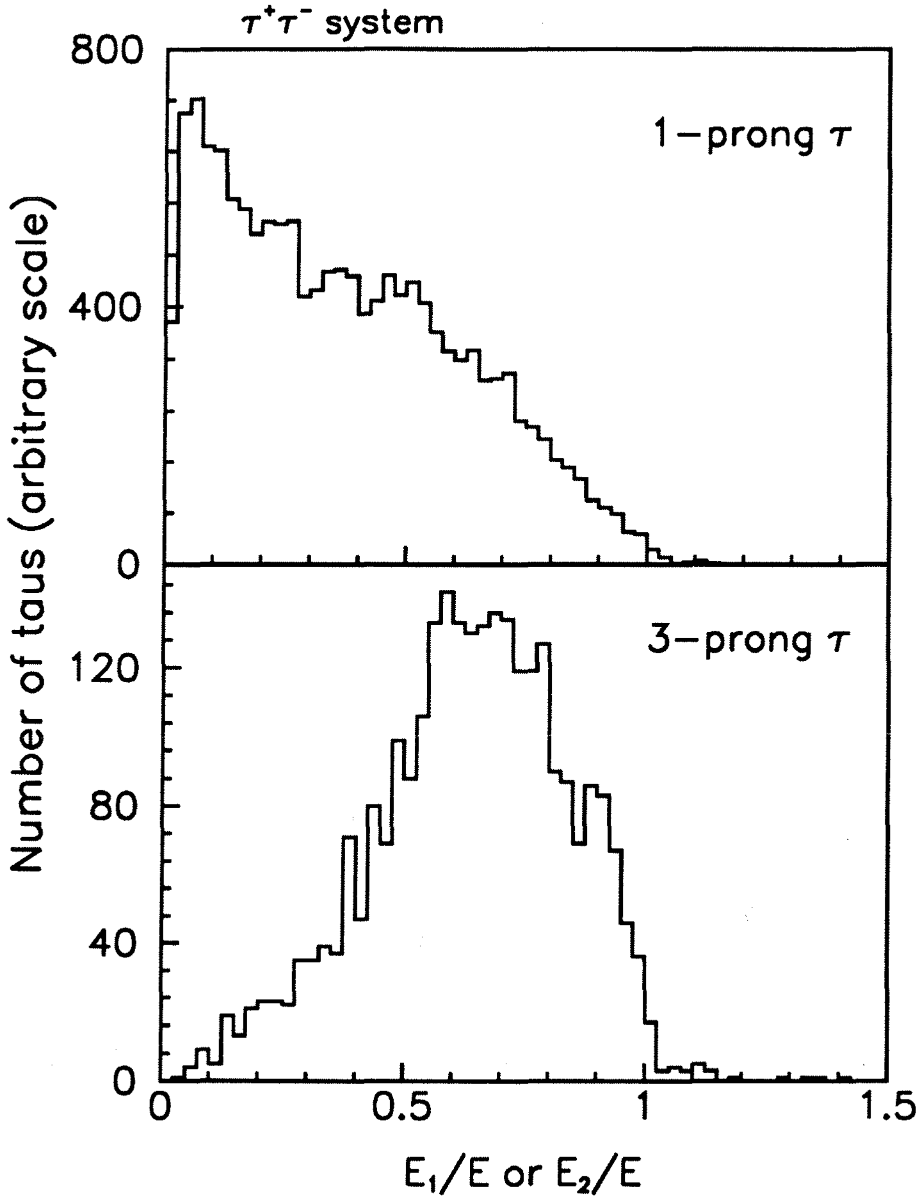

Figure 2.7: The energy ratio between the measured tau decay product and the tau lepton, for 1-prong and 3-prong tau decays. The distribution is calculated from the simulated $Z \longrightarrow \tau^+\tau^-$ events.

2.2.7 Classifying the events

The same variables E_1/E and E_2/E as defined in the previous section can also be used to separate the four-track $\tau^+\tau^-V$ from the e^+e^-V and $\mu^+\mu^-V$ events. Namely, a four-track event (or rather the event under a specific V hypothesis) is called a $\tau^+\tau^-V$ candidate if

$$E_1/E < 0.9, E_2/E < 0.9 \textit{ and } E_1/E + E_2/E < 1.2 .$$

Otherwise, if

$$E_1/E > 0.8 \textit{ and } E_2/E > 0.8,$$

it is called a e^+e^-V or $\mu^+\mu^-V$ candidate. (to be further classified later by the particle identifications).

Hypotheses falling outside both categories are called non-classifiable and rejected. After this cut, fifty two events remain having at least one classifiable V assumption.

The E_1/E vs E_2/E plots for e^+e^-, $\mu^+\mu^-$, and $\tau^+\tau^-$ events are shown in figure 2.8 to figure 2.10. One note that the most of the events are correctly classified and the crosstalk between $\tau^+\tau^-$ and e^+e^- (or $\mu^+\mu^-$) is already very small at a few percent level. The total energy cut described later reduced the crosstalk further to be less than 0.1%.

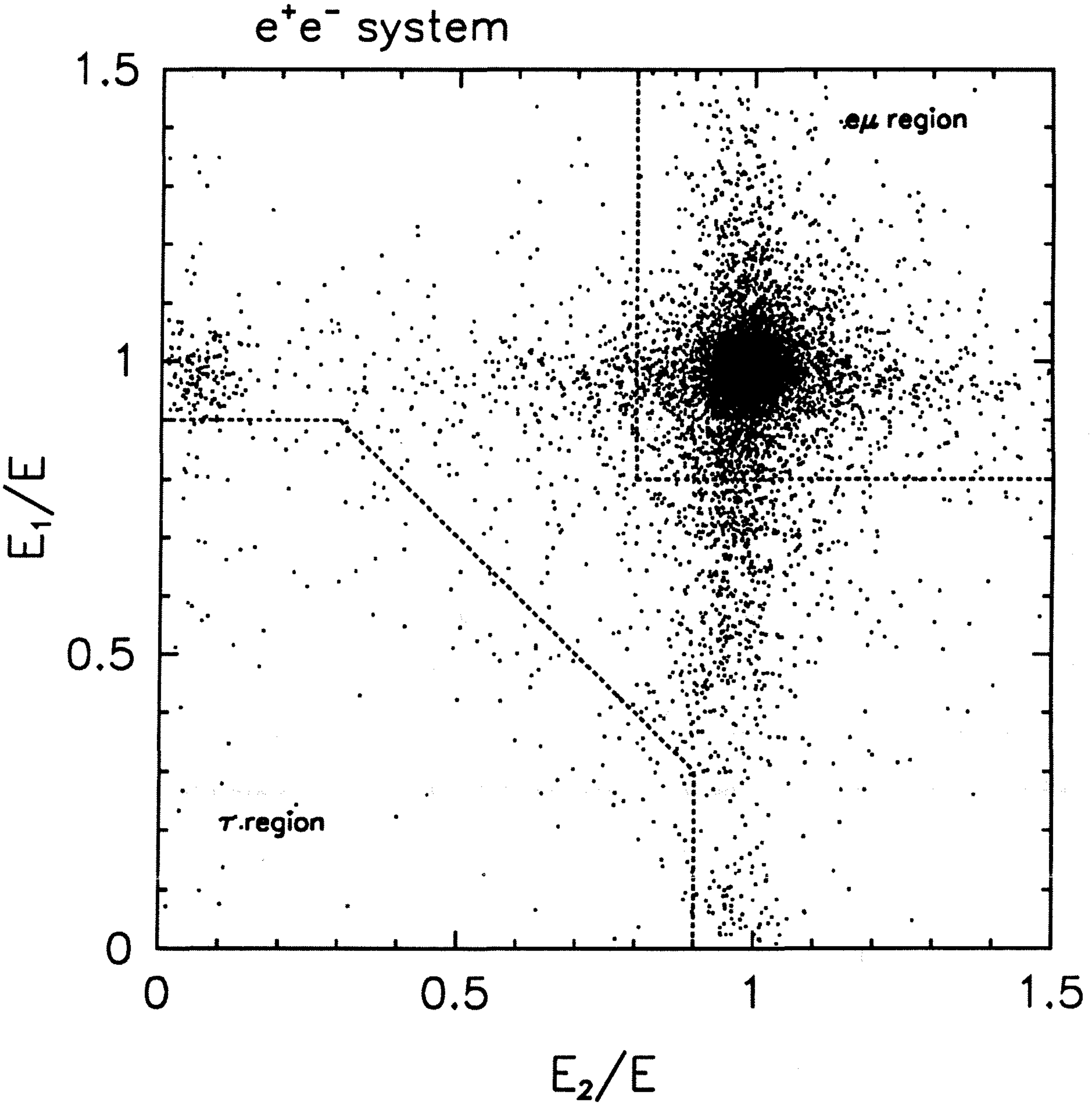

Figure 2.8: E_1/E versus E_2/E for the e^+e^- system. $Z \longrightarrow e^+e^-$ Monte Carlo events are used in calculation. Both taus are required to decay into one charged track.

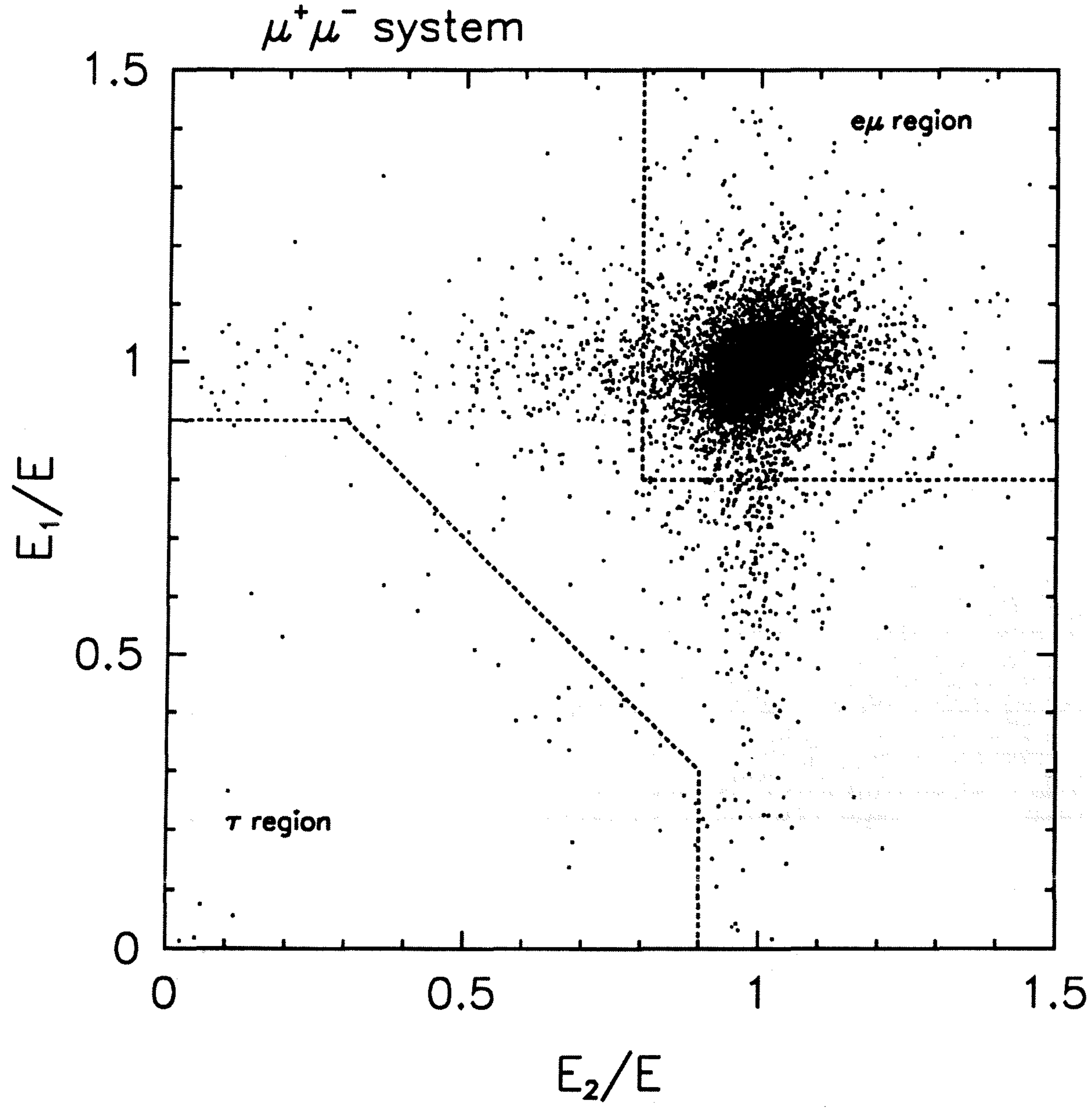

Figure 2.9: E_1/E versus E_2/E for the $\mu^+\mu^-$ system. $Z \longrightarrow \mu^+\mu^-$ Monte Carlo events are used in calculation. Both taus are required to decay into one charged track.

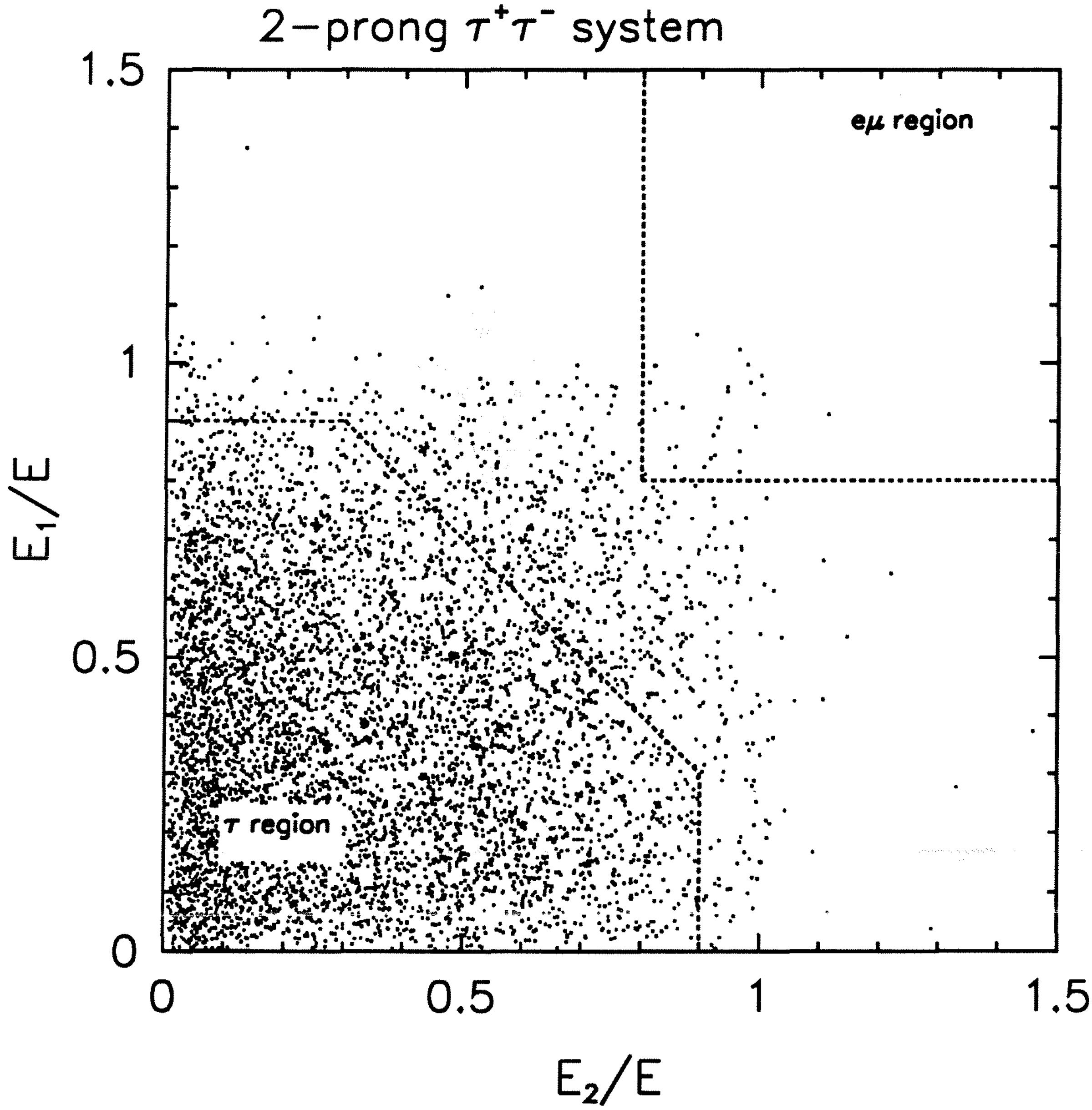

Figure 2.10: E_1/E versus E_2/E for the $\tau^+\tau^-$ system. $Z \longrightarrow \tau^+\tau^-$ Monte Carlo events are used in calculation. Both taus are required to decay into one charged track.

2.2.8 The total energy cut

Under a certain V assumption, if an event is classified into $\tau^+\tau^-V$ channel, then the total energy of the event should not exceed 80 GeV. Otherwise, this V assumption is rejected. This is to reduce further the hadronic contamination, and also to reduce the misclassification of the e^+e^-V and $\mu^+\mu^-V$ as the $\tau^+\tau^-V$ events. After this cut there are 44 events remaining.

The total energy of the event is calculated using an algorithm which makes comprehensive use of the information from the calorimeters and the tracking devices. Details of the algorithm can be found in Ref. [10].

2.2.9 Particle identification

Particle identification is now made for all the tracks in the remaining events. Particle ID is done at this point because the number of events (and hence the number of tracks) is small. Therefore the possible error introduced by the the particle ID is also small. As briefly discussed in the last chapter, information from the ECAL, the HCAL, the muon chambers, and the energy loss in the TPC (dE/dx) are used together to provide identify the particles .

It is required that the V be consistent with being a particle-antiparticle pair (e^+e^- , $\mu^+\mu^-$, or $\pi^+\pi^-$) and the lepton tracks be consistent with the kinematic classification performed before.

Three events fail this particle ID requirement: one probable $\tau^+\tau^-V$ and one probable $\mu^+\mu^-V$ in which the correct combinations fail the kinematic cuts due to radiated photons, and the third is most likely to be a hadronic event.

Among the remaining events, there are four events having more than one V assumption. In such cases, the V with lowest mass is taken as the "V" in a event.

2.2.10 Tight conversion cut

As seen in figure 2.3, there are still converted pairs passing our previous loose conversion cut (cut 3) and hence the background due to the photon conversion in di-lepton events still remains. With the particle identification done, we can use a more strict conversion cut. Obviously, this should be applied only to the $V = e^+e^-$ case. Under the tighten cut, an e^+e^- pair is called conversion if either

$$M_{pair} < 20\ MeV \ or\ M_{pair} < 100\ MeV/cm \times (1 - |\delta_{xy}|),$$

where M_{pair} and δ_{xy} are calculated in section 2.2.4. Events with a converted V are removed. In this way, 6 events, two of each channel, are rejected.

Events passing all the cuts described in this and the previous sections make up our final sample of the l^+l^-V events. There are thirty five, of which there are 10 e^+e^-V , 10 $\mu^+\mu^-V$, and 15 $\tau^+\tau^-V$ events.

Chapter 3

The l^+l^-V Results

In this chapter, some properties of the events selected as the l^+l^-V events will be discussed. These include the event rates, their distributions over the three lepton channels, and some interesting physics quantities of the events. The possible contributions from the known processes, including both background and signal processes, will also be studied using the Monte Carlo method. At the end, the Monte Carlo prediction will be compared with the observed data.

3.1 The selected events

There are thirty five l^+l^-V events selected from the whole ALEPH data sample collected in 1989 and 1990. The integrated luminosity of the data sample is 8.5 pb^{-1} (equivalent to 6.2 pb^{-1} at the peak). Main properties of each of these 35 events are listed in table 3.1 and table 3.2. The variables in these two tables are explained as following:

- *Run* and *Event* are two numbers from the ALEPH event numbering system. They have no physics meaning and are listed only for book keeping purposes.

- E_{cm} is the center of mass energy (in GeV) for the event. The E_{cm} distribution of the l^+l^-V events is in agreement with that of the 1989 and 1990 ALEPH data.

- N_{tk} is the charged track multiplicity in the event. All the e^+e^-V and $\mu^+\mu^-V$ events have four charged tracks. Among the fifteen $\tau^+\tau^-V$ events, ten have four prongs and the other five have six prongs. This ratio is about as predicted from the tau decay branching ratios.

- E_{ch} is the measured charged energy of the event. From the table, one can see that the E_{ch}'s for the e^+e^-V and $\mu^+\mu^-V$ events are in most cases very close to the corresponding E_{cm}'s, whilst the E_{ch}'s for the $\tau^+\tau^-V$ events are lower due to the missing neutrinos.

  However, we do see some of the e^+e^-V events having lower charged energies. This is because of the bremsstrahlungs of the tracks. The energy re-scaling prescription introduced in section 2.2.5 corrects for this effect.

- l^+l^- specifies the lepton type of the l^+l^-V events.

- The column under the heading "V" lists the identified types of the V in the observed l^+l^-V events. None of the three V types prevails over the others.

- M_{ll} is the invariant mass of the l^+l^- pair in the event calculated from E_{cm} and the V four-momentum. Its distribution is shown in figure 3.1 .

	Run	Event	E_{cm}	N_{trk}	E_ch	l^+l^-V	V	M_V	M_{ll}	E_V
1	8898	5940	91.2	4	86.0	ee	ee	0.341	47.22	33.39
2	8960	749	88.2	4	61.0	ee	ee	1.454	84.77	3.39
3	9011	4093	91.2	4	83.3	ee	ee	2.297	72.50	16.82
4	7339	5121	91.2	4	83.5	ee	$\mu\mu$	3.457	65.67	22.05
5	7849	456	91.2	4	95.3	ee	$\mu\mu$	22.996	49.15	35.27
6	6975	1389	91.2	4	94.2	ee	$\pi\pi$	0.565	80.17	10.39
7	9010	5607	91.2	4	92.1	ee	$\pi\pi$	0.565	33.74	39.36
8	7422	2873	91.2	4	89.9	ee	$\pi\pi$	0.590	50.61	31.57
9	8163	2748	89.2	4	82.4	ee	$\pi\pi$	0.706	75.91	12.32
10	8334	7367	91.2	4	85.1	ee	$\pi\pi$	0.794	65.44	22.15
11	7339	1745	91.2	4	90.5	$\mu\mu$	ee	0.135	89.26	1.95
12	5825	51	91.5	4	80.5	$\mu\mu$	ee	1.063	55.65	28.85
13	8855	3264	92.2	4	90.5	$\mu\mu$	ee	1.063	55.92	29.16
14	8804	3691	90.2	4	84.1	$\mu\mu$	ee	1.232	76.17	12.96
15	5821	3675	91.5	4	92.2	$\mu\mu$	$\mu\mu$	0.257	83.97	7.25
16	4515	750	91.3	4	95.3	$\mu\mu$	$\mu\mu$	0.277	89.69	1.61
17	8899	4745	91.2	4	90.5	$\mu\mu$	$\mu\mu$	2.288	76.14	13.86
18	8775	1605	91.2	4	88.6	$\mu\mu$	$\mu\mu$	8.329	75.78	14.52
19	8803	2443	90.2	4	90.2	$\mu\mu$	$\mu\mu$	38.855	36.57	46.06
20	7496	3332	91.2	4	90.9	$\mu\mu$	$\pi\pi$	0.811	58.77	26.68
21	5509	2667	92.3	6	67.4	$\tau\tau$	ee	0.185	66.78	21.98
22	7743	8370	91.2	6	52.2	$\tau\tau$	ee	0.402	83.43	7.46
23	7253	357	90.2	6	65.9	$\tau\tau$	ee	0.833	83.90	6.11
24	7958	3841	91.2	6	49.4	$\tau\tau$	ee	0.830	89.56	1.64
25	7681	2160	88.2	4	33.8	$\tau\tau$	ee	1.072	71.00	15.55
26	8335	1133	91.2	4	43.1	$\tau\tau$	ee	1.819	76.96	13.17
27	7858	8314	90.2	6	50.2	$\tau\tau$	$\mu\mu$	0.484	56.25	27.58
28	5166	981	91.3	4	43.6	$\tau\tau$	$\mu\mu$	0.803	85.58	5.53
29	8623	158	91.2	4	28.6	$\tau\tau$	$\mu\mu$	1.187	68.39	19.98
30	8865	6111	91.2	4	17.7	$\tau\tau$	$\mu\mu$	1.275	82.62	8.20
31	8537	4398	91.2	4	40.4	$\tau\tau$	$\pi\pi$	0.694	87.39	3.76
32	8833	4673	91.2	4	38.0	$\tau\tau$	$\pi\pi$	0.767	80.55	10.05
33	6972	4547	91.2	4	38.0	$\tau\tau$	$\pi\pi$	0.772	87.41	3.73
34	8126	771	91.2	4	33.3	$\tau\tau$	$\pi\pi$	0.829	65.67	21.98
35	8796	4675	91.2	4	39.3	$\tau\tau$	$\pi\pi$	1.022	83.03	7.82

Table 3.1: Propterties of the selected l^+l^-V events. (continues in the next table)

	Run	Event	$M(3\pi)$	E_1/E	E_2/E	$\theta-\theta_1-\theta_2$	θ_{open}	θ_V	$\cos\theta_D$	E_{tot}
1	8898	5940	6.87	0.94	0.92	-1.9	2.3	19.8	0.86	89.9
2	8960	749	8.60	1.24	0.95	-0.3	59.3	28.1	-0.55	90.8
3	9011	4093	4.63	0.87	0.94	-1.2	16.5	8.0	-0.31	89.1
4	7339	5121	5.68	1.01	0.98	-0.3	18.0	6.7	0.04	92.8
5	7849	456	43.04	1.01	1.11	0.1	93.9	83.1	-0.60	95.3
6	6975	1389	2.21	1.03	1.04	0.2	5.5	5.4	0.19	94.8
7	9010	5607	3.33	1.17	1.00	1.0	1.5	11.0	-0.45	92.1
8	7422	2873	23.91	0.98	0.95	0.7	1.9	63.1	-0.15	89.9
9	8163	2748	19.30	1.00	0.95	-0.3	7.2	55.8	-0.67	89.3
10	8334	7367	8.47	0.94	0.99	-0.8	4.2	21.7	0.44	89.8
11	7339	1745	3.19	1.01	0.98	-0.3	9.0	17.3	0.46	90.3
12	5825	51	30.14	0.95	0.99	1.3	4.4	75.2	-0.26	90.6
13	8855	3264	9.58	0.97	1.15	0.8	8.1	22.6	-0.86	93.0
14	8804	3691	3.02	0.96	0.89	-1.3	33.2	3.7	0.95	84.8
15	5821	3675	17.73	0.99	1.02	-0.1	2.3	62.7	0.30	92.2
16	4515	750	5.11	1.00	1.09	0.5	12.8	33.2	-0.22	91.6
17	8899	4745	4.69	1.00	0.98	-0.4	19.0	6.0	-0.07	90.5
18	8775	1605	28.54	0.97	0.96	-0.9	74.6	71.6	-0.39	90.0
19	8803	2443	50.19	1.03	0.91	1.0	115.1	77.9	0.07	90.8
20	7496	3332	5.88	0.99	1.01	-0.2	3.7	14.6	0.56	90.9
21	5509	2667	66.78	21.98	22.47	0.52	0.74	-2.3	1.0	75.7
22	7743	8370	83.43	7.46	17.36	0.41	0.66	-2.1	6.2	92.4
23	7253	357	83.90	6.11	8.86	0.50	0.97	1.3	17.0	32.2
24	7958	3841	89.56	1.64	2.99	0.30	0.90	0.8	61.6	16.5
25	7681	2160	71.00	15.55	3.29	0.17	0.61	-3.6	31.7	18.6
26	8335	1133	76.96	13.17	2.08	0.67	0.37	-3.3	35.5	16.3
27	7858	8314	56.25	27.58	17.63	0.10	0.94	-4.3	2.3	46.2
28	5166	981	85.58	5.53	8.93	0.10	0.83	-3.8	18.3	37.2
29	8623	158	68.39	19.98	8.55	0.74	0.17	-2.1	9.1	51.9
30	8865	6111	82.62	8.20	4.31	0.09	0.14	-10.0	19.4	35.1
31	8537	4398	87.39	3.76	3.68	0.59	0.23	-1.7	20.2	33.0
32	8833	4673	80.55	10.05	4.33	0.58	0.07	-1.9	8.3	48.7
33	6972	4547	87.41	3.73	3.24	0.44	0.28	-2.9	32.1	18.3
34	8126	771	65.67	21.98	6.71	0.19	0.34	-6.4	4.1	37.6
35	8796	4675	83.03	7.82	2.15	0.65	0.15	-5.6	24.2	1.9

Table 3.2: Propterties of selected l^+l^-V events. (continued from previous table)

- M_V is the mass of the "V" in a $l^+l^- V$ event. We note that, as shown in figure 3.2, there are events with large M_V's (> 3 GeV) in both $e^+e^- V$ and $\mu^+\mu^- V$ channels, while in the $\tau^+\tau^- V$ channel the V masses are all less than 2 GeV.

- E_V denotes the energy of the V in GeV.

- θ_{open} is the opening angle of the two tracks forming the V.

- $M(3\pi)$ is the smaller of the two invariant masses the V making with the two leptons. Because of the triplet mass cut in section 2.2.3, all these masses should be larger than 1.7 GeV and indeed they are all well above that value.

- E_1/E , E_2/E , and $\theta - \theta_1 - \theta_2$ are described in section 2.2.6. Their distributions are in good agreement with the expectation.

- θ_V is the angle between the V and the closest lepton l, in the laboratory system. Its distribution bears the characteristic of the radiative processes. Also we note that there are more low θ_V events in the $e^+e^- V$ and $\mu^+\mu^- V$ channels than in the $\tau^+\tau^- V$ channel. This is because in $\tau^+\tau^- V$ events, tracks from the τ decays are usually softer, and hence need larger θ_V in order to pass the triplet mass cut.

- $\cos\theta_D$ is the cosine of the V decay angle (see figure 3.3), and its distribution is plotted in figure 3.3. The distribution suggests that the V is not highly polarized.

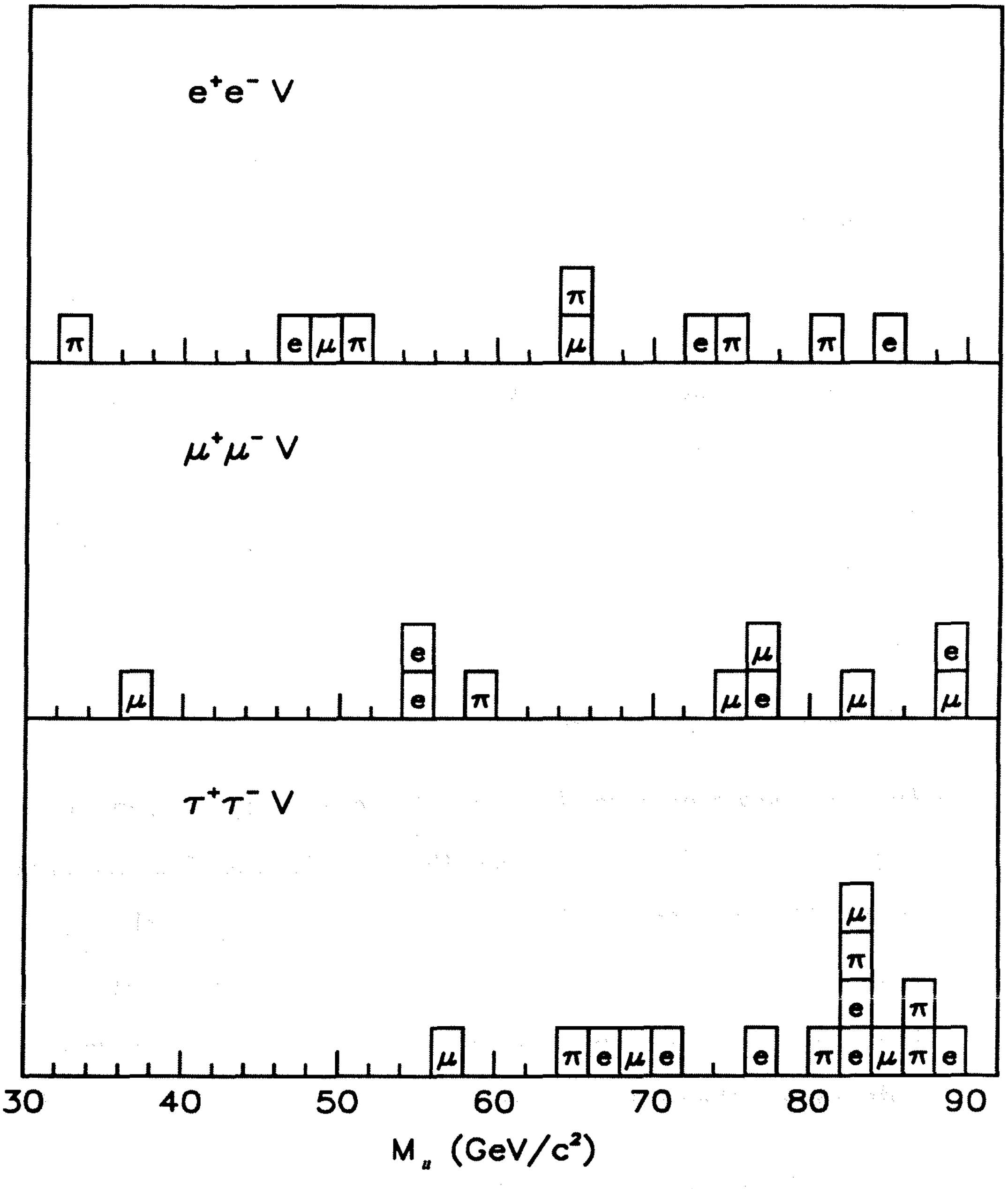

Figure 3.1: The M_{ll} distribution for the selected e^+e^-V , $\mu^+\mu^-V$, and $\tau^+\tau^-V$ events. Each box represents one event. The letters inside the boxes denote the V types.

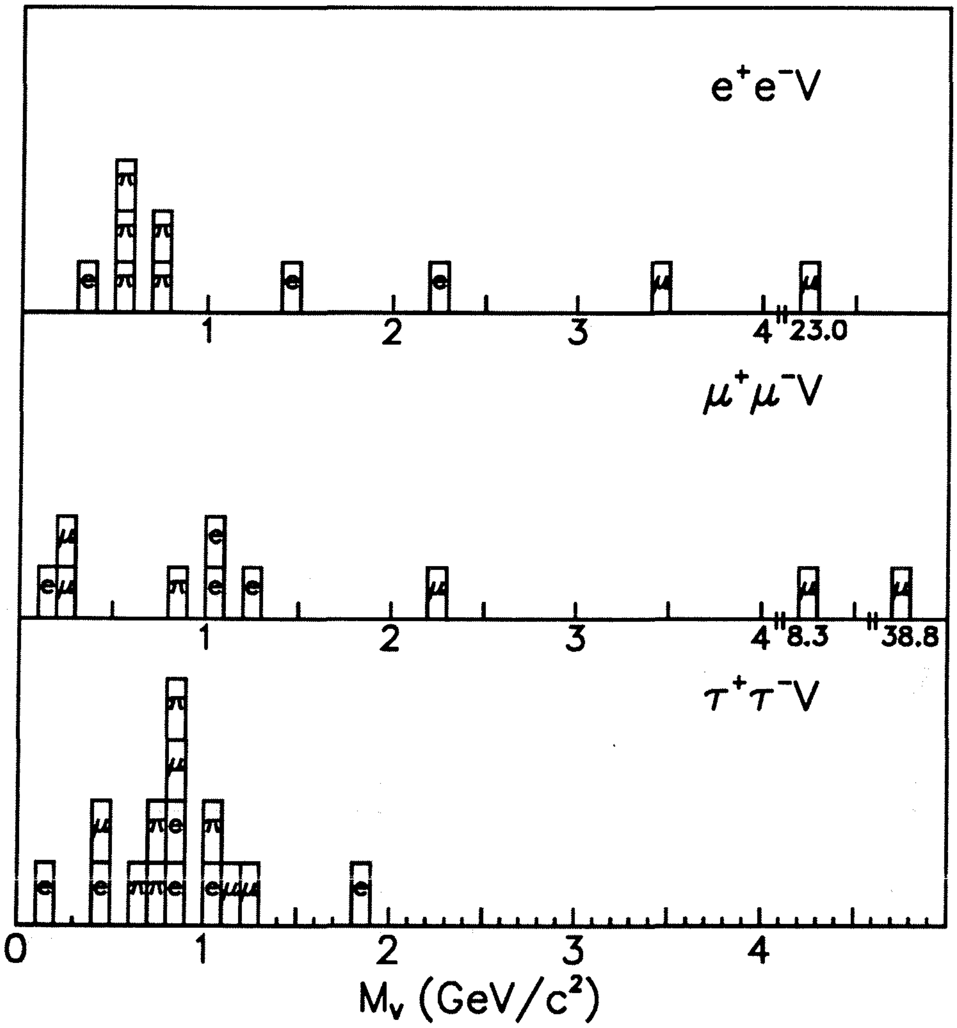

Figure 3.2: The M_V distribution for the selected e^+e^-V , $\mu^+\mu^-V$, and $\tau^+\tau^-V$ events. Each box represents one event. The letters inside the boxes denote the V types.

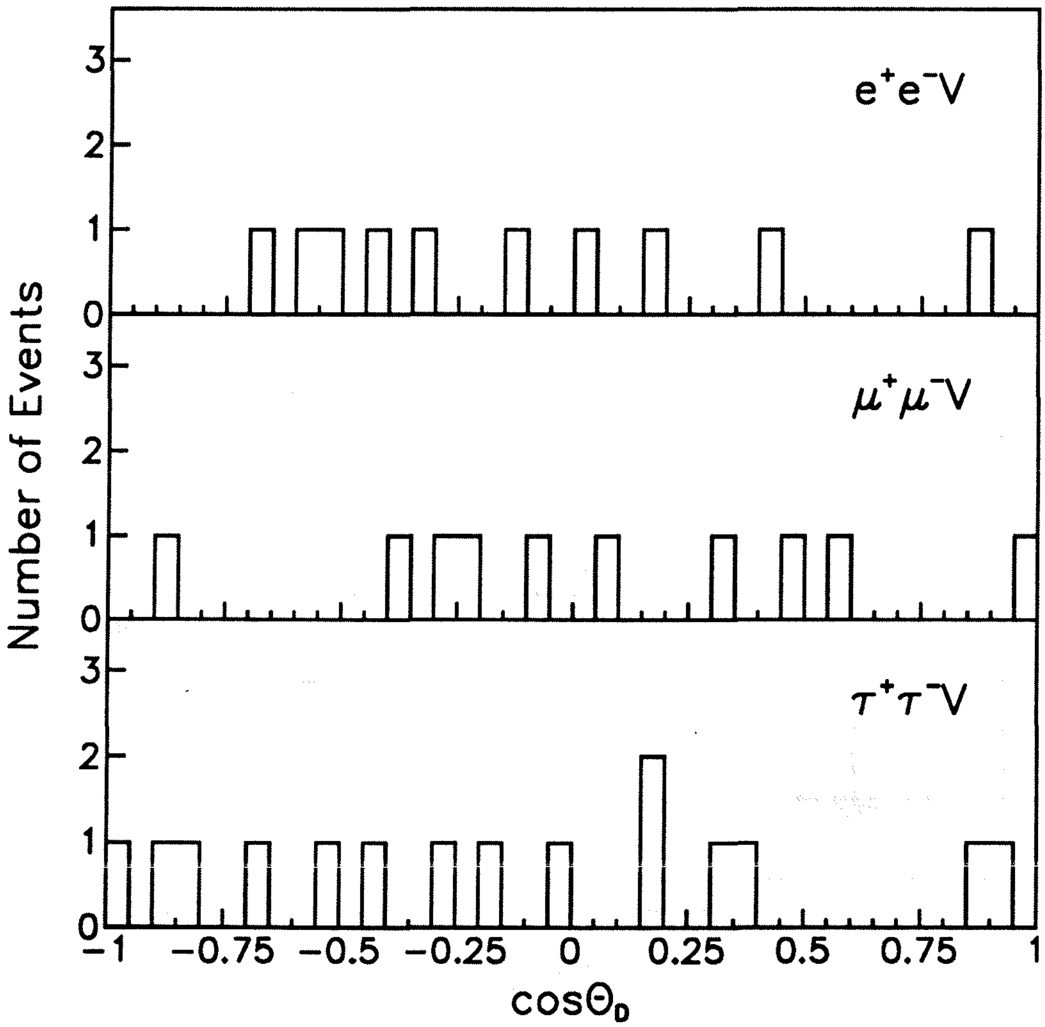

Figure 3.3: The V decay angle distribution for the selected $l^+l^- V$ events.

- And finally, E_{tot} is the total energy in GeV of the event.

3.1.1 Measured tau decay modes

Decay modes of all the taus in the $\tau^+\tau^-V$ events are identified. They are listed in table 3.3.

Run	Event	N_{trk}	Type	$\tau^+ \rightarrow$	$\tau^- \rightarrow$
5509	2667	6	$\tau\tau ee$	$3\pi\nu$	$\pi\pi^0\pi^0\nu$
7743	8370	6	$\tau\tau ee$	$3\pi\nu$	$\mu\nu$
7253	357	6	$\tau\tau ee$	$3\pi\nu$	$\mu\nu$
7958	3841	6	$\tau\tau ee$	$3\pi\nu$	$\rho\nu$
7681	2160	4	$\tau\tau ee$	$e\nu\nu$	$\pi\pi^0\pi^0\nu$
8335	1133	6	$\tau\tau ee$	$\rho\nu$	$e\nu\nu$
7858	8314	6	$\tau\tau\mu\mu$	$3\pi\nu$	$\rho\nu$
5166	981	4	$\tau\tau\mu\mu$	$\mu\nu\nu$	$\pi\nu$
8623	158	4	$\tau\tau\mu\mu$	$\pi\nu$	$\rho\nu$
8865	6111	4	$\tau\tau\mu\mu$	$\mu\nu\nu$	$e\nu\nu$
8537	4398	4	$\tau\tau\pi\pi$	$\pi\nu$	$\mu\nu\nu$
8833	4673	4	$\tau\tau\pi\pi$	$\rho\nu$	$\rho\nu$
6973	4547	4	$\tau\tau\pi\pi$	$\rho\nu$	$\pi\nu$
8126	771	4	$\tau\tau\pi\pi$	$e\nu\nu$	$\rho\nu$
8796	4675	4	$\tau\tau\pi\pi$	$\rho\nu$	$\mu\nu\nu$

Table 3.3: Identified tau decay modes for the taus in the $\tau^+\tau^-V$ events.

Decay mode	Calculated from $\tau^+\tau^-V$	Measured from $\tau^+\tau^-$
$\tau \rightarrow e\nu\nu$	$4/25 = 0.16 \pm 0.09$	$0.18/0.84 = 0.21$
$\tau \rightarrow \mu\nu\nu$	$6/25 = 0.24 \pm 0.11$	$0.18/0.84 = 0.21$
$\tau \rightarrow \pi\nu, \pi 2\pi^0\nu, \ldots$	$6/25 = 0.24 \pm 0.11$	$0.23/0.84 = 0.27$
$\tau \rightarrow \rho\nu$	$9/25 = 0.36 \pm 0.14$	$0.25/0.84 = 0.30$
$\tau \rightarrow 3 - prong$	$5/30 = 0.17 \pm 0.08$	0.14

Table 3.4: A comparison of the tau branching ratio calculated from the $\tau^+\tau^-V$ events with the measurement [11] from the $\tau^+\tau^-$ events. 1-prong tau decay modes are normalized by themselves. 0.84 is the sum of measured branching of the 1-prong decay modes listed.

A comparison with the predicted tau branching ratios is made in table 3.4. The agreement is reasonably good, given the small sample size.

3.2 Standard model contribution to the l^+l^-V signature

Many of the Standard Model processes produce events with four or six charged tracks. They are thus the potential sources of the l^+l^-V signature. These processes include:

1. Hadronic Z decays: $Z \longrightarrow q\bar{q}(g)$
2. Radiative di-lepton processes: $Z \longrightarrow l^+l^-\ (\gamma)$
3. Two photon processes with hadronic final states:

   $e^+e^- \longrightarrow e^+e^-\ hadrons$
4. Electroweak processes with the final states of four leptons or two leptons and two pions: $e^+e^- \longrightarrow e^+e^-e^+e^-$, $e^+e^-\mu^+\mu^-$, $e^+e^-\tau^+\tau^-$, $\mu^+\mu^-\mu^+\mu^-$, $\mu^+\mu^-\tau^+\tau^-$, $\tau^+\tau^-\tau^+\tau^-$, $e^+e^-\pi^+\pi^-$, $\mu^+\mu^-\pi^+\pi^-$, $\tau^+\tau^-\pi^+\pi^-$.

The first three types of processes are found to be unlikely to have any significant contribution to the l^+l^-V signal. They are hence called the background processes. The last category bears the exact l^+l^-V signature. Their actual contribution to the l^+l^-V signal has to be studied.

3.2.1 Background processes

(a) Hadronic Z decays

Hadronic events from the Z decays generally have much higher multiplicity than that of the $l^+l^- V$ events. Nevertheless, since its cross section is large, the low multiplicity tail can not be simply neglected without careful studies.

A Monte Carlo sample corresponding to 7.4×10^5 hadronic Z decays, four times of the data sample, is used to estimate this source of background. To save computer time, a portion (60%) of these events were selected to have low multiplicity before passing through the detector simulation. A total of three events from this sample pass the selection criteria. They all have six tracks and contain no leptons. Limited by the size of the Monte Carlo sample and the fact that low multiplicity hadronic Z decays might not be well modeled, the possible contamination from this source in future data can not be completely ruled out. However, it has been noticed that all the five six-track $l^+l^- V$ events selected contain at least two leptons and there are only two out of the ten four-track $\tau^+\tau^- V$ events containing no lepton in their final states. The tau decay modes of these two events are well understood. This fact makes it very unlikely for the selected $\tau^+\tau^- V$ events to be hadronic in origin. The other fact supporting this is that along the selection chain, the total energy requirement in section 2.2.8 rejects 29 events out of this 740000 event sample, to be compared with 8 out of 189000 hadronic events rejected this way in the data sample. This shows that the Monte Carlo and the data are in good agreement as far as the cuts in this analysis are concerned.

The e^+e^-V and $\mu^+\mu^-V$ events are generally immune from this source of background.

(b) Radiative di-lepton processes. Events from this type of processes that may contaminate the signal are those with the radiated photon converted in the material of the detector. This occurs only in the low mass V=e^+e^- cases. In the l^+l^-V sample, there are three events, one in each lepton channel, with V=e^+e^- and $M_V < 400$ MeV. However their locations on the $M_{pair} - \delta_{xy}$ plot are too far away from the area populated by Monte Carlo simulated conversions. Also, in 20 pb^{-1} of these di-lepton Monte Carlo events fed through the selection chain, no event is found to pass.

(c) Two photon processes $e^+e^- \longrightarrow e^+e^-$ hadrons. Study has been made on 50 pb^{-1}, about eight times the data luminosity, of simulated events of these processes and no event has been found passing the selection cuts. If the Monte Carlo simulation of this type of events is reasonably correct, it is believed that the chance of the selected l^+l^-V events coming from this source of process is very small. This claim is also supported by the fact that both of the only two $\tau^+\tau^-V$ events that contain no leptons have a much higher transverse momentum than expected from the two photon events. Figure 3.4 demonstrates this.

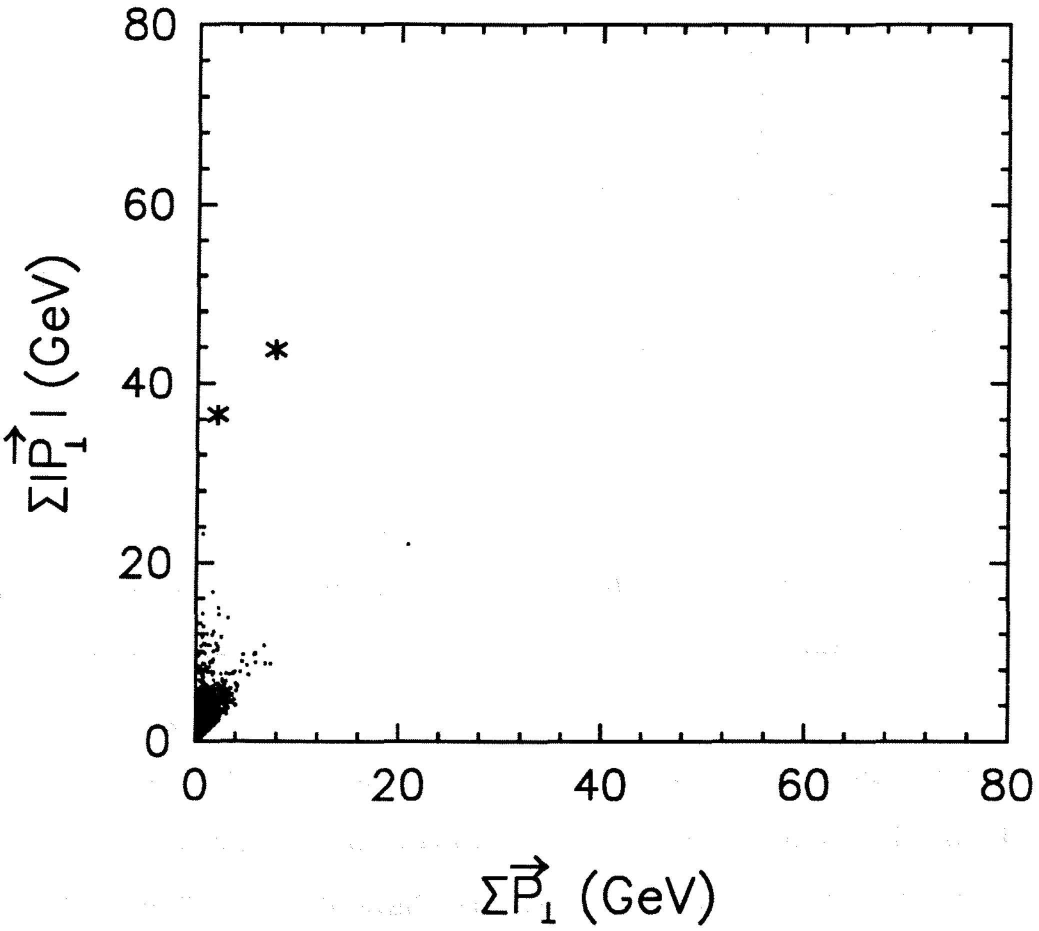

Figure 3.4: Transverse Momentum distribution for the $e^+e^- \longrightarrow e^+e^-$ *hadrons* events (dots). The vertical and the horizontal axes are respectively the scalar and vector sum of the transverse momentum of the tracks in the event. Asterisks are the two $\tau^+\tau^-V$ events with no lepton in the final state.

final state	A(%)	C(%)	B(%)	M(%)
$eeee$	60	5	34	1
$ee\mu\mu$	79	6	13	1
$\mu\mu\mu\mu$	94	6	0	0
$\tau\tau ee$	86	8	3	3

Table 3.5: Relative contributions of the four diagram to the four-lepton cross sections. A=annihilation, C=conversion, B=bremsstrahlung, and M=multiperipheral. The cross sections are calculated requiring all final state leptons to have an angle of at least 15° with the beam axis. Each row may not add up to 100% due to the roundoff.

3.2.2 Signal processes

As mentioned before, production of $l^+l^- V$ events is expected from electroweak processes with 4-lepton or 2-lepton + 2-pion final states. Many diagrams contribute to these processes, and they belong to one of the four classes: annihilation, conversion, bremsstrahlung, and multiperipheral. The graphs of these classes are shown in figure 3.5. Not all the processes contribute equally to the $l^+l^- V$ signal. The processes with annihilation through the Z contribute by far the most, while the multiperipheral processes have little contribution since the going out electrons and positrons tend to escape through beam pipe. In all these cases, the radiative Z^* contribution is very small and can be neglected [12].

The estimated relative contributions of the four classes of processes to various final states at the Z peak are tabled in table 3.5.

These processes have been calculated by Berends, Daverveld and Kleiss[13]. They have also produced an event generator for the pure QED part of the diagrams. A modification of this generator has been made by Daverveld to

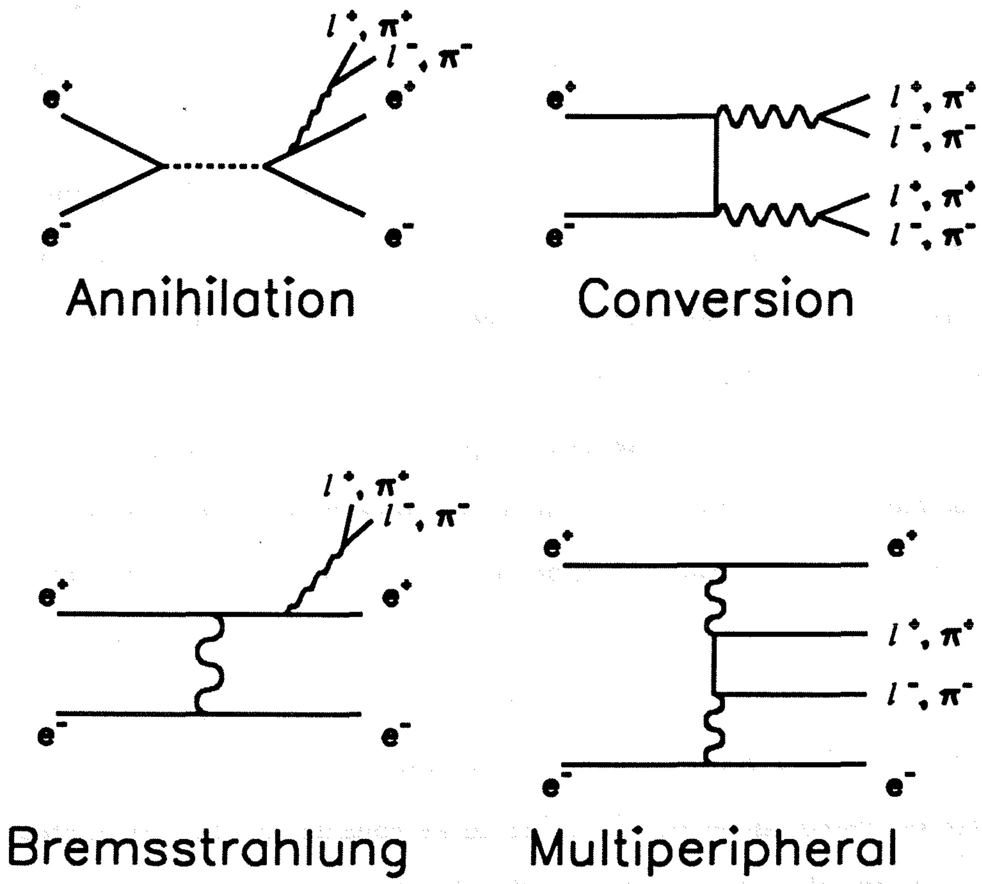

Figure 3.5: The Standard Model processes contributing to the l^+l^-V signal.

incorporate the Z diagrams[14]. This modified generator is used here to generate four lepton events and to calculate the cross sections of the processes.

One problem related to this generator is that it does not include initial or final state radiation, and it uses a constant value of 1/137 as the electromagnetic coupling constant at all vertices. These simplifications affect the analysis in both cross section calculation and the efficiency determination. The cross section can be corrected by a multiplication of an overall factor of $0.8 = (137/128)^2 \times 0.7$ to the values calculated by the generator. The $(137/128)^2$ factor takes into account the proper value of electromagnetic coupling constant at the Z for two of the vertices, and 0.7 is an approximation for the correction to the peak cross section due to initial state radiation. In principle, these corrections are good only for the annihilation processes. But since the annihilation processes are the dominating processes among the others, this method makes a good approximation to the cross sections with errors at about a few percent level. However, this introduces a source of systematic error which has to be considered. The calculated cross sections for the these final states are listed in table 3.6.

The effect on the efficiencies due to the lack of initial and final state radiations can be estimated using a low-mass Higgs generator with and without these radiations. It is found that for e^+e^-V and $\mu^+\mu^-V$ events, the including of ISR and FSR brings in about 10% reduction on the efficiency, and for $\tau^+\tau^-V$ the reduction is much smaller at about 3%.

In order to study the contribution of these electroweak processes, events with each of the final states $e^+e^-e^+e^-$, $e^+e^-\mu^+\mu^-$, $e^+e^-\tau^+\tau^-$, $\mu^+\mu^-\mu^+\mu^-$, $\mu^+\mu^-\tau^+\tau^-$and $\tau^+\tau^-\tau^+\tau^-$are generated using the above mentioned generator. To

state	$m > 50$ MeV	$m > 300$ MeV
$ee\ ee$	1.30	0.57
$ee\ \mu\mu$	0.65	0.55
$\mu\mu\ ee$	0.83	0.36
$\mu\mu\ \mu\mu$	0.45	0.39
$\tau\tau\ ee$	0.65	0.33
$\tau\tau\ \mu\mu$	0.38	0.34

Table 3.6: Calculated four-lepton cross sections (picobarns). The second pair of particles in each state listed is the least massive oppositely charged pair of particles of the same type. m is the mass of lowest mass oppositely charged pair of particles of the same type. The cross sections are calculated requiring all final state leptons to have an angle of at least 15° with the beam axis.

save computer time, events are generated only at E_{cm} of 91.2 GeV. In addition, to avoid the divergence at the low angle, it has been required that all tracks in the events are at least 15° away from beam.

All the generated events are passed through the full detector simulation. The simulated events are then fed into the selection procedure where the selection efficiencies for all the channels are calculated.

Although the above generator used does not generate $l^+l^-\pi^+\pi^-$ events, it can still be used to evaluate the $l^+l^-\pi^+\pi^-$ contribution. The cross section is estimated by weighting each $l^+l^-\mu^+\mu^-$ event by the $\pi^+\pi^-$ to $\mu^+\mu^-$ ratio R as measured in the low energy e^+e^- annihilation and some fixed target experiments[15]. This ratio R is determined by the time like pion form factor F_{π^2} as $R = F_{\pi^2}/4$. To have an idea how well this method works, the results of this calculation are compared with those calculated by Abraham and van der Bij[16] and by Bergsrom and Robinett[17]. It turns out the results are 30-50% higher. This information is used in the estimation of the systematic errors.

To determine the efficiency of the $l^+l^-\pi^+\pi^-$ processes, it is assumed that replacing $\mu^+\mu^-$ by $\pi^+\pi^-$ does not change much the kinematics and hence the efficiencies of the corresponding $l^+l^-\mu^+\mu^-$ processes are used for the $l^+l^-\pi^+\pi^-$ processes. With these treatments, it is estimated that the pion-pair contribution can be understood within 30%-50%.

After the cross sections and the efficiencies are determined with various corrections applied, the expected number of events in each channel is calculated with proper normalization. Since the data events are collected at different LEP scan energy points while the Monte Carlo events are all generated at the Z peak, an effective integrated luminosity of N_z/σ_z is used. (N_z is the number of Z and σ_Z is the Z peak cross section. The t-channel contribution is underestimated this way, but the effect is expected to be small at no more than a few percent.

3.3 Comparison between the observed data and the Monte Carlo prediction

The Monte Carlo predicted number of $l^+l^- V$ events and the number of observed $l^+l^- V$ events in the data are compared in table 3.7. The numbers are divided into three lepton channels, each with three V composing variations of e^+e^- , $\mu^+\mu^-$, and $\pi^+\pi^-$. The comparison shows that the number of observed events in the $\tau^+\tau^-V$ channel is considerably larger than the Monte Carlo prediction and in the e^+e^-V and $\mu^+\mu^-V$ channel such prediction is reasonably well reproduced, though the numbers observed in the data is also somewhat higher. For example, 15 $\tau^+\tau^-V$ events are observed compared to 3.2 expected, while a comparison of 10 observed to about 7 expected as in e^+e^-V or $\mu^+\mu^-V$ channel is more

	all θ_V		$\theta_V > 11.5^\circ$	
	all M_V	$M_V > 2$ GeV	all M_V	$M_V > 2$ GeV
Final State	N_{exp} N_{obs}	N_{exp} N_{obs}	N_{exp} N_{obs}	N_{exp} N_{obs}
ee ee	2.2 3	0.4 1	1.8 2	0.4 0
ee $\mu\mu$	2.0 2	0.4 2	1.7 1	0.3 1
ee $\pi\pi$	3.0 5	0.0 0	2.4 3	0.0 0
ee total	7.2 10	0.8 3	5.8 6	0.8 1
$\mu\mu$ ee	2.0 4	0.3 0	1.6 3	0.3 0
$\mu\mu$ $\mu\mu$	1.8 5	0.4 3	1.5 4	0.4 2
$\mu\mu$ $\pi\pi$	2.8 1	0.0 0	2.2 1	0.0 0
$\mu\mu$ total	6.6 10	0.7 3	5.3 8	0.7 2
$\tau\tau$ ee	1.1 6	0.2 0	1.0 6	0.2 0
$\tau\tau$ $\mu\mu$	0.9 4	0.2 0	0.8 4	0.2 0
$\tau\tau$ $\pi\pi$	1.2 5	0.0 0	1.1 4	0.0 0
$\tau\tau$ total	3.2 15	0.5 0	2.9 14	0.4 0
grand total	17.0 35	2.0 6	14.0 28	1.8 3

Table 3.7: Comparison of selected events with Monte Carlo predictions. N_{exp} is the expected number of events from electroweak processes, N_{obs} is the observed number of events.

comfortable. In terms of the fraction of $\tau^+\tau^-V$ events in the whole sample, 18.8% is predicted, but 42.9% is observed. Such an excess in $\tau^+\tau^-V$ channel does not populate any of the three V types preferentially, that is, the relative rates for V=e^+e^- , $\mu^+\mu^-$, and $\pi^+\pi^-$ are consistent with the expectation.

Other features of the events are also compared and no obvious inconsistency is observed. Comparisons between the data and the Monte Carlo for several interesting kinematic variables are shown in figure 3.6, to figure 3.10. In all the cases, the shape of the data distribution bears no distinction as compared with the expectation; the observed V energy distribution shows the expected enhancement at low energies. The distribution of angle θ_V between the V and the lepton shows a peak at small angles as expected for a dominantly radiative process. We note, however, as the observed number of events is rather small such comparisons are subject to large statistical uncertainty, especially for those variables not quite sensible under a variety of physics situations.

3.4 Systematic errors on the expected rates

Systematic errors exist in many aspects of this analysis. We discuss here the most important ones, namely the errors in the expectation of the rates of the $l^+l^- V$ events. These errors come in two fashions; one affects the absolute, i.e. channel independent, normalization of the $l^+l^- V$ processes, and the other affects the relative rates among the three channels.

The largest systematic error comes from the selection procedure. As the number of selected data events is small, it is forseeable that a different selection may select the same data but have different efficiency. Indeed, it is found that such variances on the efficiency can be as large as 20% [18]. Some other mechanisms also contribute. For example, nuclear interactions will change the track momenta and produce extra tracks; the 15° requirement we imposed when generating the four lepton events maybe too close to the 18.2° cut we used in section 2.2.1. Taking into account all these factors, we conservatively estimate that the systematic error on the absolute normalization contributed by the selection procedure to be 30% and the channel to channel error from the same source to be 15%.

Another factor that affects the absolute normalization is the $l^+l^-\pi^+\pi^-$ cross section calculation. As mentioned before, the $l^+l^-\pi^+\pi^-$ cross sections calculated using the method in this analysis are about 30%-50% higher than those

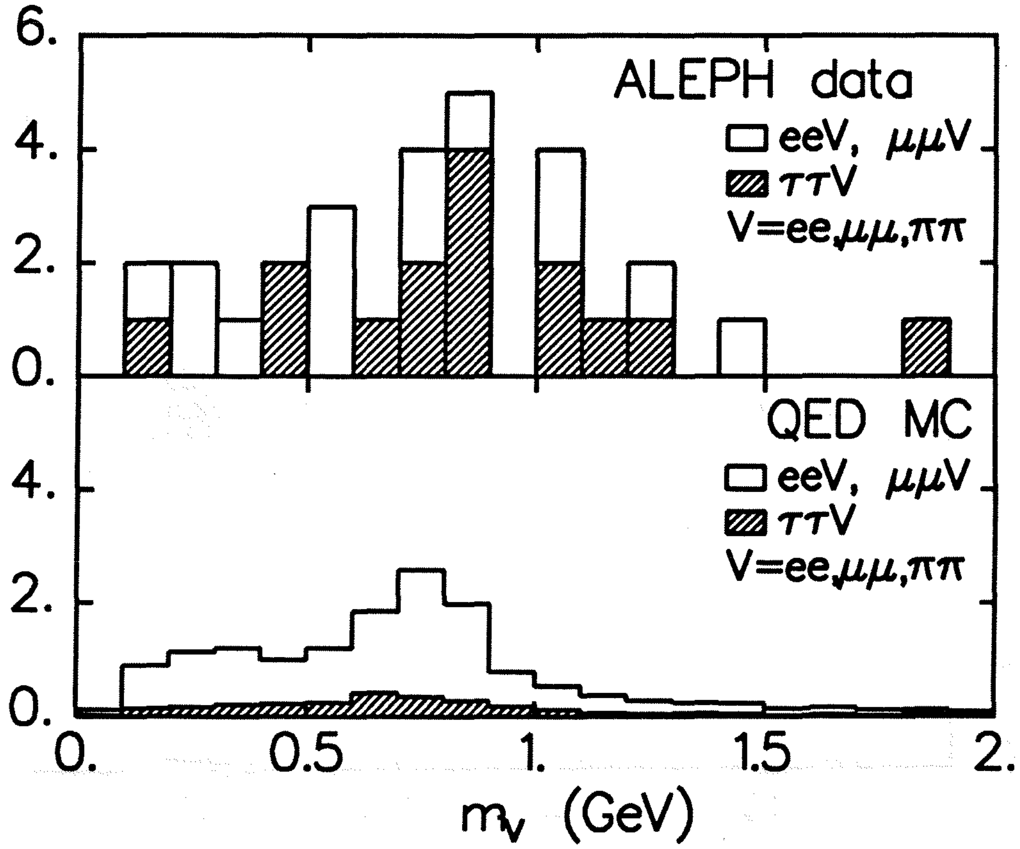

Figure 3.6: Comparison of the M_V of the observed l^+l^-V events with the Monte Carlo prediction.

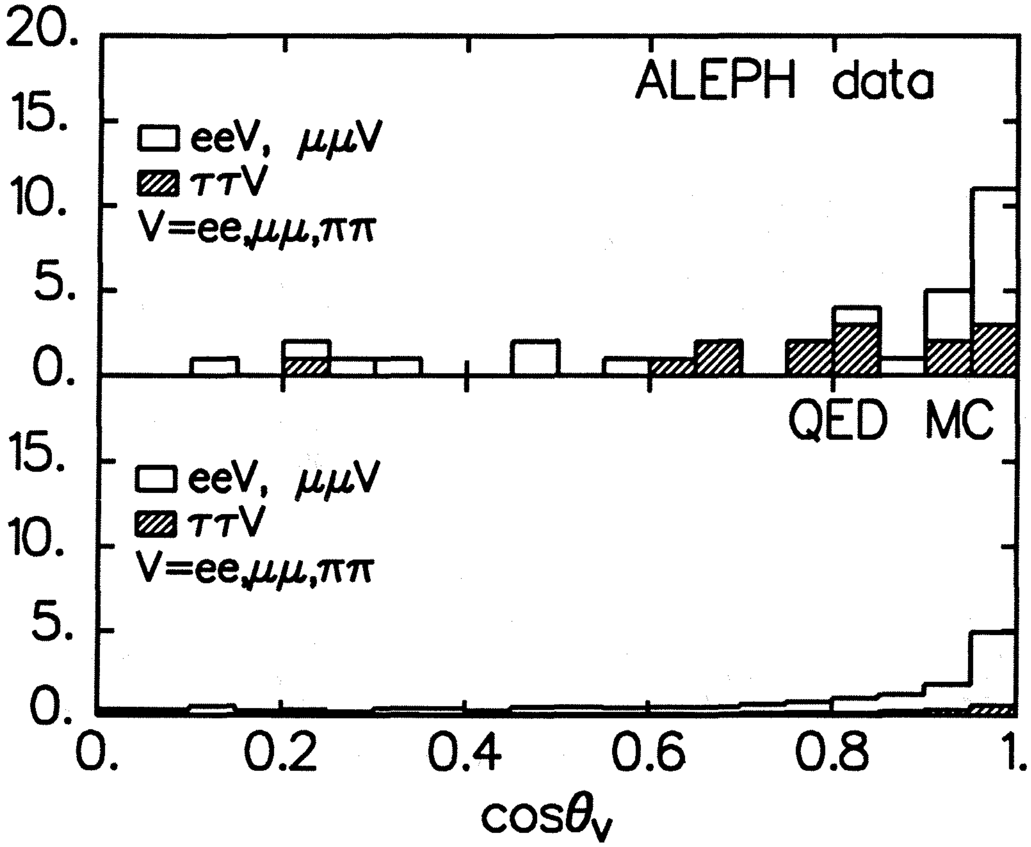

Figure 3.7: Comparison of the θ_V of the observed $l^+l^-\ V$ events with the Monte Carlo prediction.

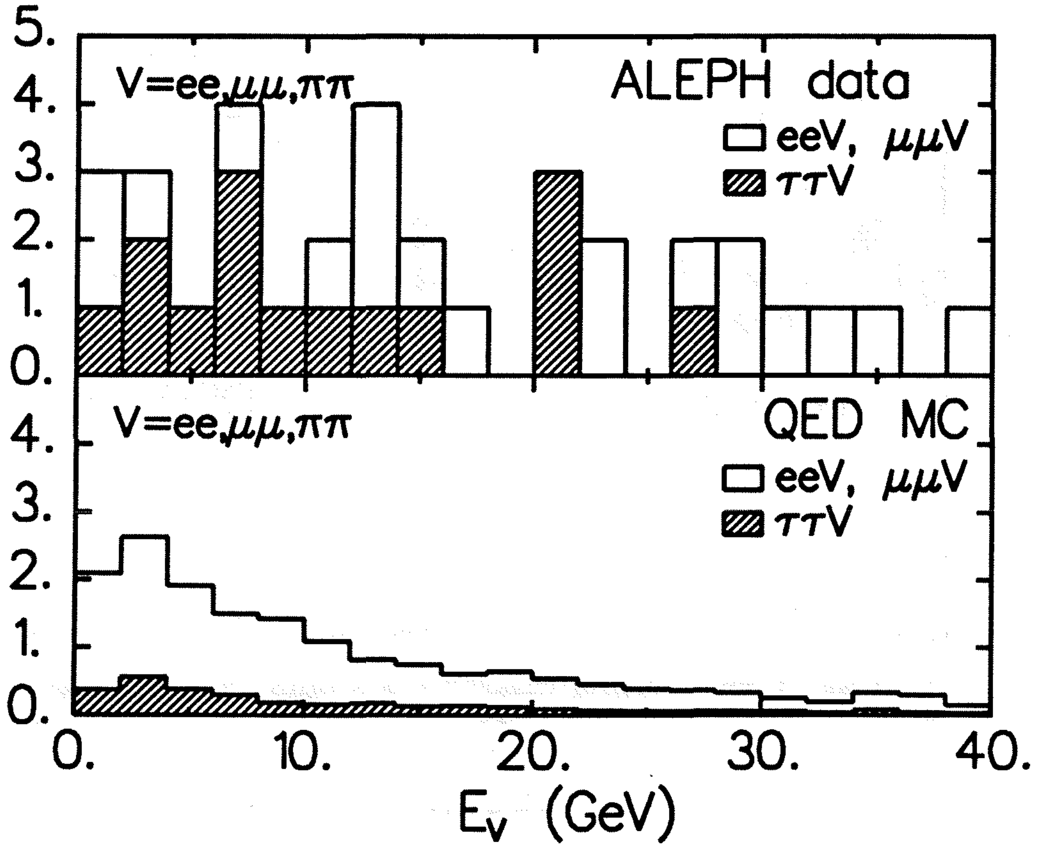

Figure 3.8: Comparison of the E_V of the observed $l^+l^- V$ events with the Monte Carlo prediction.

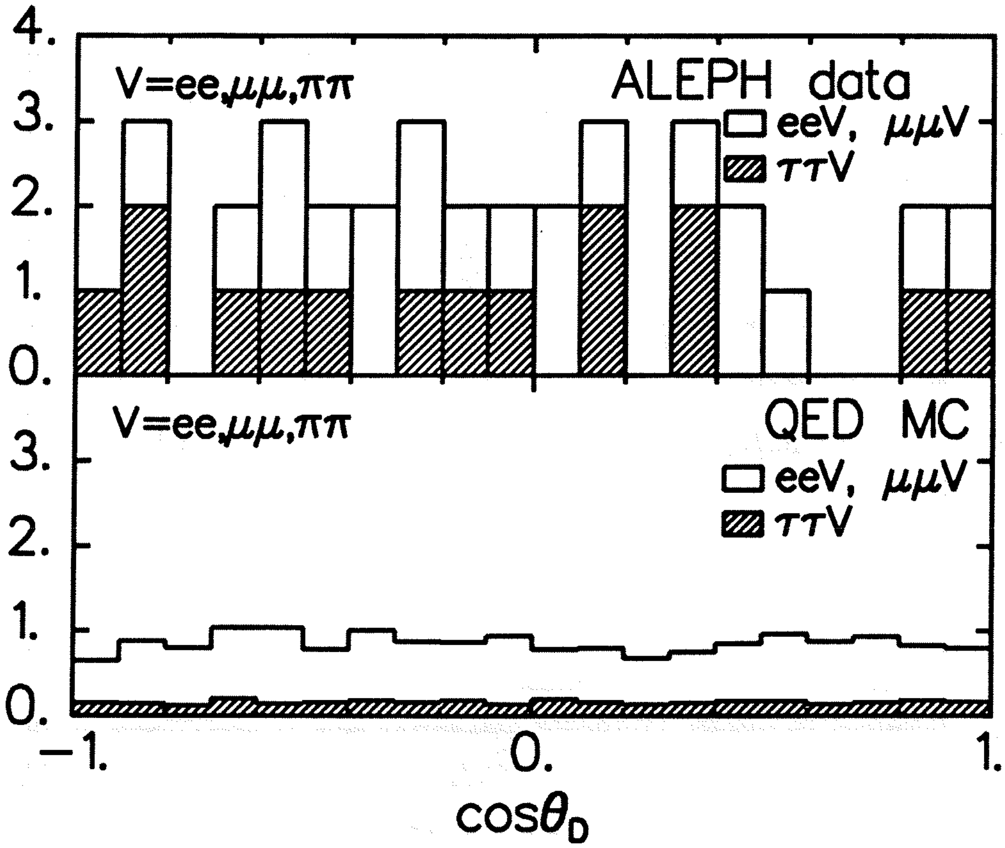

Figure 3.9: Comparison of the θ_d of the observed l^+l^-V events with the Monte Carlo prediction.

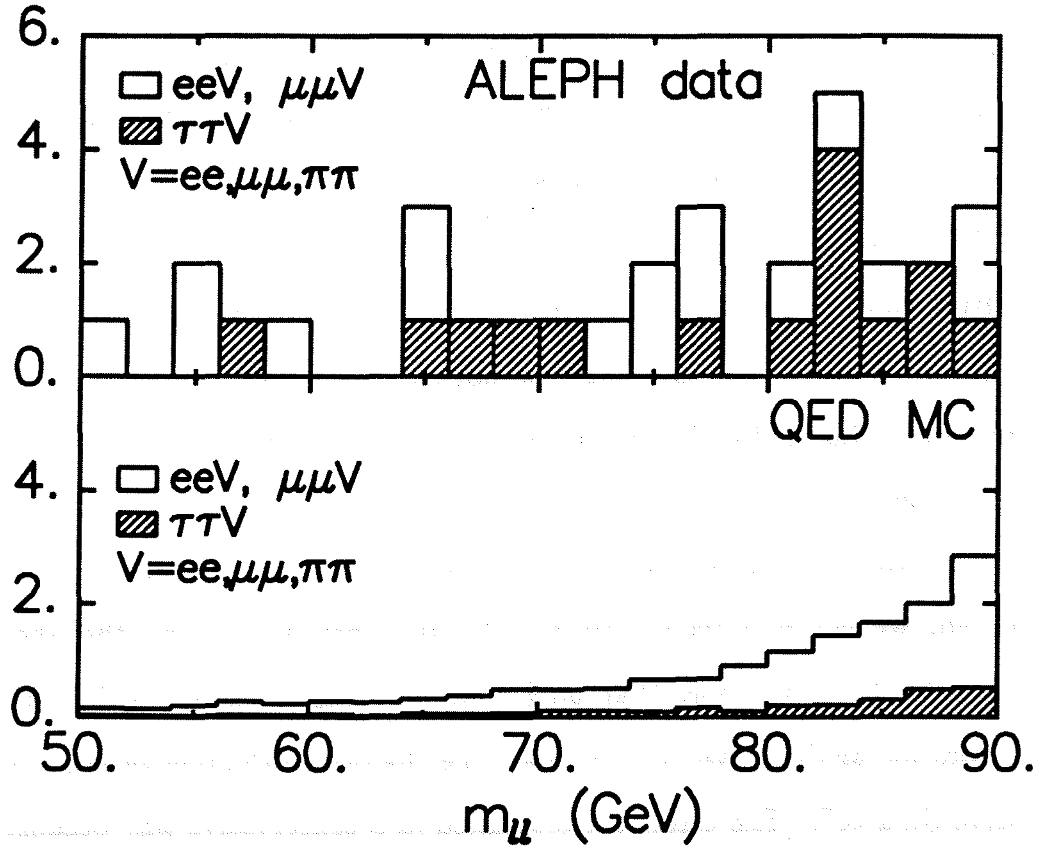

Figure 3.10: Comparison of the M_{ll} of the observed l^+l^-V events with the Monte Carlo prediction.

calculated elsewhere. Since about 40% of the $l^+l^- V$ events are $l^+l^-\pi^+\pi^-$, this source of systematic error can be as large as 20%.

The four-lepton generator used, as mentioned before, incorporates a simplified treatment of the electroweak coupling constant and does not include the initial and final state radiation. Although a correction is made for that, it works only for the annihilation processes. The other processes, though small, are non negligible. The effects of this are channel dependent, they are estimated to be from 3% to 10%.

Although the error in the ALEPH luminosity measurement is only about 1% [19], the method used to calculate the normalization (see section 3.2.2) introduces more. This is also channel dependent and a typical 5% error is expected.

Other sources like the detector simulation, the internal statistical limits of the Monte Carlo generators, are expected to have smaller effects.

In all, we conservatively estimate the systematics error on the absolute $l^+l^- V$ rates to be no more than 30% from the cross section calculations and 30% from the analysis. We also estimate the channel to channel variation to be no more than 20%. The errors are estimated in a conservative way because the Monte Carlo sample involved is small and the corrections made are only to the first order.

3.5 Probability of statistic fluctuation

Failing to show a better agreement between the data and the Monte Carlo prediction in the $\tau^+\tau^- V$ channel, one would like to investigate whether the excess is simply a result of statistical fluctuation. The probability of such a fluctuation can be estimated in various ways, and different answers are obtained. With this principle in mind, we first add all the possible systematic errors to the $\tau^+\tau^-V$ expected number of events, which is less than observed, before calculating any statistical probability. Since the gap between the two numbers is narrower in this way, we will always get a higher value of the probability of the fluctuation and hence are in the conservative direction.

To begin with, we note that even in the e^+e^-V and $\mu^+\mu^-V$ channel, the numbers of events expected are smaller than the observed. This suggests a possible overall cross section underestimation due to the inaccuracy of the Monte Carlo calculation. The bias of the selection criteria may also contribute to the overall normalization. As discussed in section 3.4, the absolute cross section uncertainty is expected to be as large as 30% and the overall selection uncertainty can be up to an another 30%. Adding this two in quadrature yields a possible 45% correction to all channels. Scaling up the prediction by this amount gives a much better agreement in the e^+e^-V and $\mu^+\mu^-V$ channels. This fact somewhat justifies the above estimations. Furthermore, taking into the consideration of the 20% channel to channel variation also described in section 3.4 , a total of 65% is then added to the $\tau^+\tau^-V$ expectation. In calculating the probability, a number of $5.3 = 3.2 \times 1.65$, instead of 3.2, is used as the Monte Carlo predicted Standard Model contribution to $\tau^+\tau^-V$ events. Now the Possion probability of observing 15 or more events when 5.3 are expected can be calculated: the result is 4×10^{-4}.

The excess is also indicated by the fact that while only a fraction of 18.8% of all the selected l^+l^-V events is expected to be $\tau^+\tau^-V$, fifteen out of a total of thirty five are observed (more than 40%). Based on this observation, an alternative way is to estimate the probability of observing 15 or more $\tau^+\tau^-V$ events out of a 35 fixed total when the expected $\tau^+\tau^-V$ fraction is 22.6%. Here the 22.6% is the result of adding the possible channel to channel error of 20% to the expected 18.8% . It is found that the probability is 4×10^{-3}. This second method avoids the sensitivity to the absolute normalization by allowing it to float. However, it is a more conservative method since it neglects the fact that the e^+e^-V to $\mu^+\mu^-V$ ratio is much better reproduced in the data. For example, the probability includes such extreme cases as, say, 20 e^+e^-V , 0 $\mu^+\mu^-V$, and 15 $\tau^+\tau^-V$ observed.

In general, we conclude that the probability of a statistical fluctuation as the source of the excess in $\tau^+\tau^-V$ channel is on the order of 10^{-4} to 10^{-3}. We note however, if one asks what the probability is for a fluctuation to have occurred in any of the three channels, all the above probabilities should be multiplied by a factor of three; then the highest would become about 1%.

3.6 V Mass Distribution

Examining the V mass distribution plot showed in figure 3.2, one may ask whether there exists any narrow resonance or other mass structure, especially in the $\tau^+\tau^-V$ events. To study this, the detector simulated four lepton Monte Carlo events are used to estimate the V mass resolution. It is found that the mass resolution is 50 MeV for V=e^+e^- and 12 MeV for V=$\mu^+\mu^-$ and V=$\pi^+\pi^-$ cases. Assuming this resolution, no evidence for a narrow resonance is found as the source of the excess. An alternative method which estimates the error on the V mass by the propagation of the tracking errors on the event by event basis gives even smaller resolutions and hence supports the same conclusion. However we note that although both methods take into account multiple scattering of the particles in the detector material, neither consider the effect of final state radiation which will enlarge the mass resolution particularly in the case of v=e^+e^- .

On the other hand, the V's in the $\tau^+\tau^-V$ events do seem to have a narrower mass spread than those in the other two channels. This can be seen by the fact that there are twelve $\tau^+\tau^-V$ events with V mass between 400 MeV and 1.2 GeV while only five e^+e^-V events and three $\mu^+\mu^-V$ events in the same mass range. However, without the guidance of theory, it is not allowed to claim an even larger excess in such a freely chosen mass range. This kind of mass clustering could certainly give hints of the possible sources of the excess if the possibility of a fluctuation is ruled out by the future data.

3.7 Conclusion

With the data sample of about 200,000 Z decays collected by the ALEPH detector in the years of 1989 and 1990, the l^+l^-V selection results in 10 e^+e^-V events, 10 $\mu^+\mu^-V$ events and 15 $\tau^+\tau^-V$ events. The kinematic aspect of these events shows no obvious contradiction to the expectation of the electroweak radiation and internal conversion processes. However, an excess of events in the $\tau^+\tau^-V$ channel is observed. The probability of a statistical fluctuation having produced the excess depends on the reliability of the model and the detector simulation, but can be as large as 10^{-2}. The excess does not appear to populate V=e^+e^- , $\mu^+\mu^-$, or $\tau^+\tau^-$ preferentially.

If future measurements on more data eliminate the possibility of the statistical fluctuation as the source of the excess, this result will be of great interest and may point toward new physics.

Appendix A

Event displays of the 35 l^+l^-V events

This appendix collectes the event display pictures of all the 35 $l^+l^- V$ events. The pictures are compiled in the same order as in table 3.1. In each picture, an event is showed in both $r - \phi$ (in the larger square box) and $r - z$ view . The tracks with their momentum are also listed. Figure A explains the layout of the picture.

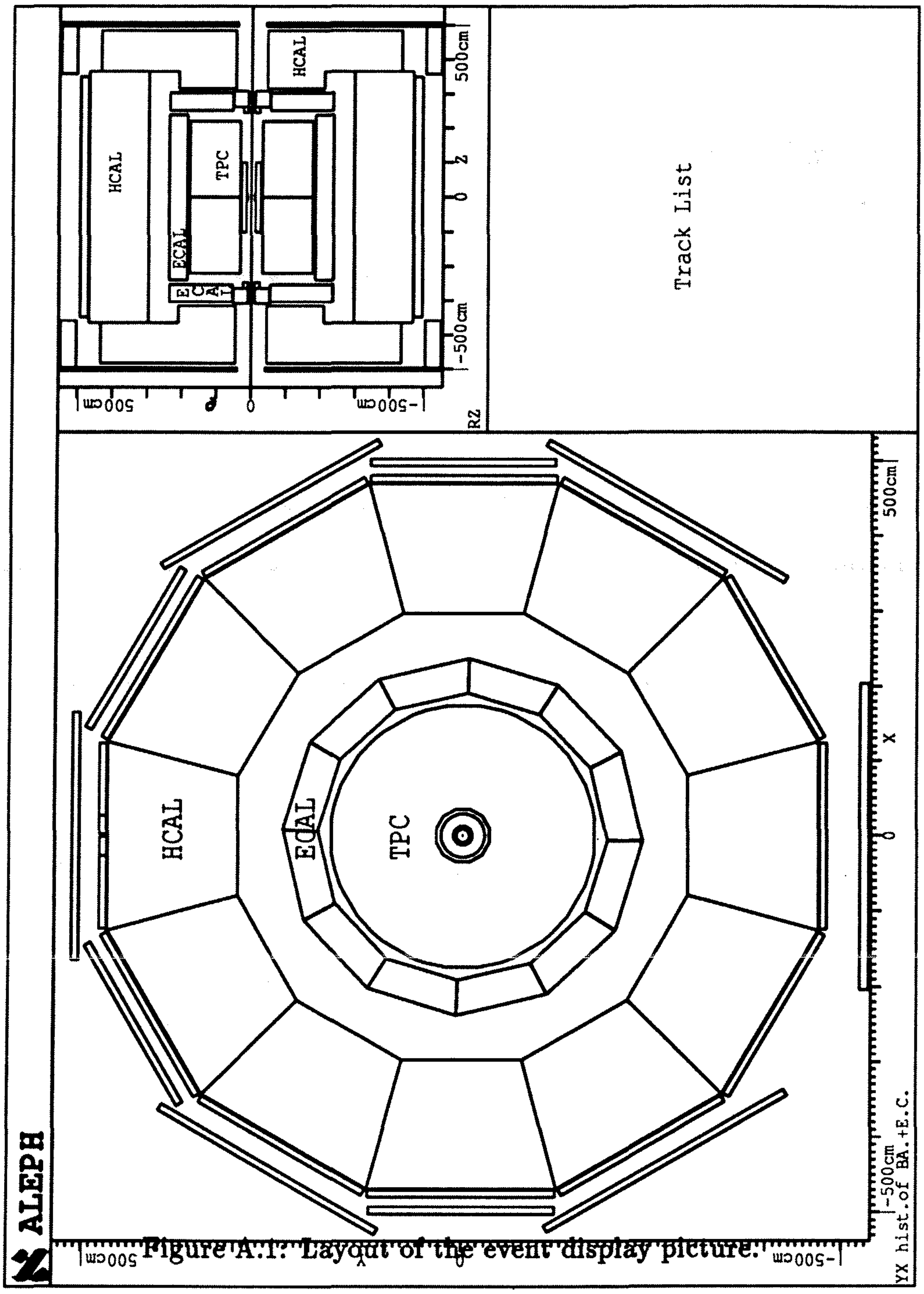

Figure A.1: Layout of the event display picture.

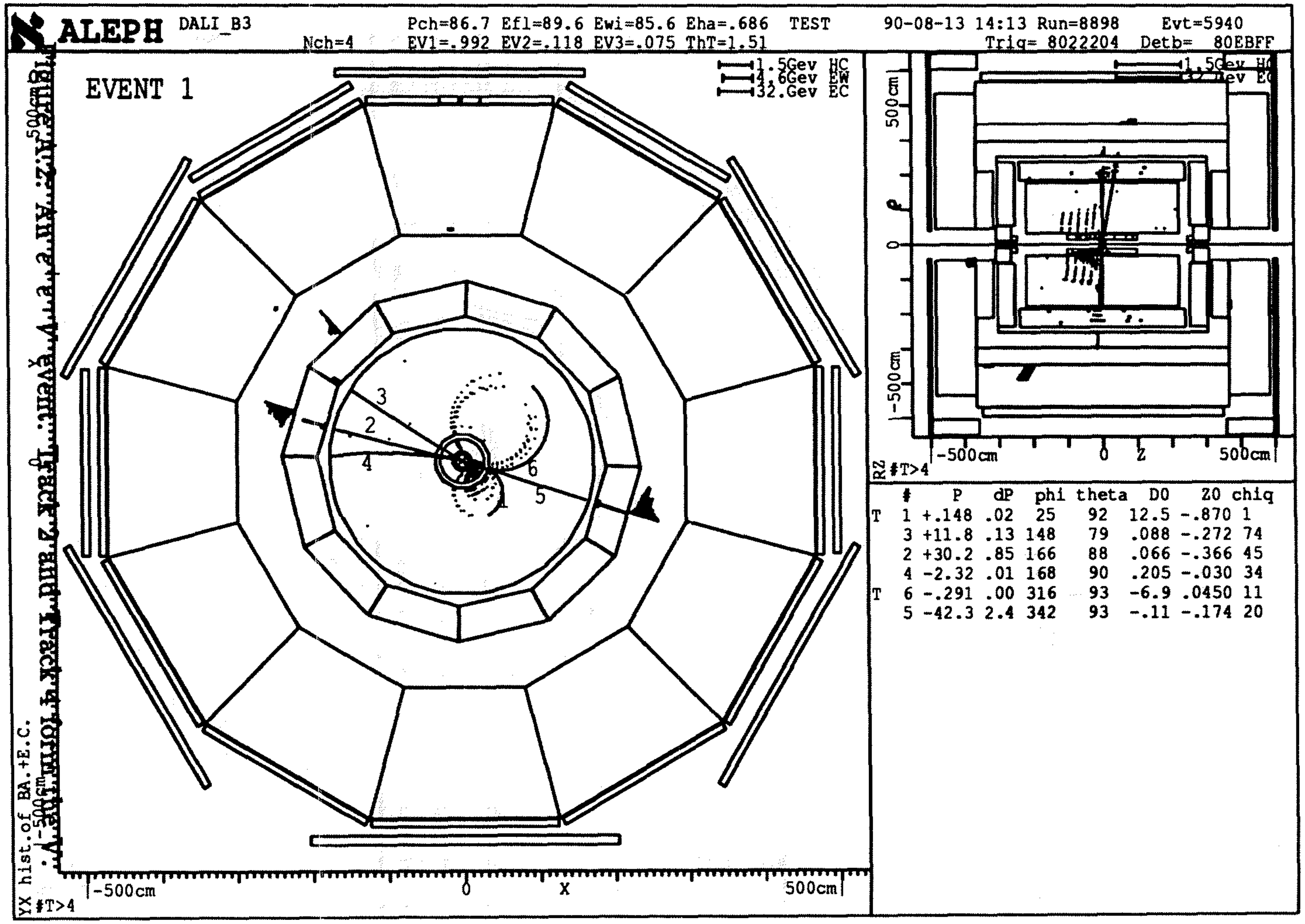

Figure A.2: An $e^+e^- \rightarrow e^+e^-$ V event. Track 2 and track 4 form the V.

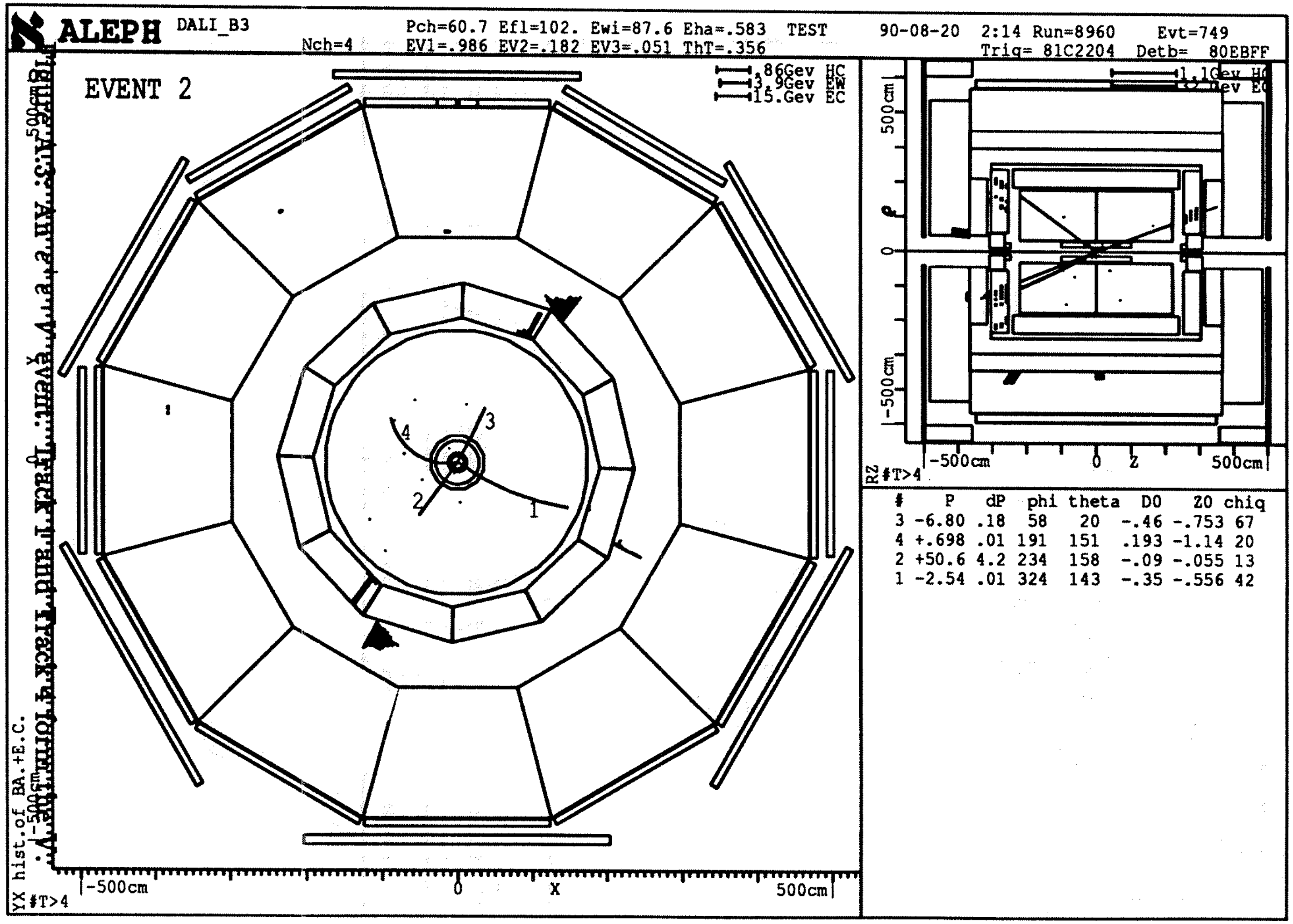

#	P	dP	phi	theta	D0	Z0	chiq
3	-6.80	.18	58	20	-.46	-.753	67
4	+.698	.01	191	151	.193	-1.14	20
2	+50.6	4.2	234	158	-.09	-.055	13
1	-2.54	.01	324	143	-.35	-.556	42

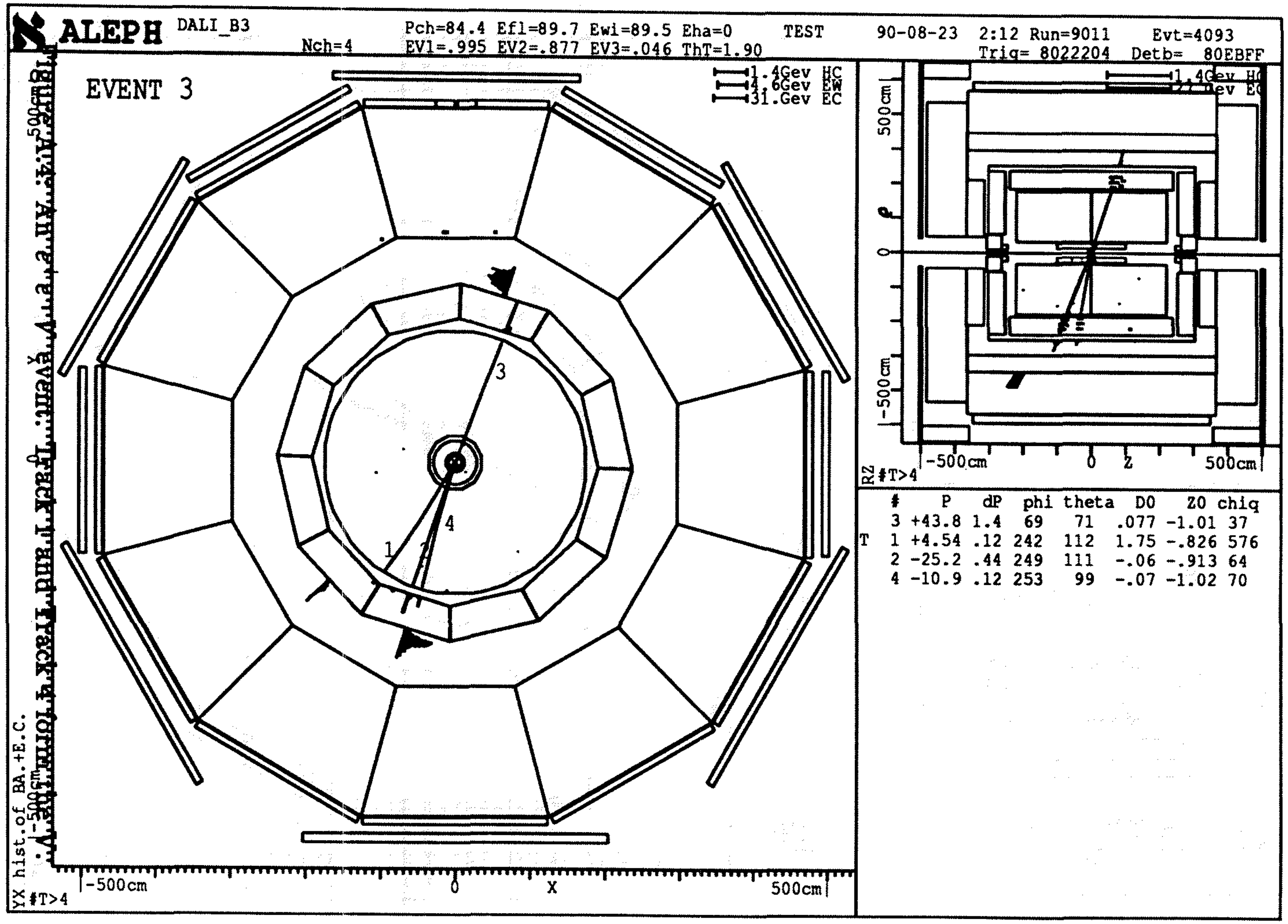

#	P	dP	phi	theta	D0	Z0	chiq
3	+43.8	1.4	69	71	.077	-1.01	37
T 1	+4.54	.12	242	112	1.75	-.826	576
2	-25.2	.44	249	111	-.06	-.913	64
4	-10.9	.12	253	99	-.07	-1.02	70

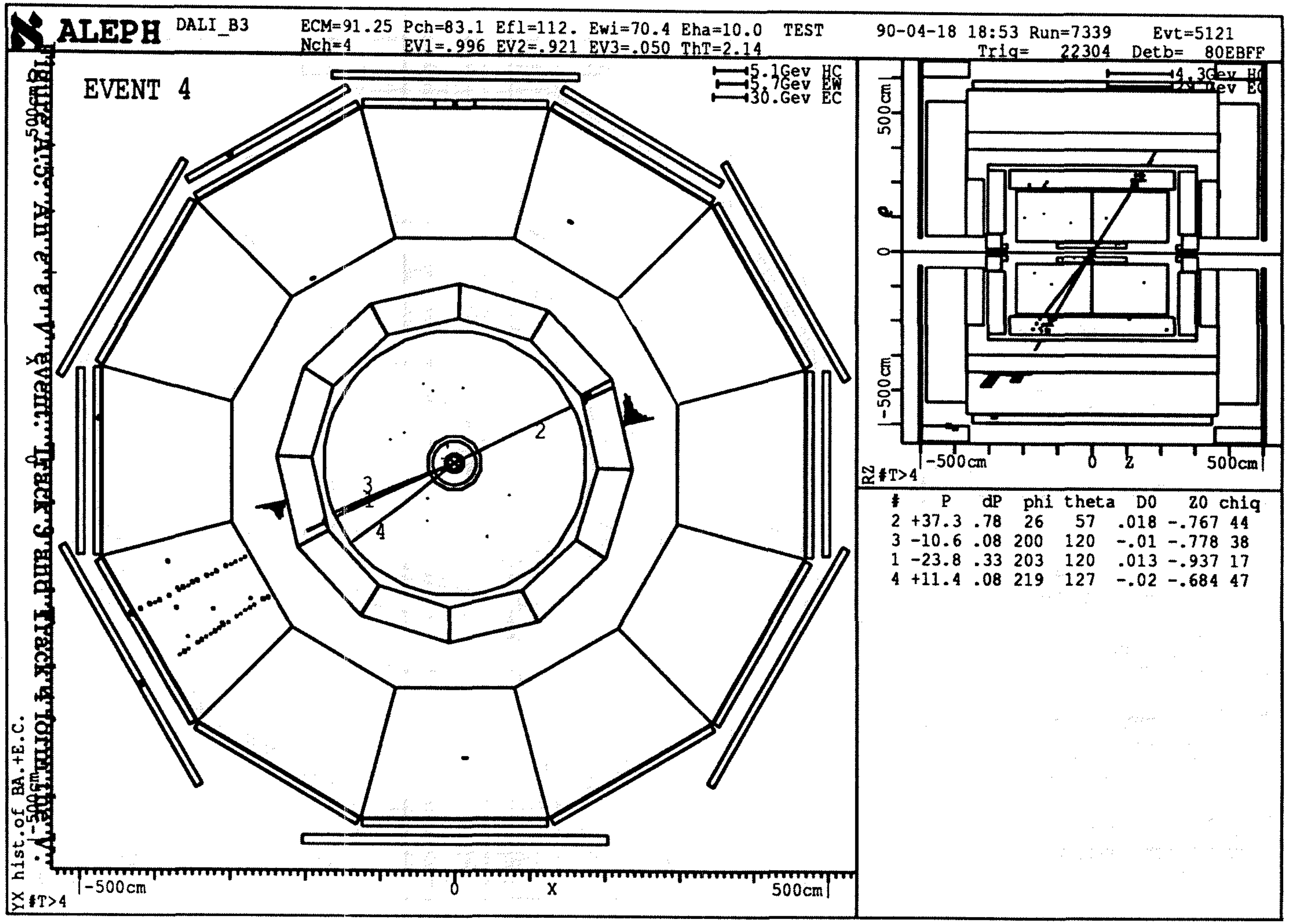
ALEPH
DALI_B3
ECM=91.25 Pch=83.1 Efl=112. Ewi=70.4 Eha=10.0 TEST
Nch=4 EV1=.996 EV2=.921 EV3=.050 ThT=2.14
90-04-18 18:53 Run=7339 Evt=5121
Trig= 22304 Detb= 80EBFF
EVENT 4
5.1Gev HC
5.7Gev EW
30.Gev EC
YX hist.of BA.+E.C.
#T>4
-500cm
500cm
X
RZ
#T>4
Z
P dP phi theta D0 Z0 chiq
2 +37.3 .78 26 57 .018 -.767 44
3 -10.6 .08 200 120 -.01 -.778 38
1 -23.8 .33 203 120 .013 -.937 17
4 +11.4 .08 219 127 -.02 -.684 47

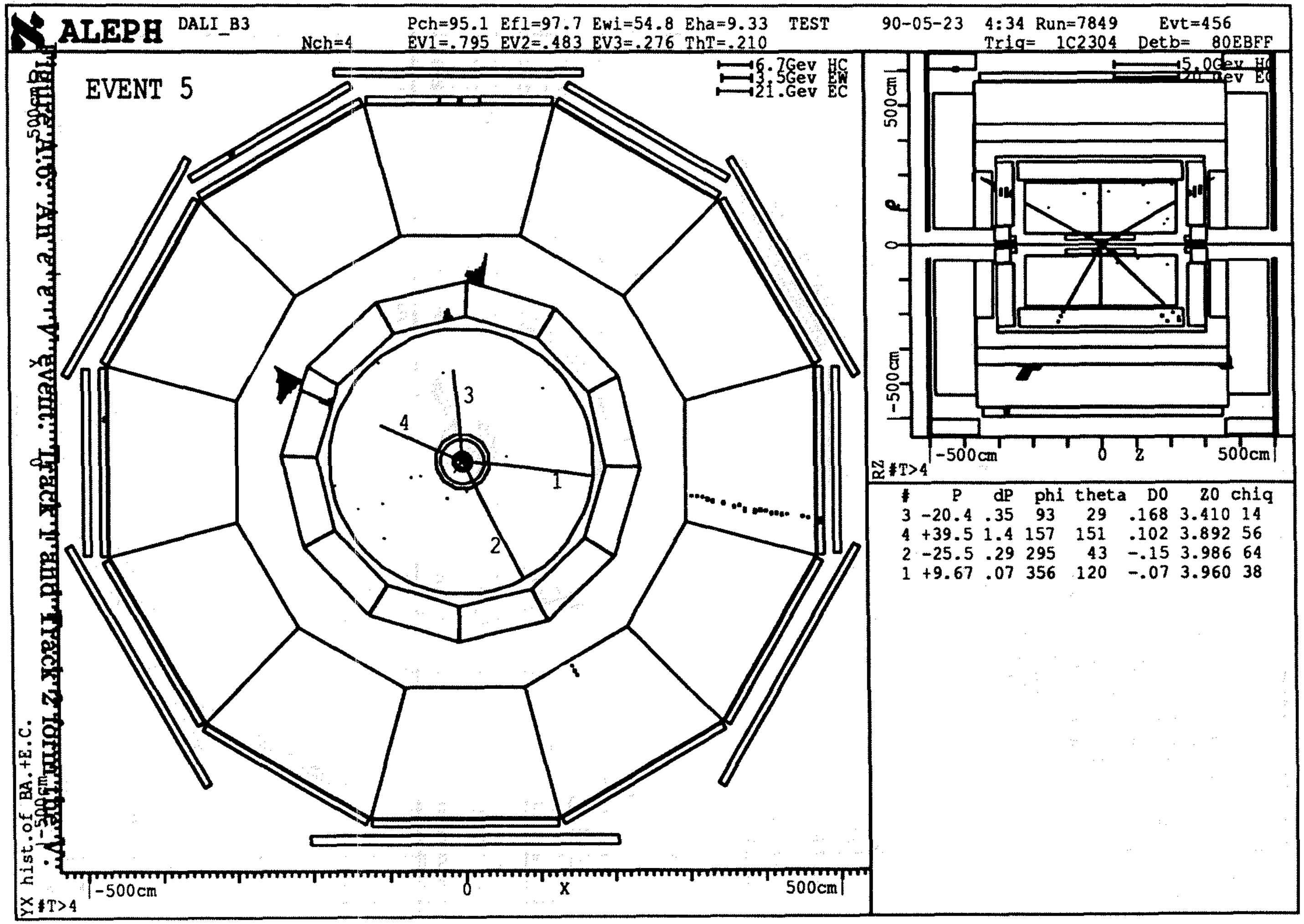
ALEPH
DALI_B3
Nch=4
Pch=95.1 Efl=97.7 Ewi=54.8 Eha=9.33 TEST
EV1=.795 EV2=.483 EV3=.276 ThT=.210
90-05-23 4:34 Run=7849 Evt=456
Trig= 1C2304 Detb= 80EBFF
EVENT 5
6.7Gev HC
3.5Gev EW
21.Gev EC
5.0Gev HC
20 Gev EC
-500cm
0
X
500cm
YX hist.of BA.+E.C.
#T>4
RZ
#T>4
Z
P dP phi theta D0 Z0 chiq
3 -20.4 .35 93 29 .168 3.410 14
4 +39.5 1.4 157 151 .102 3.892 56
2 -25.5 .29 295 43 -.15 3.986 64
1 +9.67 .07 356 120 -.07 3.960 38

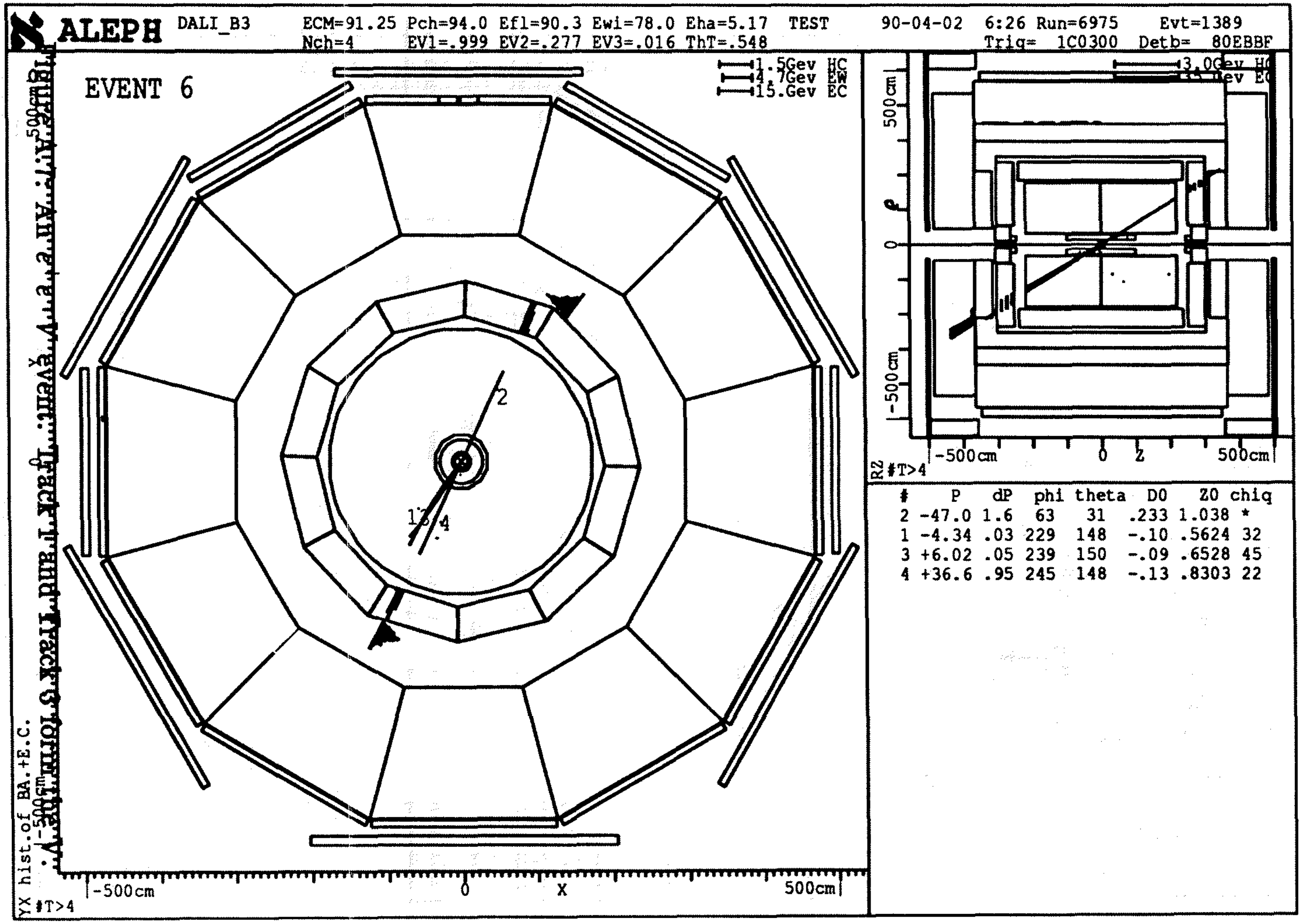

#	P	dP	phi	theta	D0	Z0	chiq
2	-47.0	1.6	63	31	.233	1.038	*
1	-4.34	.03	229	148	-.10	.5624	32
3	+6.02	.05	239	150	-.09	.6528	45
4	+36.6	.95	245	148	-.13	.8303	22

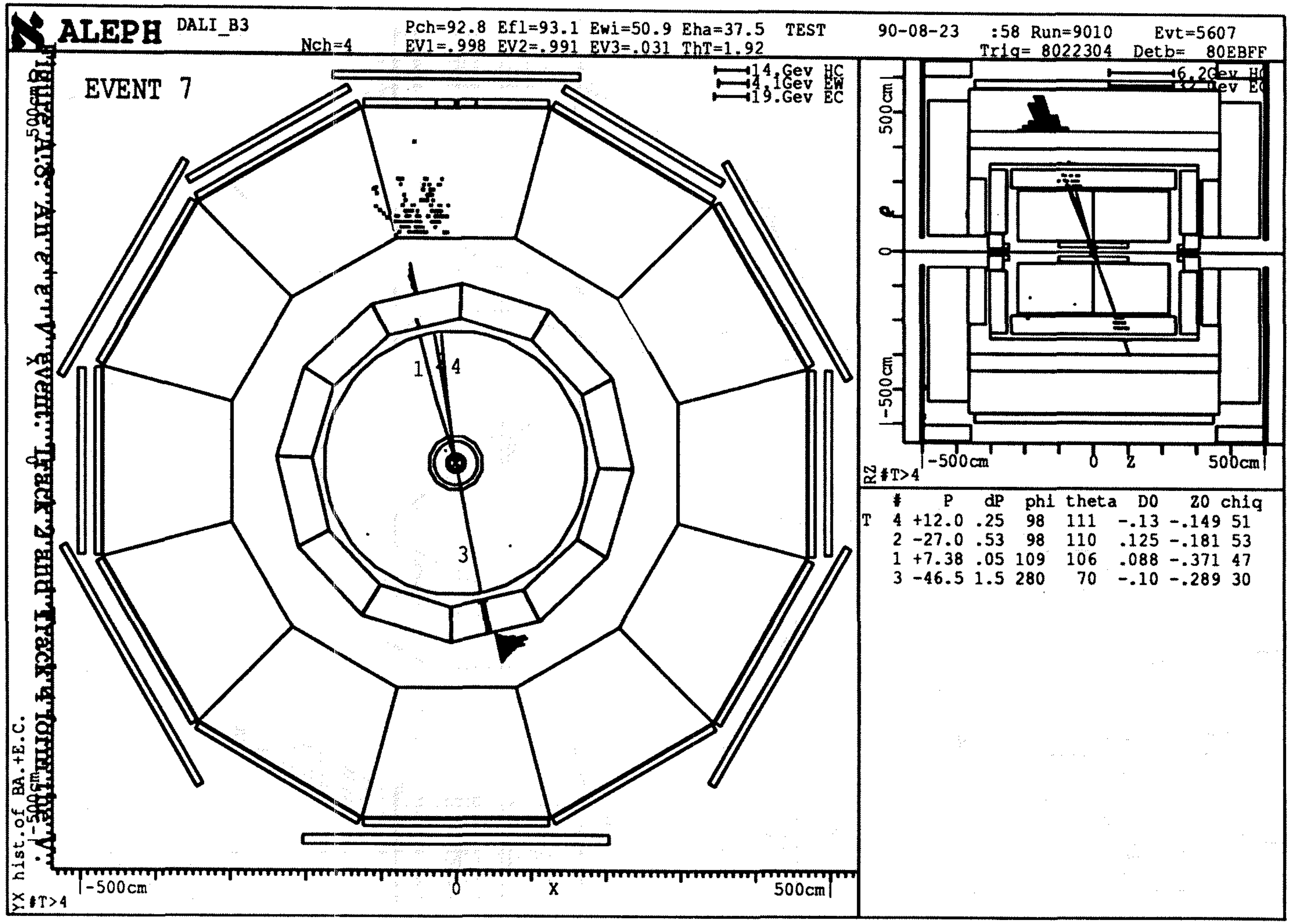

#	P	dP	phi	theta	D0	Z0	chiq
T 4	+12.0	.25	98	111	-.13	-.149	51
2	-27.0	.53	98	110	.125	-.181	53
1	+7.38	.05	109	106	.088	-.371	47
3	-46.5	1.5	280	70	-.10	-.289	30

Figure A.8: An ... event. Track 2 and Track 4 form the V.

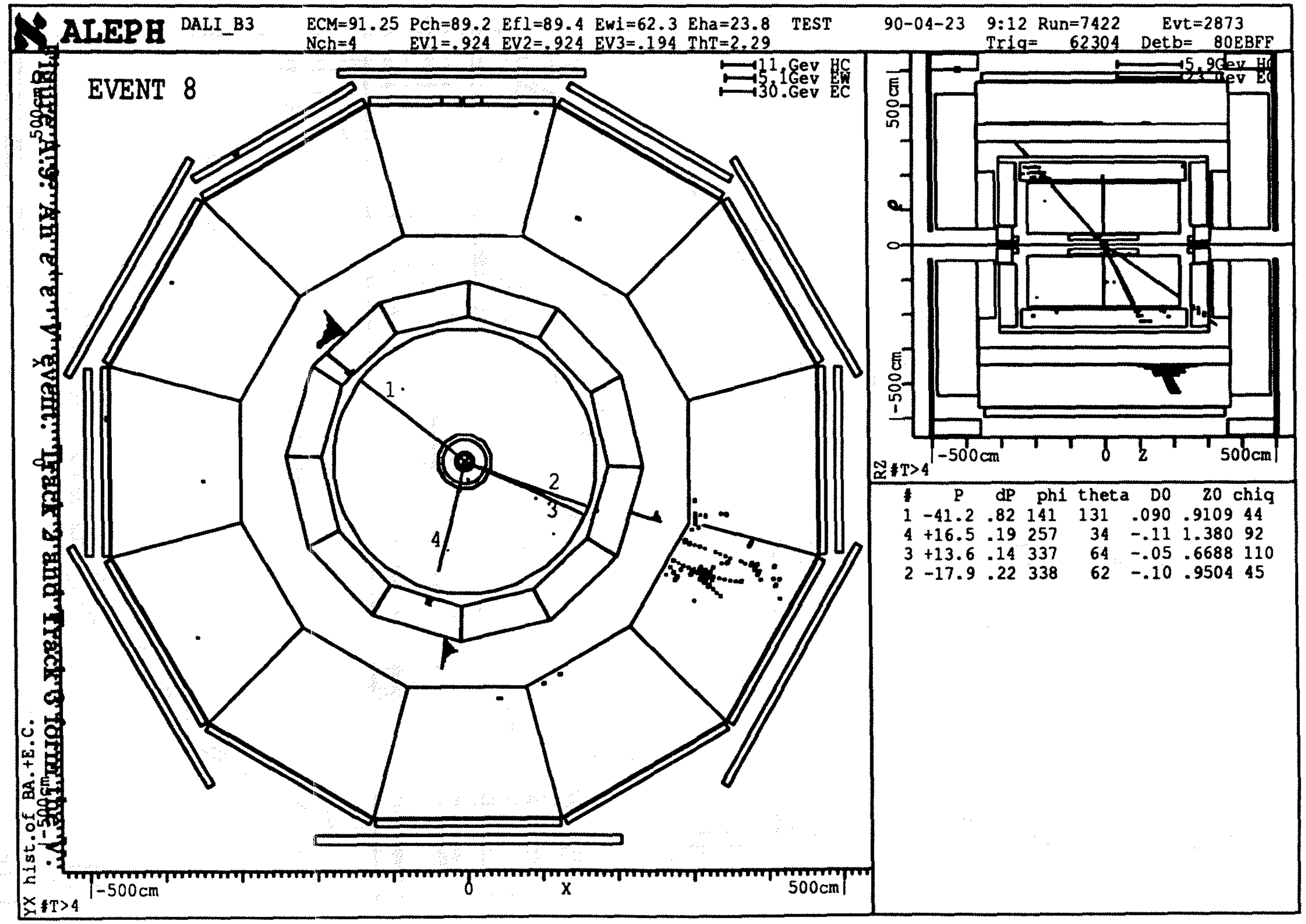
ALEPH
DALI_B3
ECM=91.25 Pch=89.2 Efl=89.4 Ewi=62.3 Eha=23.8 TEST
90-04-23 9:12 Run=7422 Evt=2873
Nch=4 EV1=.924 EV2=.924 EV3=.194 ThT=2.29
Trig= 62304 Detb= 80EBFF
EVENT 8
11.Gev HC
5.1Gev EW
30.Gev EC
1
2
3
4
-500cm
0
X
500cm
YX #T>4
hist.of BA.+E.C.
500cm
0
-500cm
0
Z
RZ #T>4
P dP phi theta D0 Z0 chiq
1 -41.2 .82 141 131 .090 .9109 44
4 +16.5 .19 257 34 -.11 1.380 92
3 +13.6 .14 337 64 -.05 .6688 110
2 -17.9 .22 338 62 -.10 .9504 45

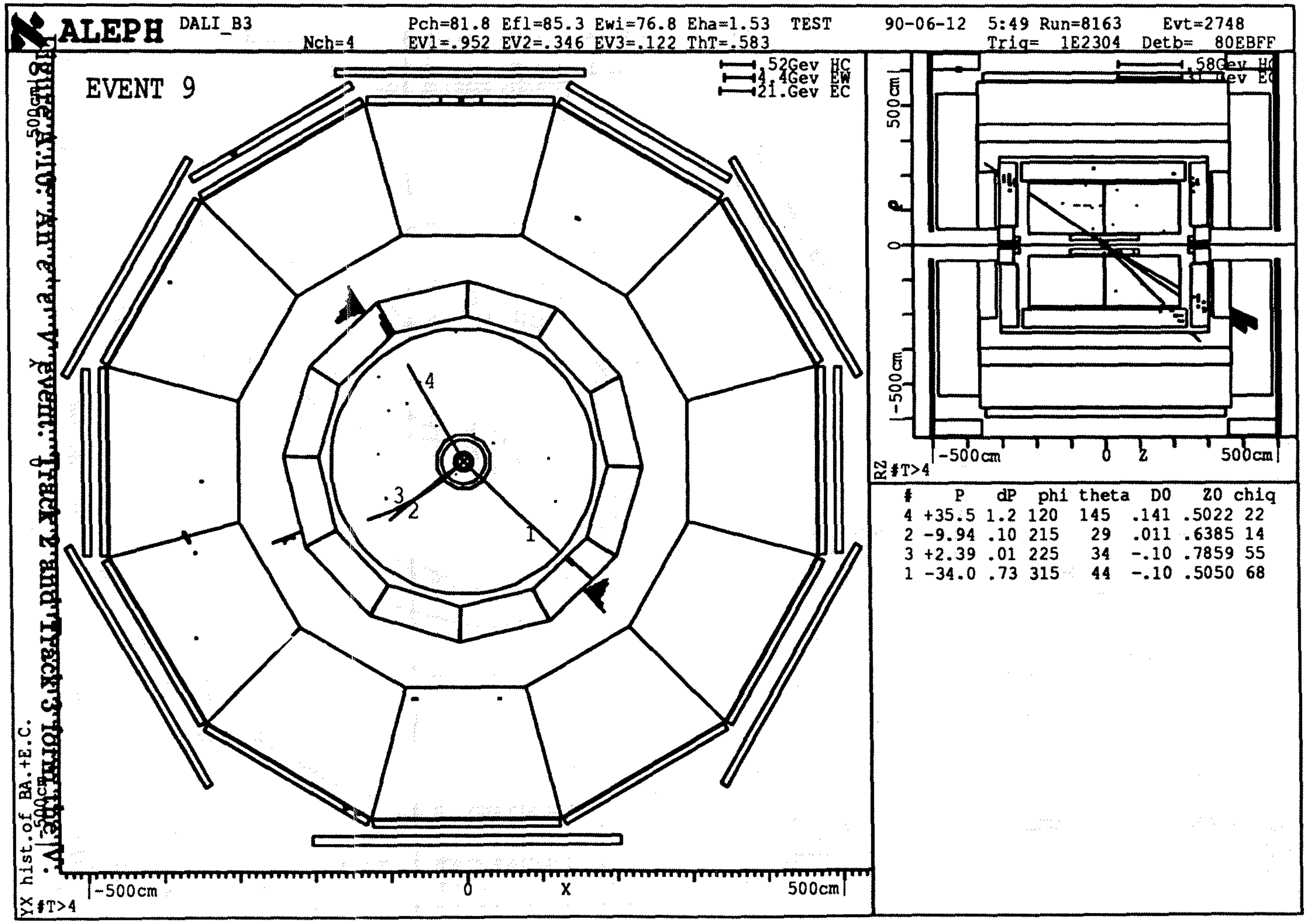
ALEPH
DALI_B3
Nch=4
Pch=81.8 Efl=85.3 Ewi=76.8 Eha=1.53 TEST
EV1=.952 EV2=.346 EV3=.122 ThT=.583
90-06-12 5:49 Run=8163 Evt=2748
Trig= 1E2304 Detb= 80EBFF
EVENT 9
.52Gev HC
4.4Gev EW
21.Gev EC
-500cm
0
X
500cm
YX hist.of BA.+E.C.
#T>4
500cm
0
-500cm
Z
RZ #T>4
P dP phi theta D0 Z0 chiq
4 +35.5 1.2 120 145 .141 .5022 22
2 -9.94 .10 215 29 .011 .6385 14
3 +2.39 .01 225 34 -.10 .7859 55
1 -34.0 .73 315 44 -.10 .5050 68

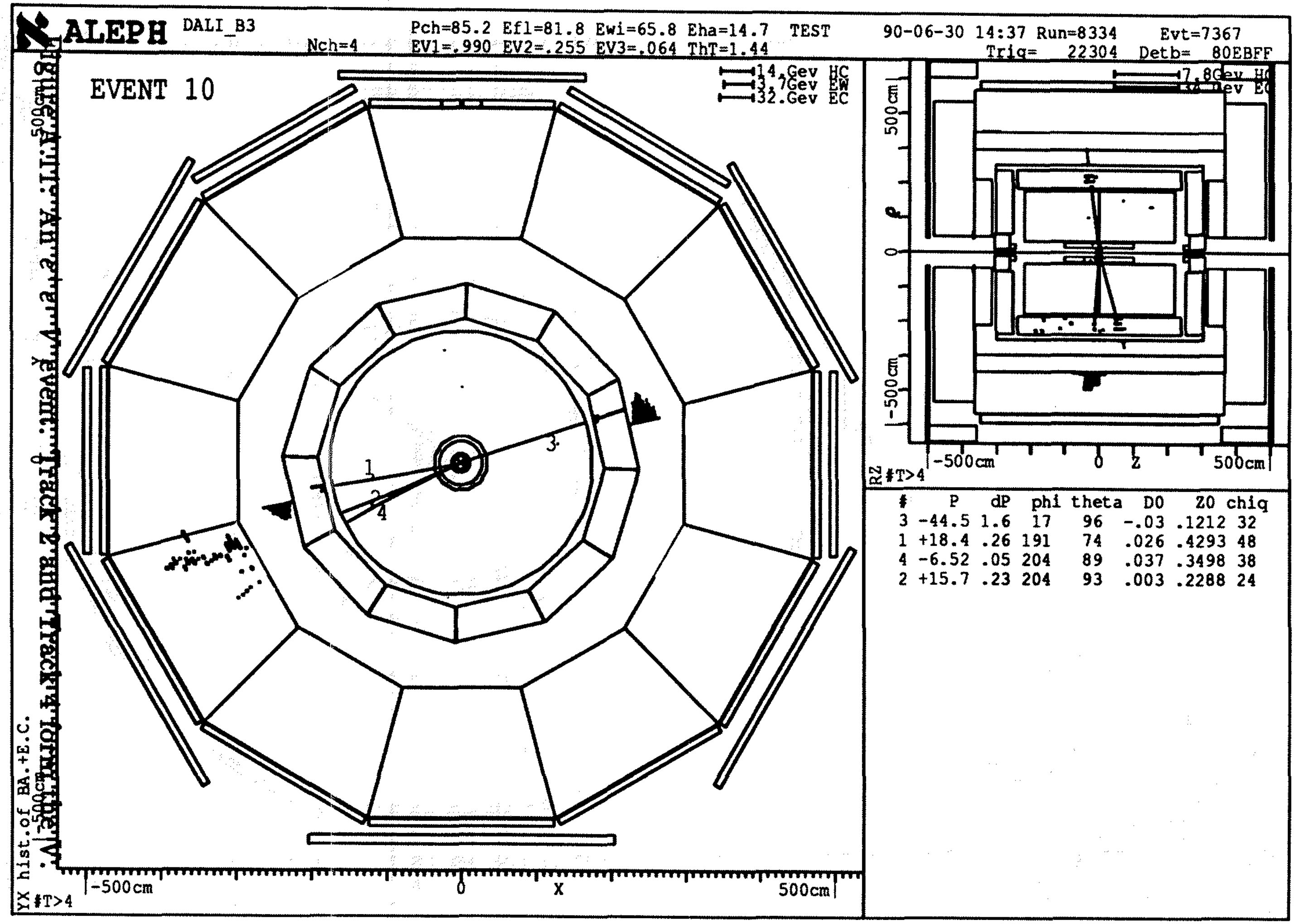
ALEPH
DALI_B3
Nch=4
Pch=85.2 Efl=81.8 Ewi=65.8 Eha=14.7 TEST
EV1=.990 EV2=.255 EV3=.064 ThT=1.44
90-06-30 14:37 Run=8334 Evt=7367
Trig= 22304 Detb= 80EBFF
EVENT 10
14.Gev HC
3.7Gev EW
32.Gev EC
1
2
3
4
-500cm
0
X
500cm
500cm
Y
YX hist.of BA.+E.C.
#T>4
7.8Gev HC
-500cm
0
Z
500cm
500cm
ρ
RZ #T>4
P dP phi theta D0 Z0 chiq
3 -44.5 1.6 17 96 -.03 .1212 32
1 +18.4 .26 191 74 .026 .4293 48
4 -6.52 .05 204 89 .037 .3498 38
2 +15.7 .23 204 93 .003 .2288 24

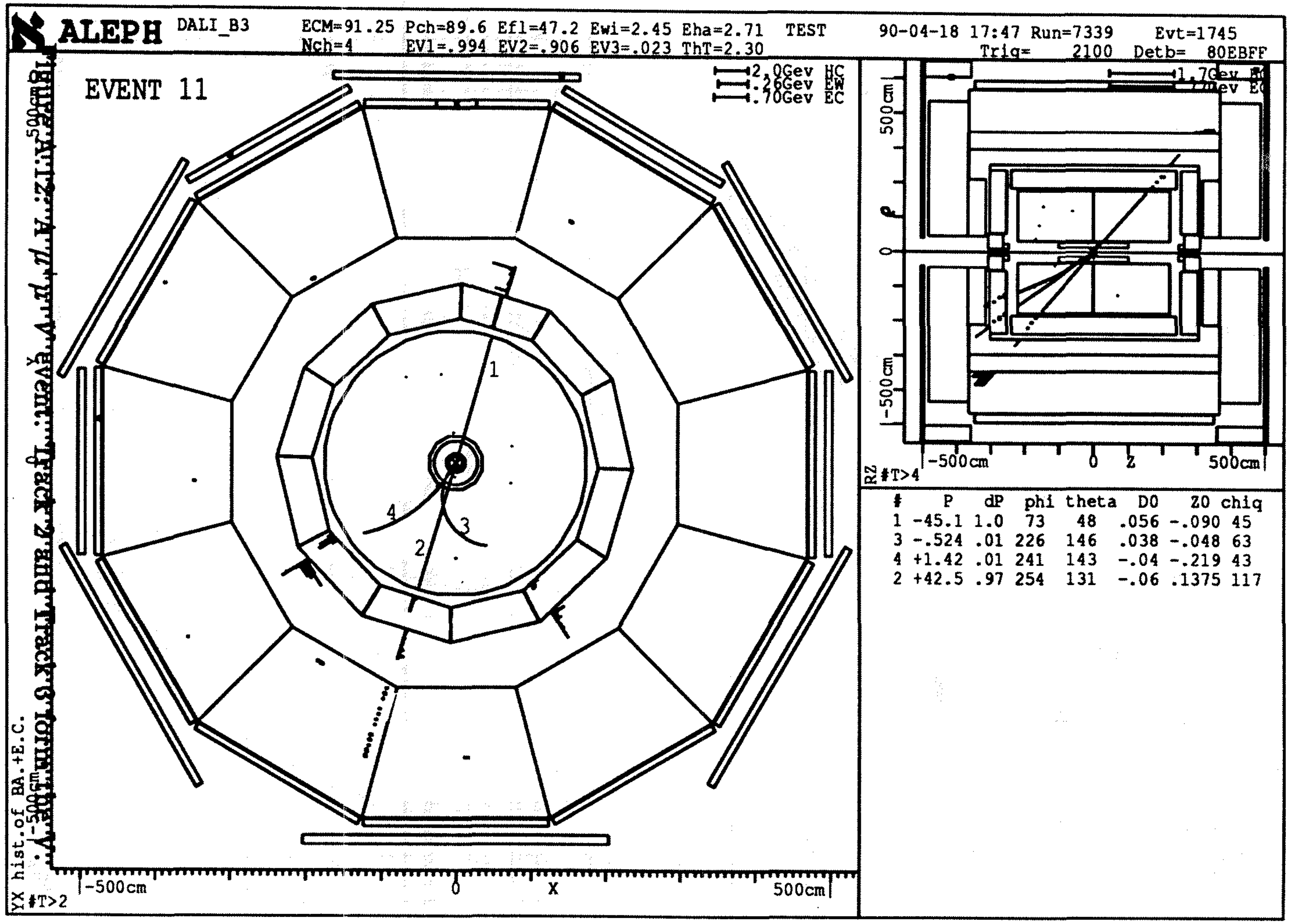

ALEPH DALI_B3
ECM=91.25 Pch=89.6 Efl=47.2 Ewi=2.45 Eha=2.71 TEST
Nch=4 EV1=.994 EV2=.906 EV3=.023 ThT=2.30
90-04-18 17:47 Run=7339 Evt=1745
Trig= 2100 Detb= 80EBFF
EVENT 11
2.0Gev HC
.26Gev EW
.70Gev EC
YX #T>2
-500cm
0
X
500cm
RZ #T>4
-500cm
0
Z
500cm
P dP phi theta D0 Z0 chiq
1 -45.1 1.0 73 48 .056 -.090 45
3 -.524 .01 226 146 .038 -.048 63
4 +1.42 .01 241 143 -.04 -.219 43
2 +42.5 .97 254 131 -.06 .1375 117

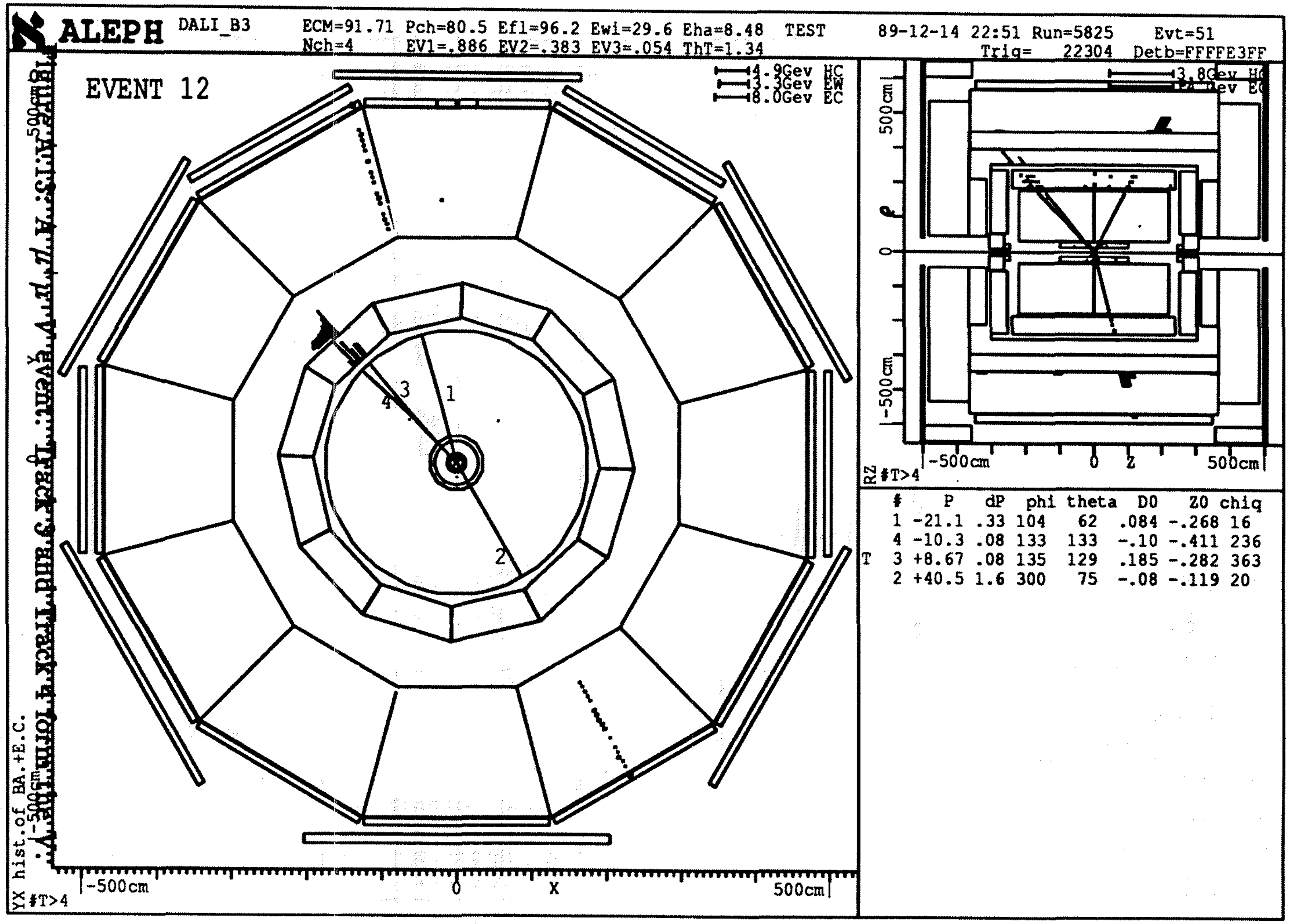

#	P	dP	phi	theta	D0	Z0	chiq
1	-21.1	.33	104	62	.084	-.268	16
4	-10.3	.08	133	133	-.10	-.411	236
3	+8.67	.08	135	129	.185	-.282	363
2	+40.5	1.6	300	75	-.08	-.119	20

Figure A.14: A $\mu\mu\gamma$ event: Track 1 and track 4 form the γ.

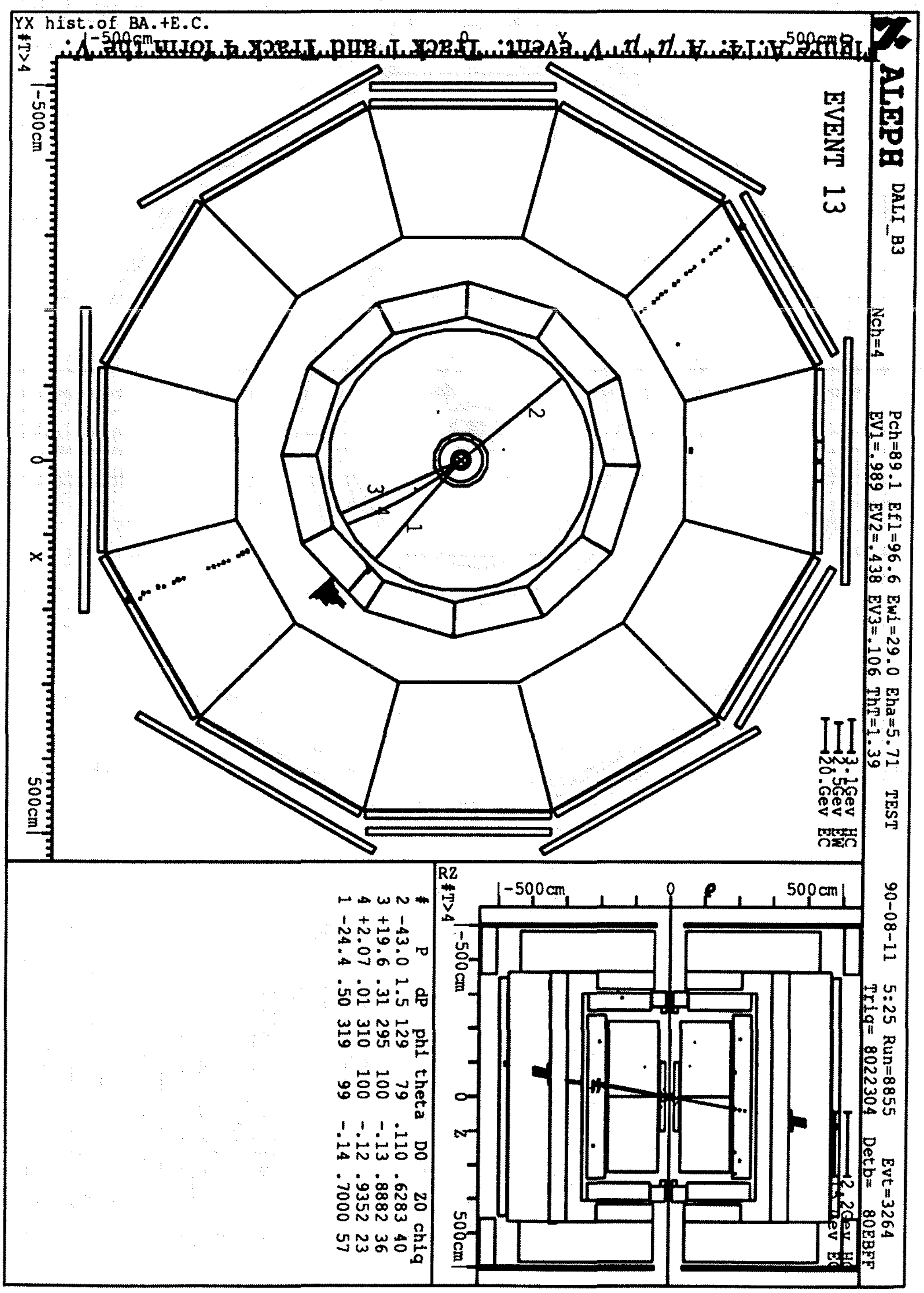

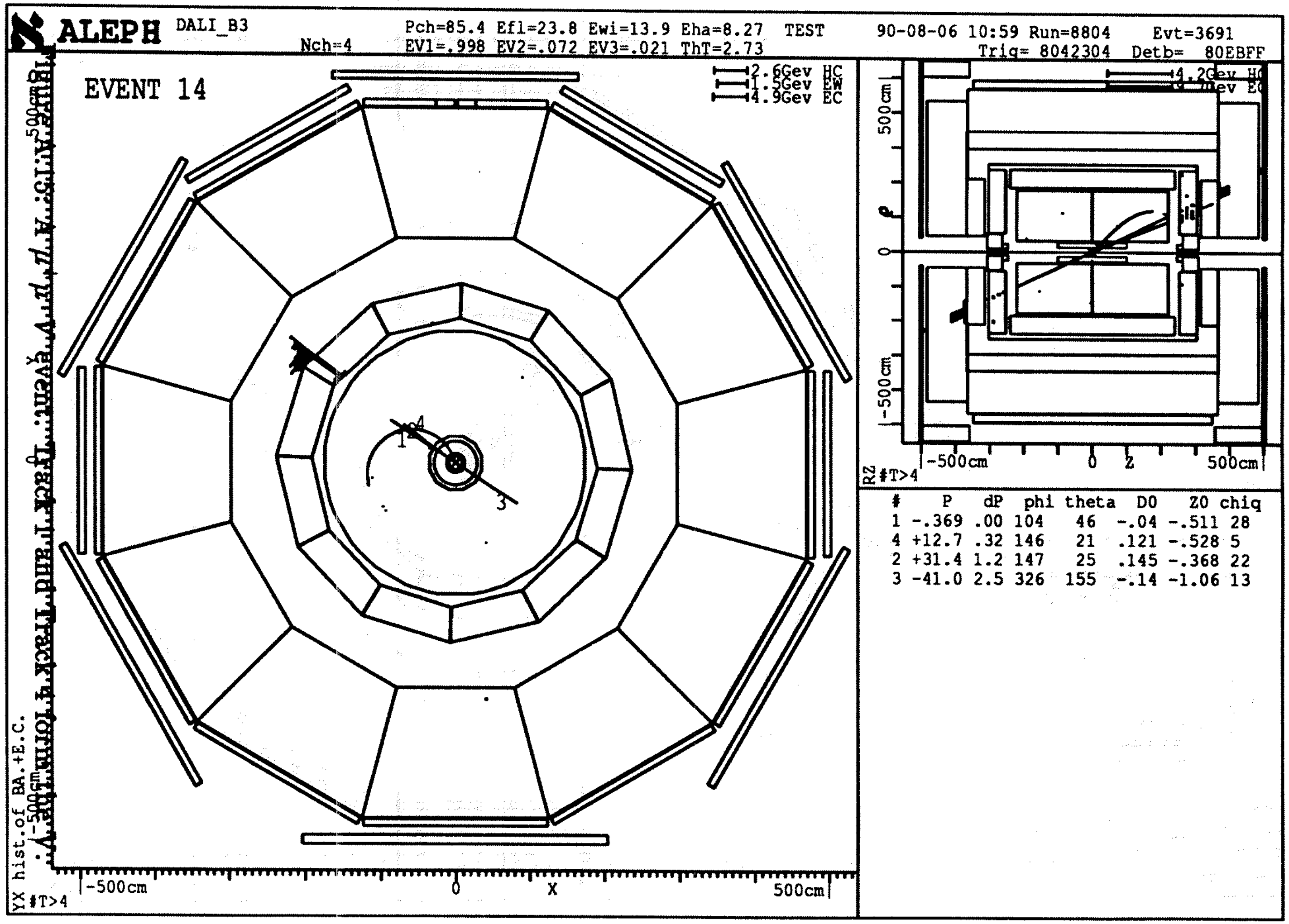
ALEPH DALI_B3
Nch=4
Pch=85.4 Efl=23.8 Ewi=13.9 Eha=8.27 TEST
EV1=.998 EV2=.072 EV3=.021 ThT=2.73
90-08-06 10:59 Run=8804 Evt=3691
Trig= 8042304 Detb= 80EBFF
EVENT 14
2.6Gev HC
1.5Gev EW
4.9Gev EC
YX hist.of BA.+E.C.
#T>4
-500cm
0
X
500cm
RZ #T>4
Z
P dP phi theta D0 Z0 chiq
1 -.369 .00 104 46 -.04 -.511 28
4 +12.7 .32 146 21 .121 -.528 5
2 +31.4 1.2 147 25 .145 -.368 22
3 -41.0 2.5 326 155 -.14 -1.06 13

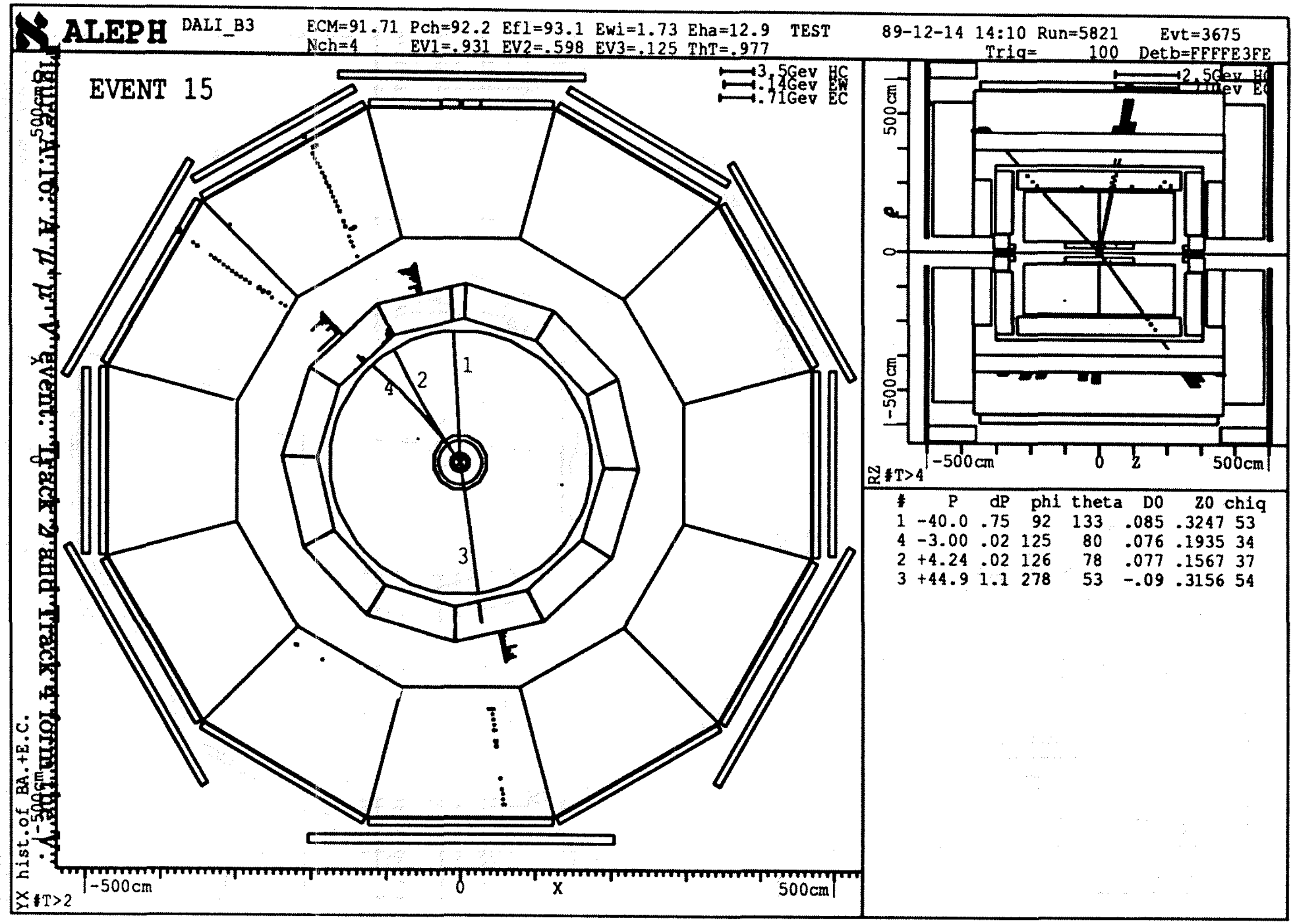

#	P	dP	phi	theta	D0	Z0	chiq
1	-40.0	.75	92	133	.085	.3247	53
4	-3.00	.02	125	80	.076	.1935	34
2	+4.24	.02	126	78	.077	.1567	37
3	+44.9	1.1	278	53	-.09	.3156	54

Figure 4.10: A $\mu\mu\gamma$ event. Track 2 and Track 4 form a

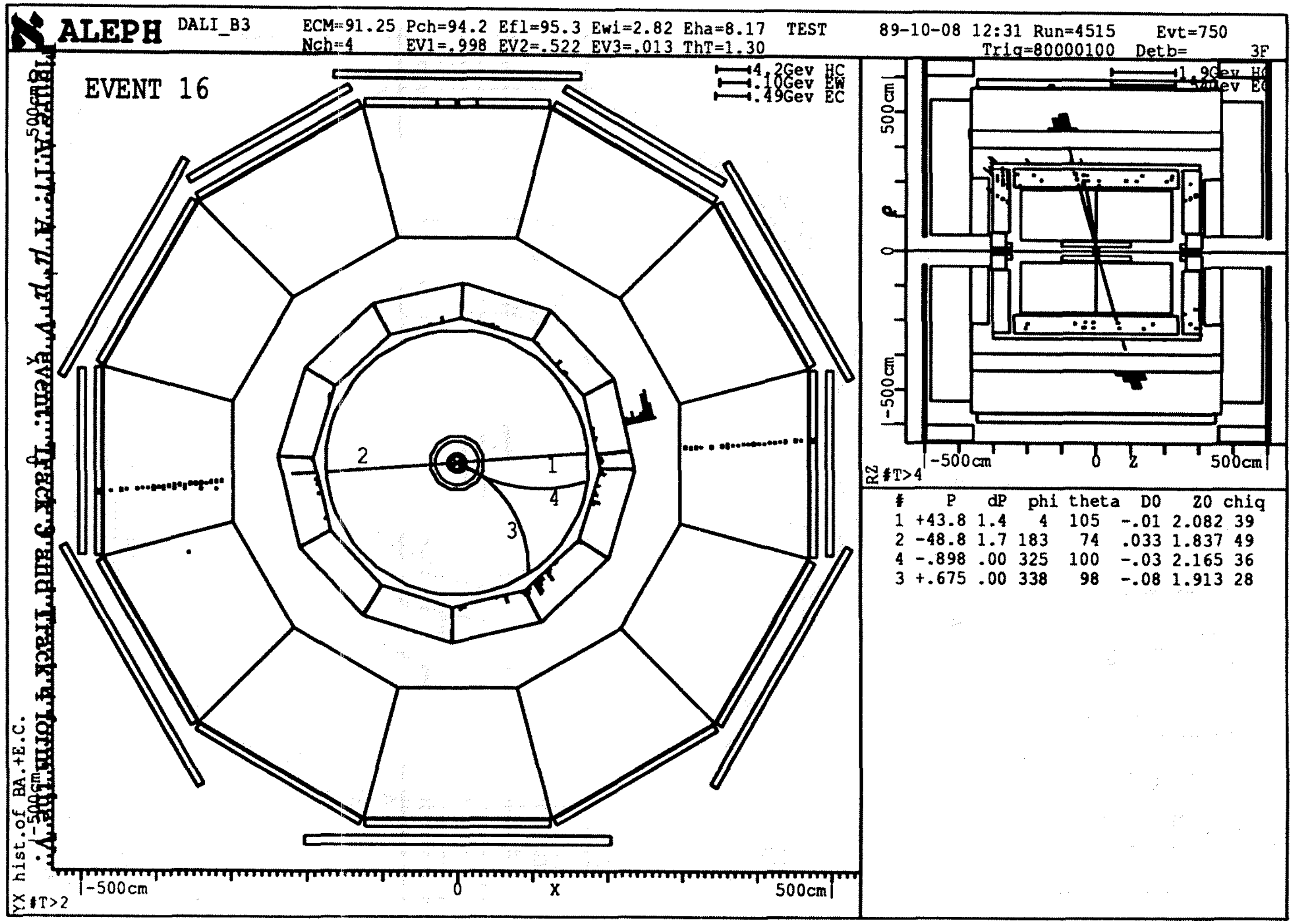

#	P	dP	phi	theta	D0	Z0	chiq
1	+43.8	1.4	4	105	-.01	2.082	39
2	-48.8	1.7	183	74	.033	1.837	49
4	-.898	.00	325	100	-.03	2.165	36
3	+.675	.00	338	98	-.08	1.913	28

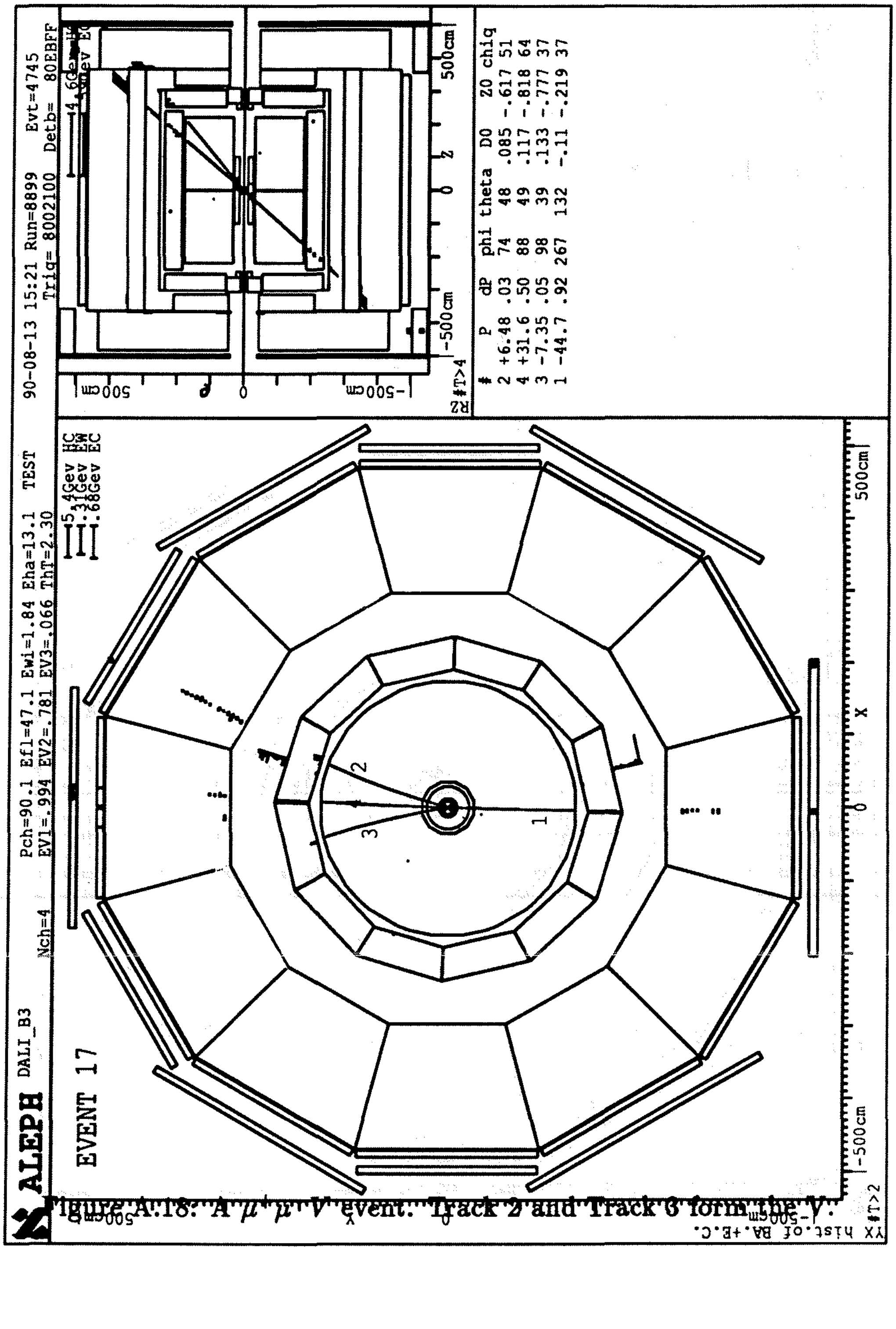

Figure A.18: A $\mu^+\mu^- V$ event. Track 2 and Track 3 form the V.

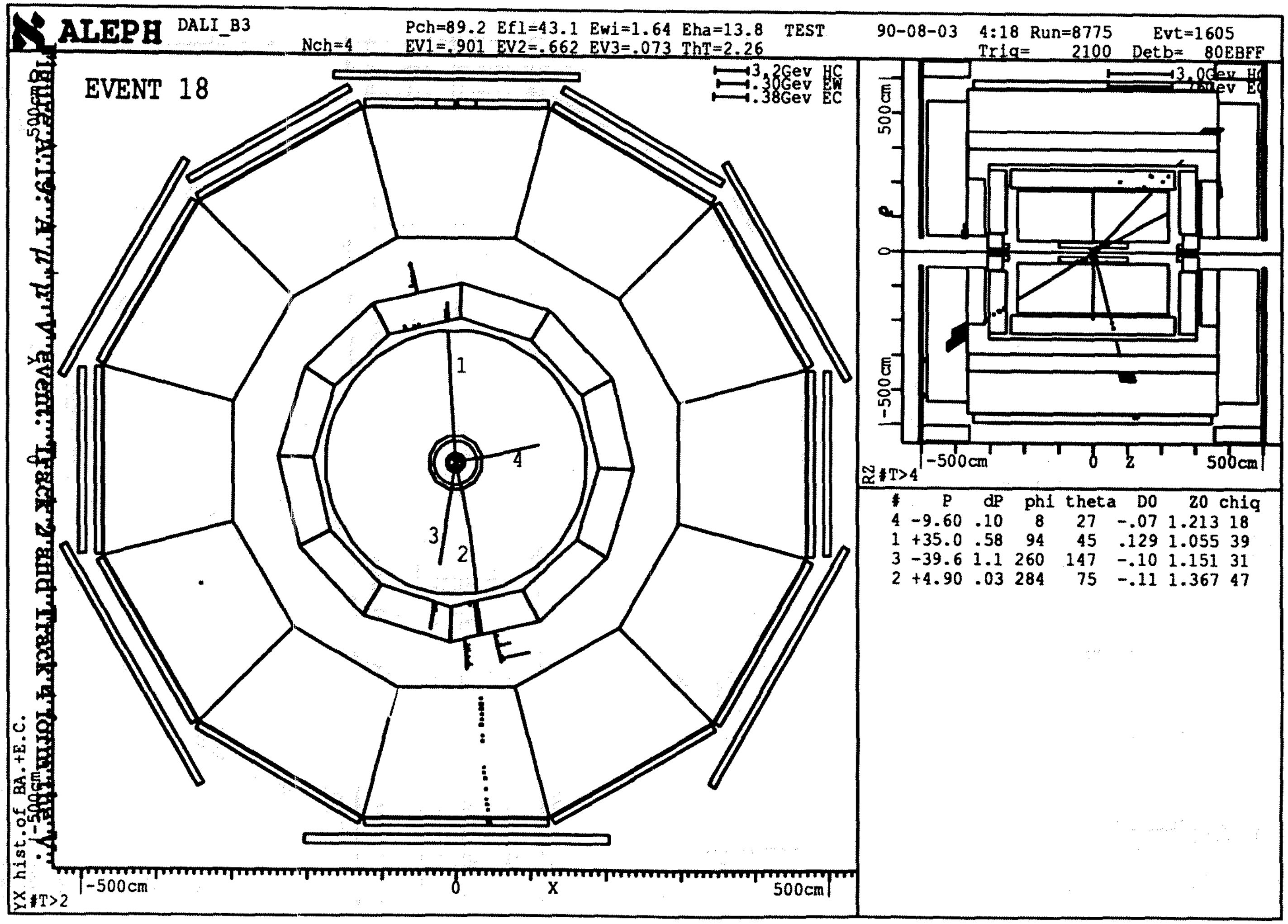
ALEPH
DALI_B3
Nch=4
Pch=89.2 Efl=43.1 Ewi=1.64 Eha=13.8 TEST
EV1=.901 EV2=.662 EV3=.073 ThT=2.26
90-08-03 4:18 Run=8775 Evt=1605
Trig= 2100 Detb= 80EBFF
EVENT 18
3.2Gev HC
.30Gev EW
.38Gev EC
1
2
3
4
-500cm
0
X
500cm
YX hist.of BA.+E.C.
#T>2
500cm
0
-500cm
Z
RZ #T>4
P dP phi theta D0 Z0 chiq
4 -9.60 .10 8 27 -.07 1.213 18
1 +35.0 .58 94 45 .129 1.055 39
3 -39.6 1.1 260 147 -.10 1.151 31
2 +4.90 .03 284 75 -.11 1.367 47

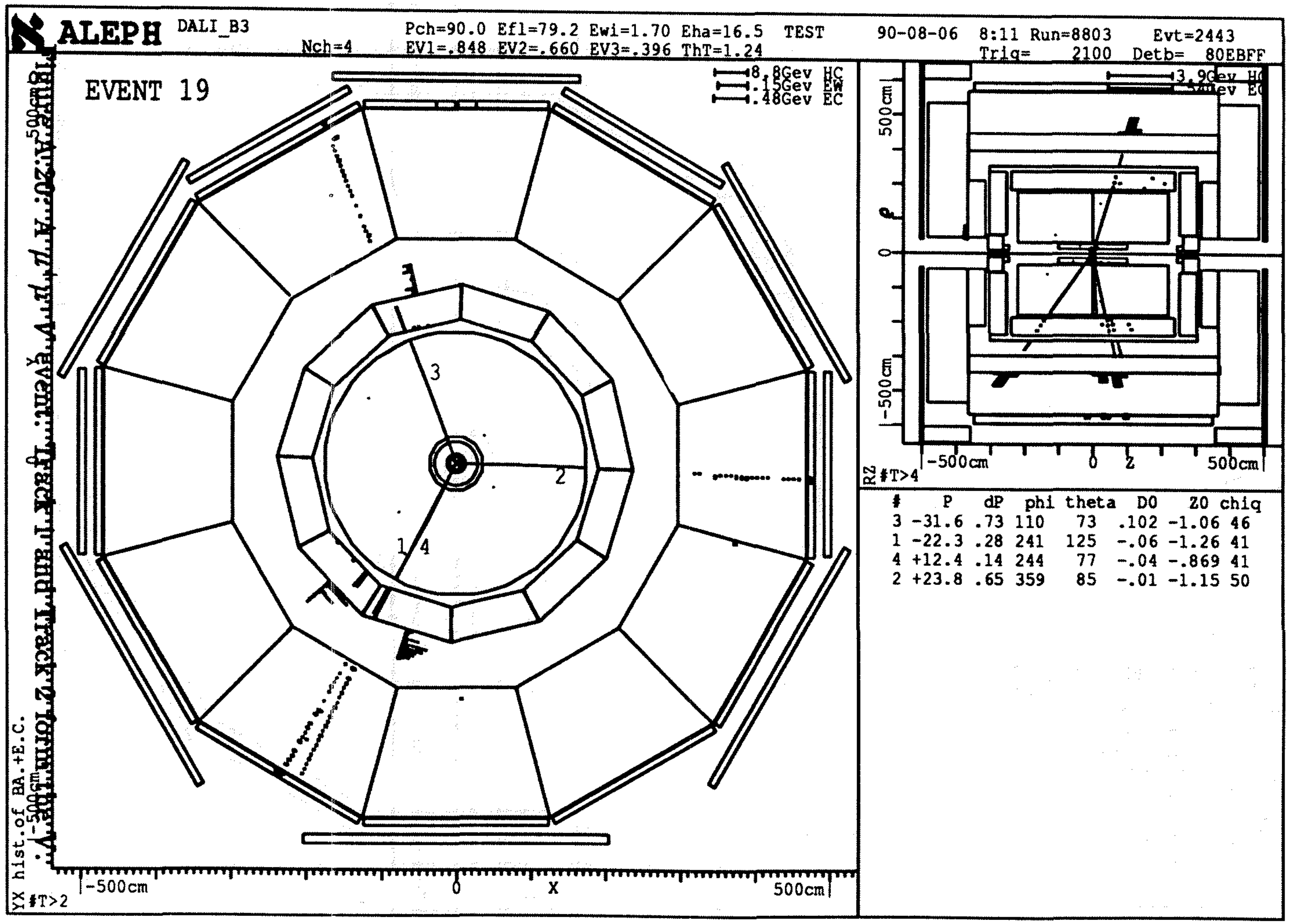
ALEPH DALI_B3
Nch=4
Pch=90.0 Efl=79.2 Ewi=1.70 Eha=16.5 TEST
EV1=.848 EV2=.660 EV3=.396 ThT=1.24
90-08-06 8:11 Run=8803 Evt=2443
Trig= 2100 Detb= 80EBFF
EVENT 19
8.8Gev HC
.15Gev EW
.48Gev EC
3.9Gev HC
-500cm
0
X
500cm
YX hist.of BA.+E.C.
#T>2
500cm
0
-500cm
Z
RZ #T>4
P dP phi theta D0 Z0 chiq
3 -31.6 .73 110 73 .102 -1.06 46
1 -22.3 .28 241 125 -.06 -1.26 41
4 +12.4 .14 244 77 -.04 -.869 41
2 +23.8 .65 359 85 -.01 -1.15 50

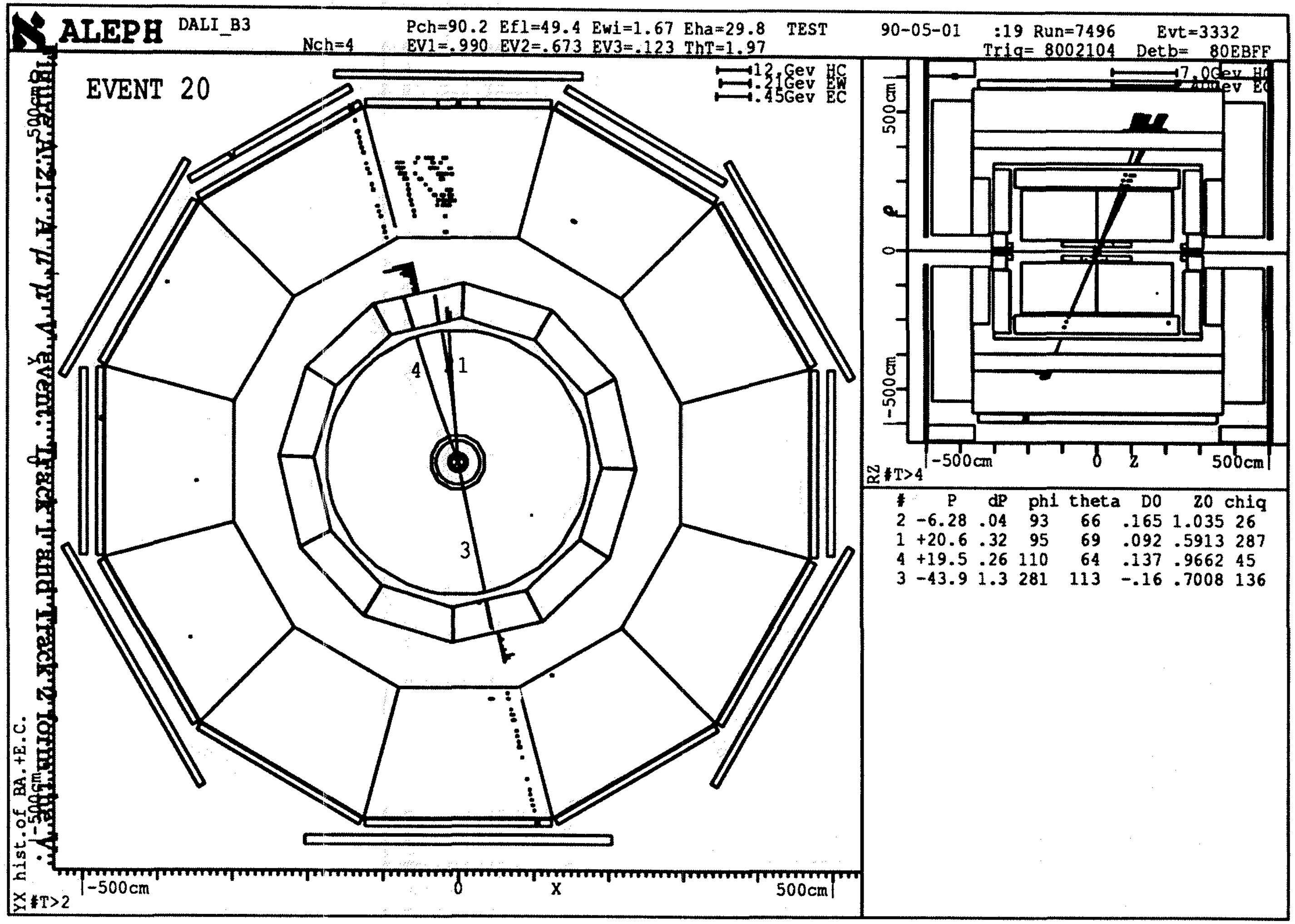

ALEPH DALI_B3
Nch=4
Pch=90.2 Efl=49.4 Ewi=1.67 Eha=29.8 TEST
EV1=.990 EV2=.673 EV3=.123 ThT=1.97
90-05-01 :19 Run=7496 Evt=3332
Trig= 8002104 Detb= 80EBFF
EVENT 20
12.Gev HC
.21Gev EW
.45Gev EC
7.0Gev HC
YX hist.of BA.+E.C.
#T>2
-500cm
0
X
500cm
Y
RZ #T>4
500cm
-500cm
Z
P dP phi theta D0 Z0 chiq
2 -6.28 .04 93 66 .165 1.035 26
1 +20.6 .32 95 69 .092 .5913 287
4 +19.5 .26 110 64 .137 .9662 45
3 -43.9 1.3 281 113 -.16 .7008 136

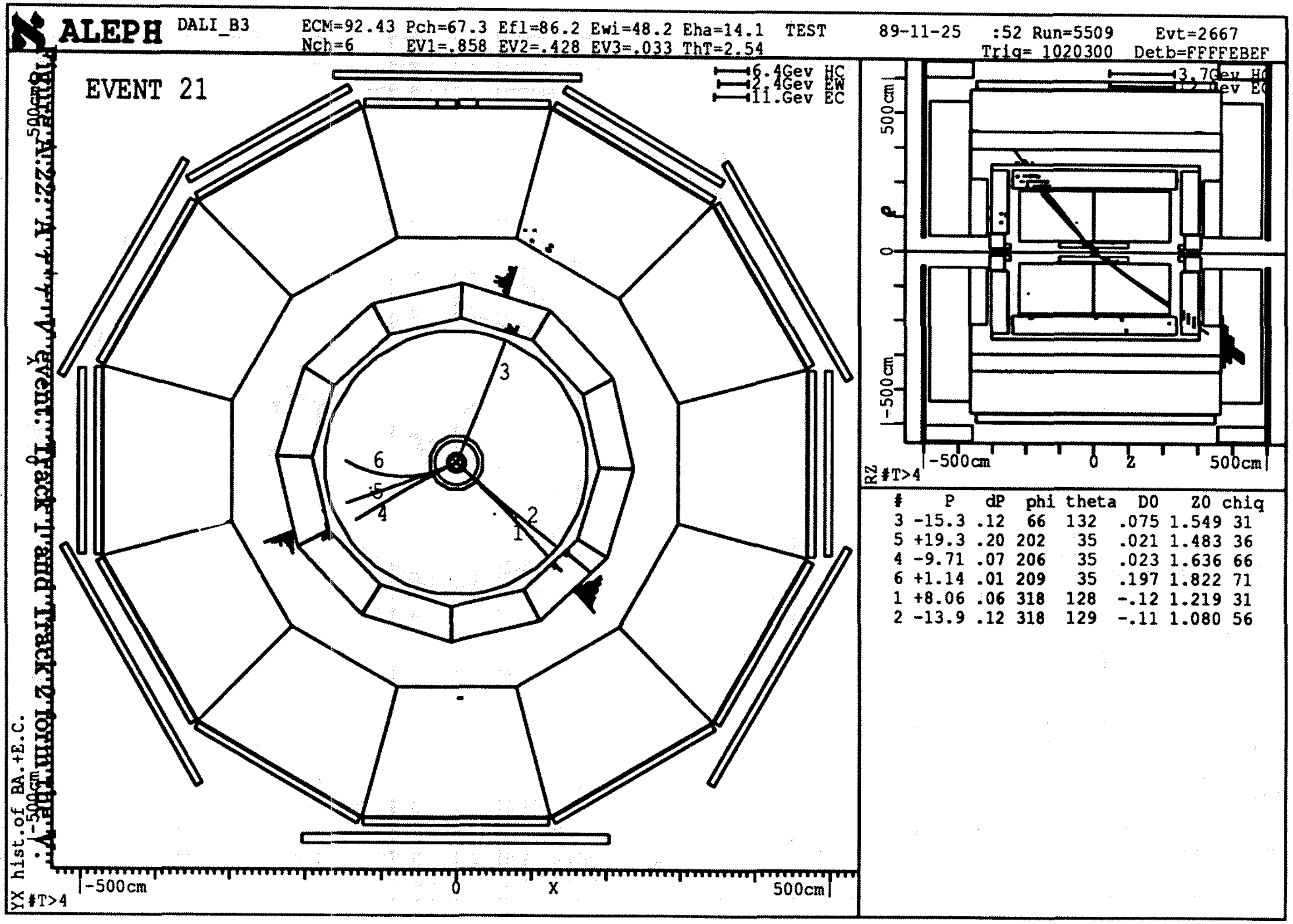

Figure A.22: A $\tau^+\tau^-$ event. Track 1 and Track 2 form the γ.

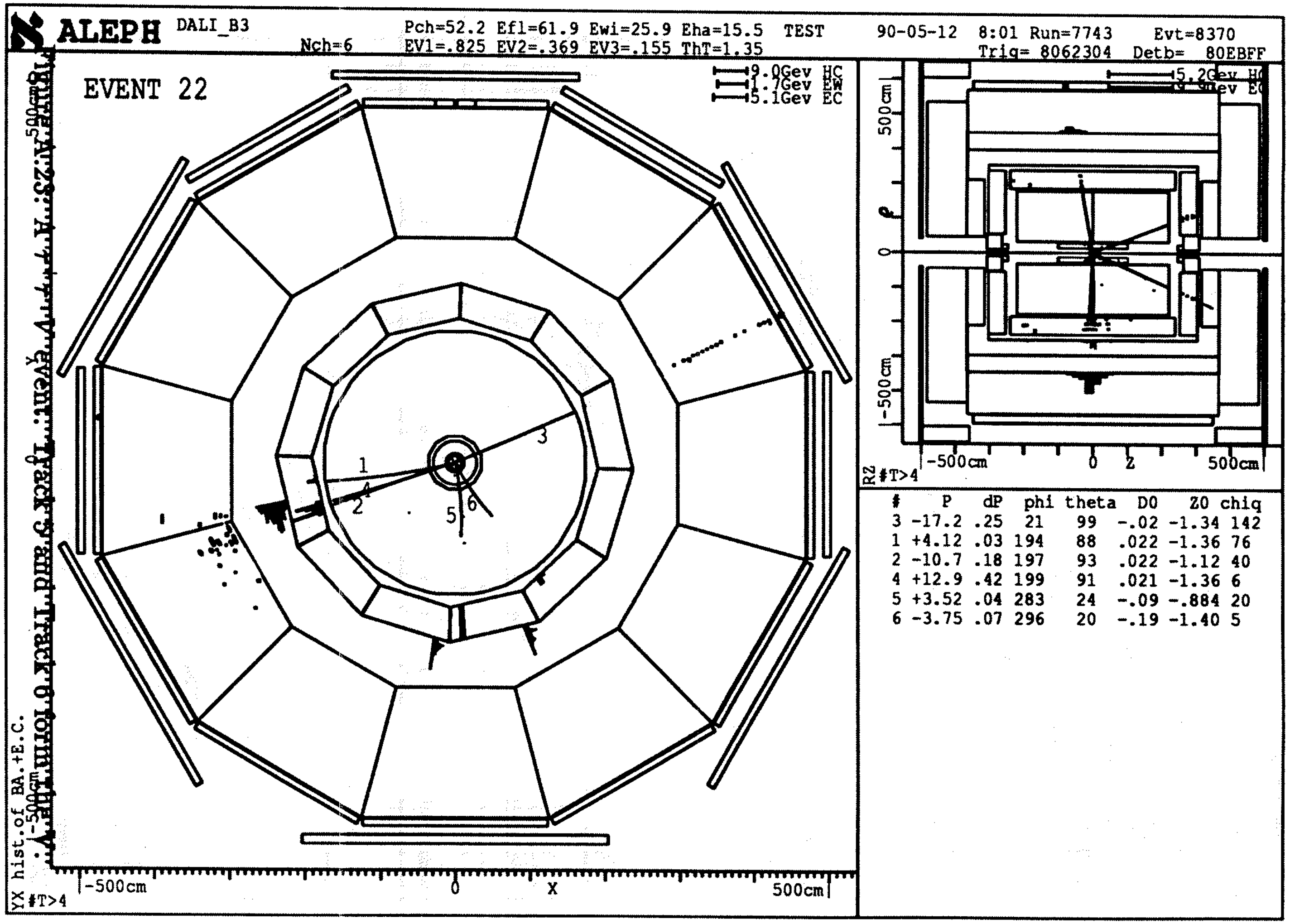
ALEPH DALI_B3
Nch=6
Pch=52.2 Efl=61.9 Ewi=25.9 Eha=15.5 TEST
EV1=.825 EV2=.369 EV3=.155 ThT=1.35
90-05-12 8:01 Run=7743 Evt=8370
Trig= 8062304 Detb= 80EBFF
EVENT 22
9.0Gev HC
1.7Gev EW
5.1Gev EC
-500cm
0
X
500cm
YX #T>4
hist.of BA.+E.C.
RZ #T>4
Z
ρ
P dP phi theta D0 Z0 chiq
3 -17.2 .25 21 99 -.02 -1.34 142
1 +4.12 .03 194 88 .022 -1.36 76
2 -10.7 .18 197 93 .022 -1.12 40
4 +12.9 .42 199 91 .021 -1.36 6
5 +3.52 .04 283 24 -.09 -.884 20
6 -3.75 .07 296 20 -.19 -1.40 5

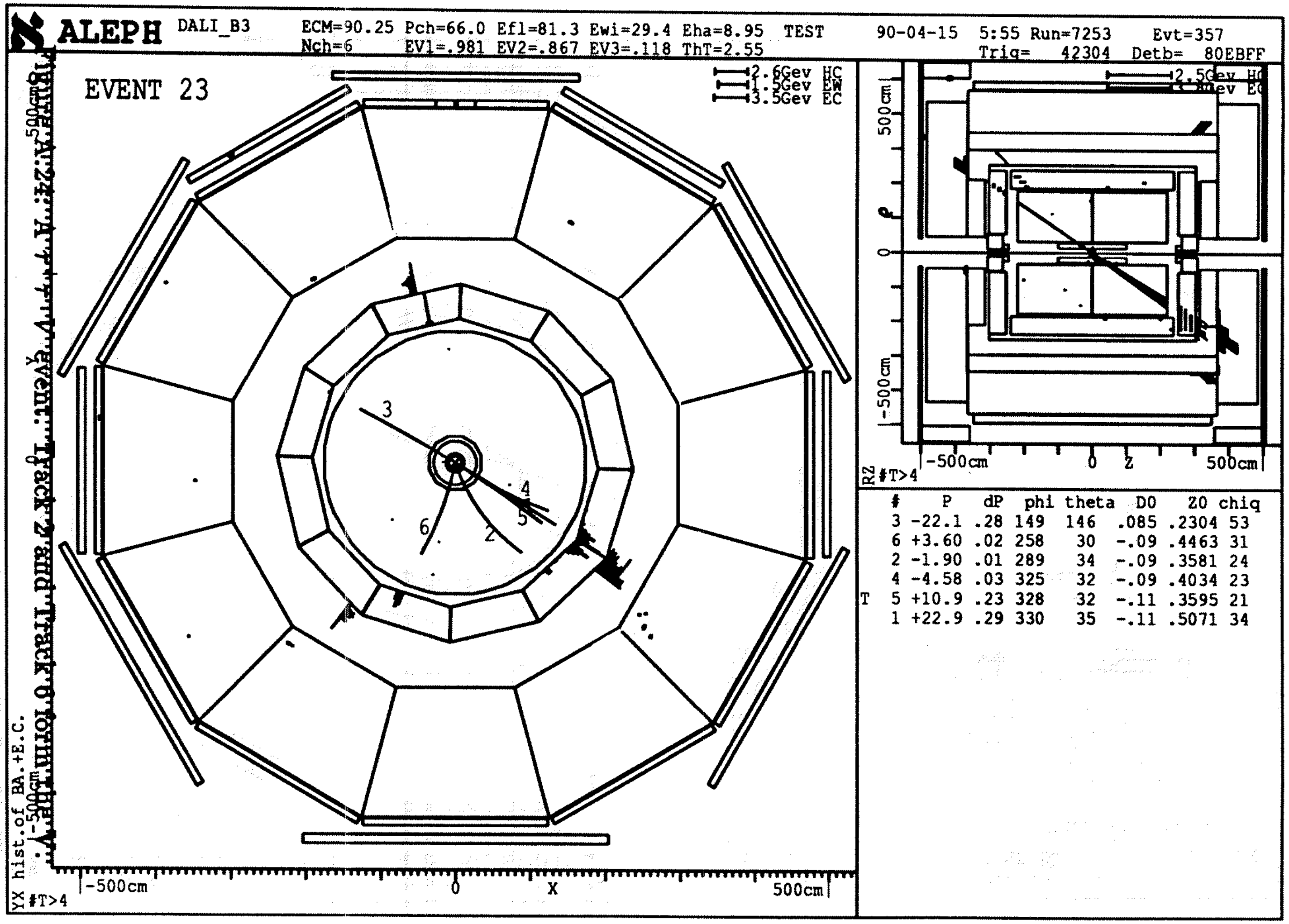

Figure A.24: A $\tau\tau\gamma$ event. Track 2 and Track 0 form the γ.

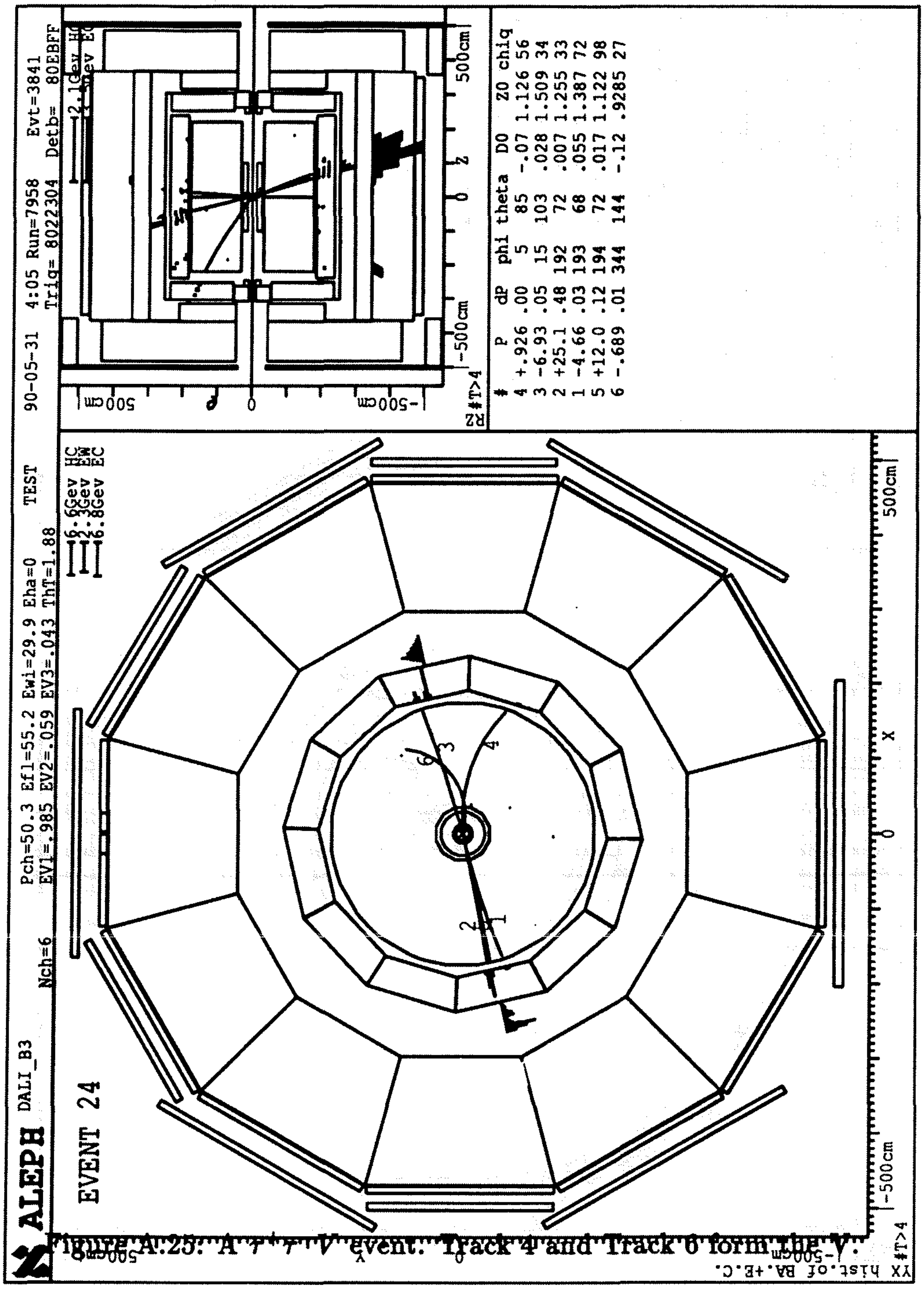

Figure A.25: A $\tau^+\tau^-V$ event. Track 4 and Track 6 form the V.

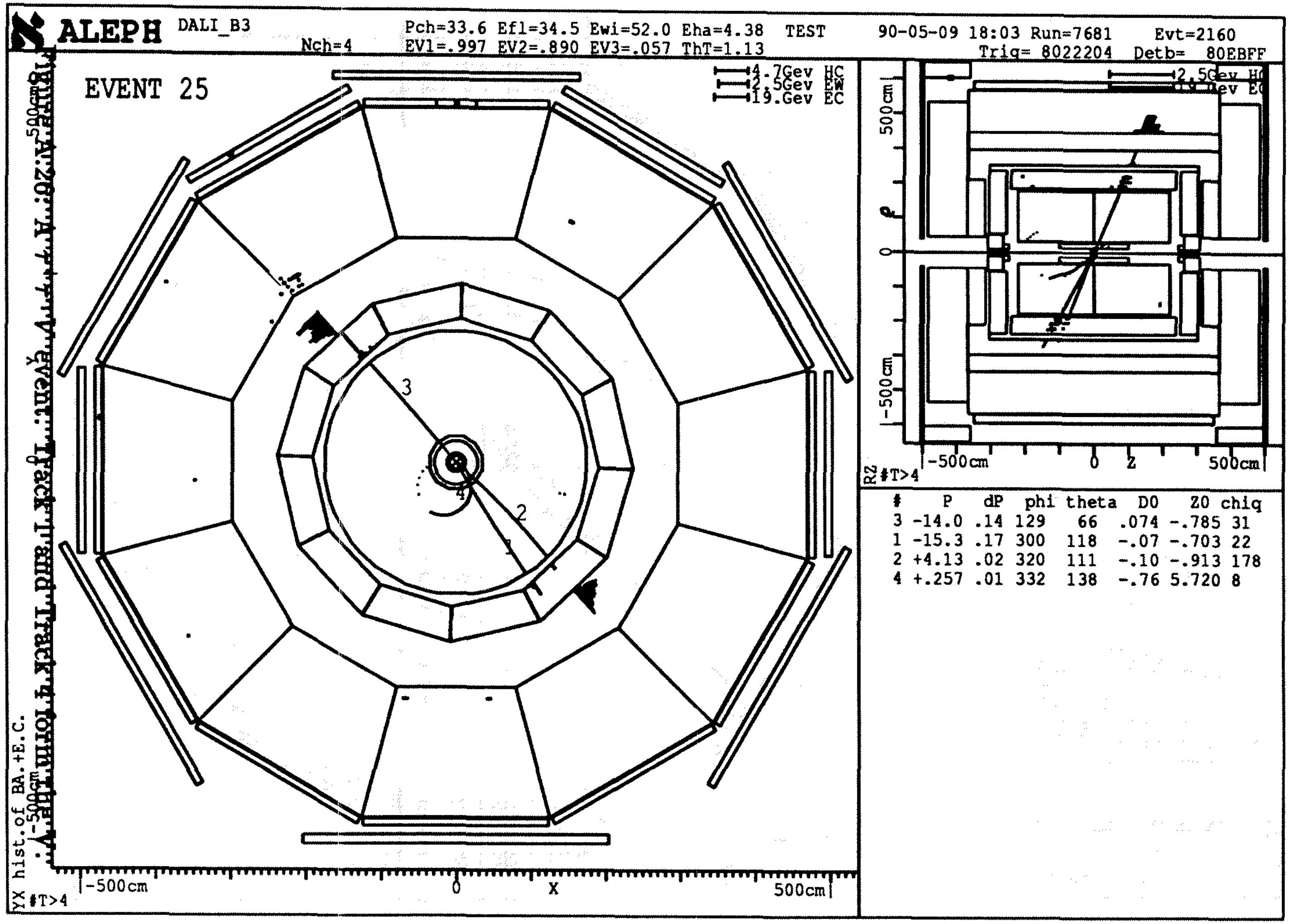

Figure A.26: A $\tau^+\tau^-$ event: Track 1 and Track 4 form

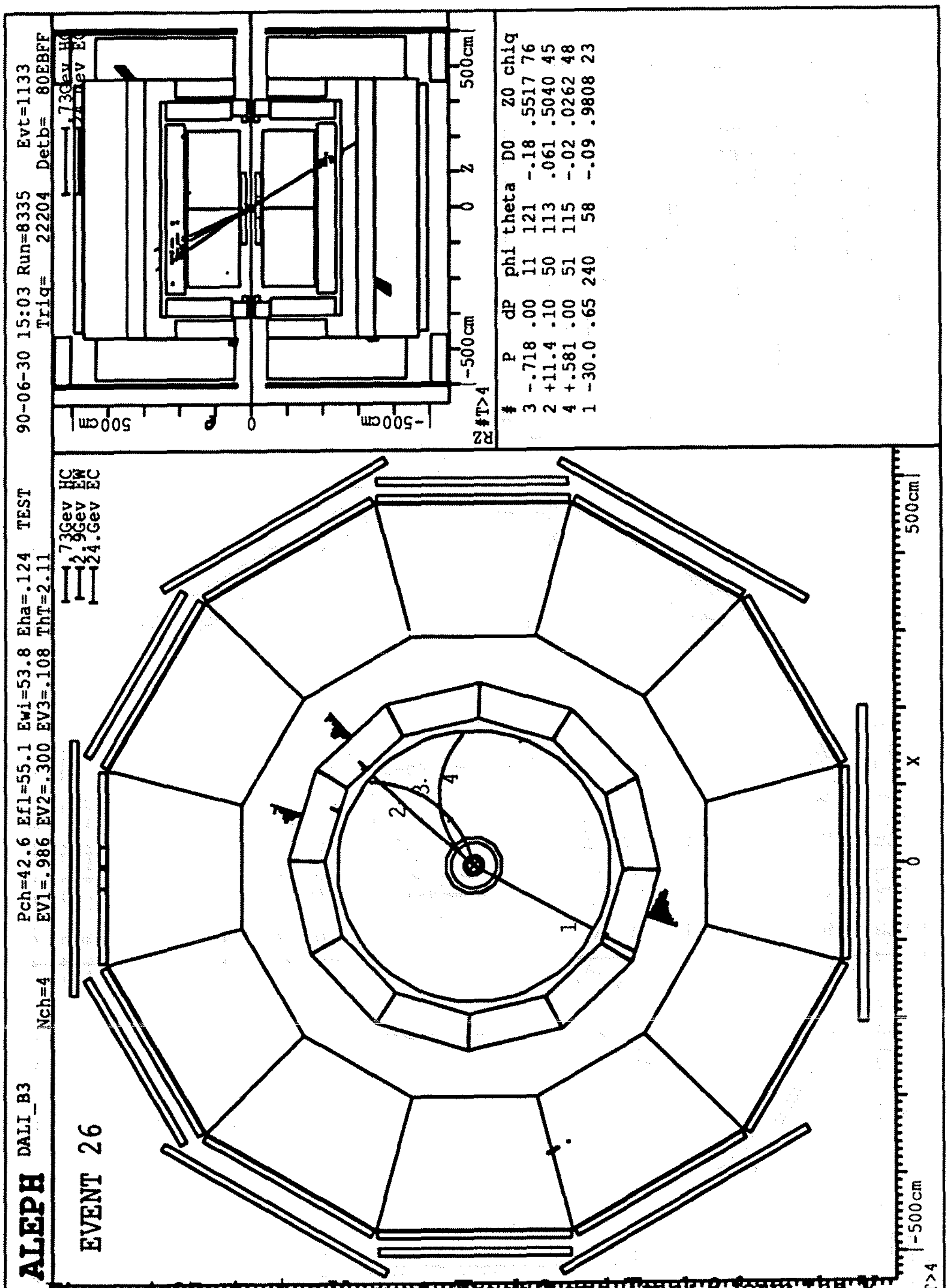

Figure A.27: A $\tau^+\tau^- V$ event. Track 2 and Track 6 form the V.

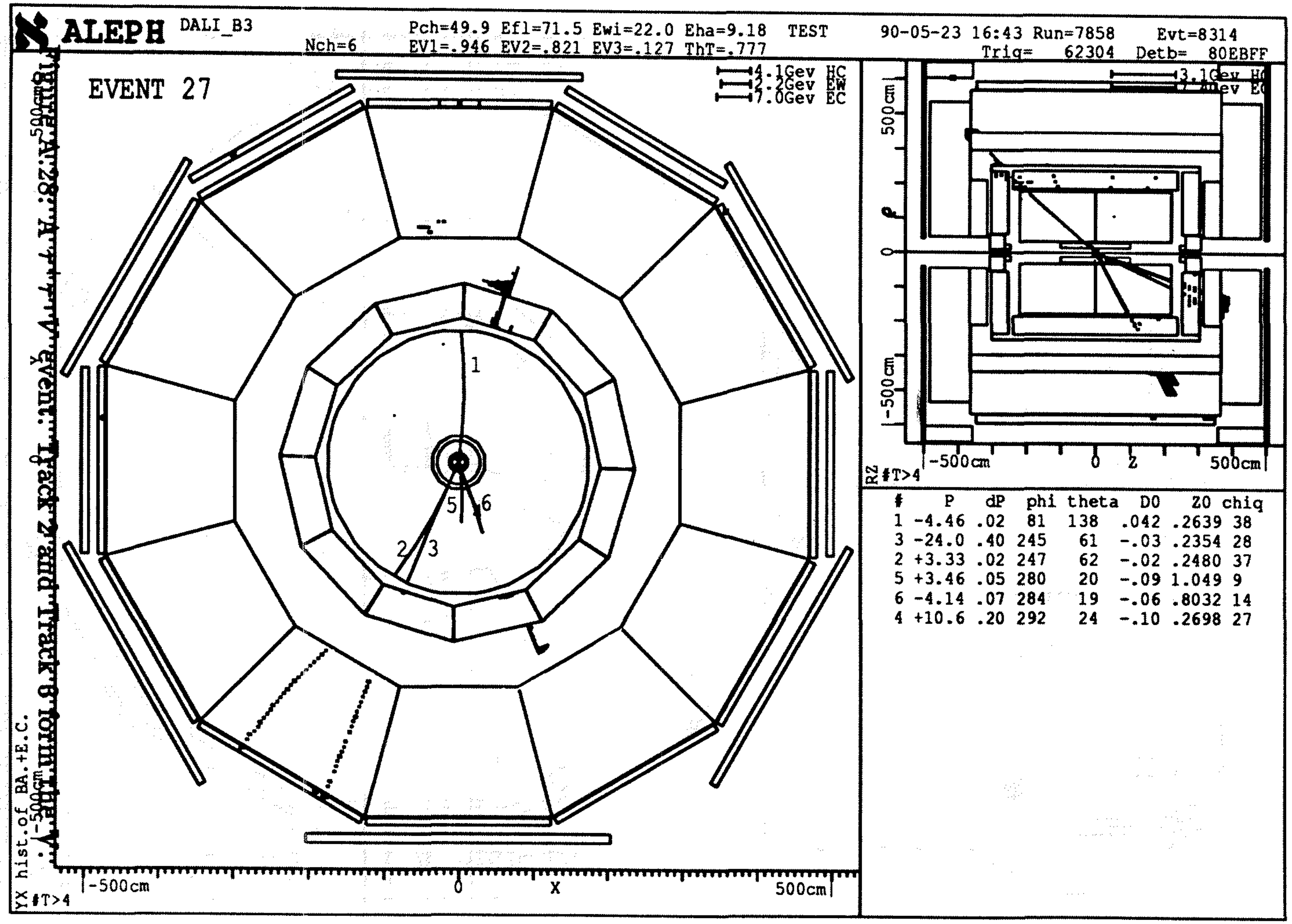

#	P	dP	phi	theta	D0	Z0	chiq
1	-4.46	.02	81	138	.042	.2639	38
3	-24.0	.40	245	61	-.03	.2354	28
2	+3.33	.02	247	62	-.02	.2480	37
5	+3.46	.05	280	20	-.09	1.049	9
6	-4.14	.07	284	19	-.06	.8032	14
4	+10.6	.20	292	24	-.10	.2698	27

Figure A.28: A [illegible] event. Track 2 and Track 6 form the [illegible]

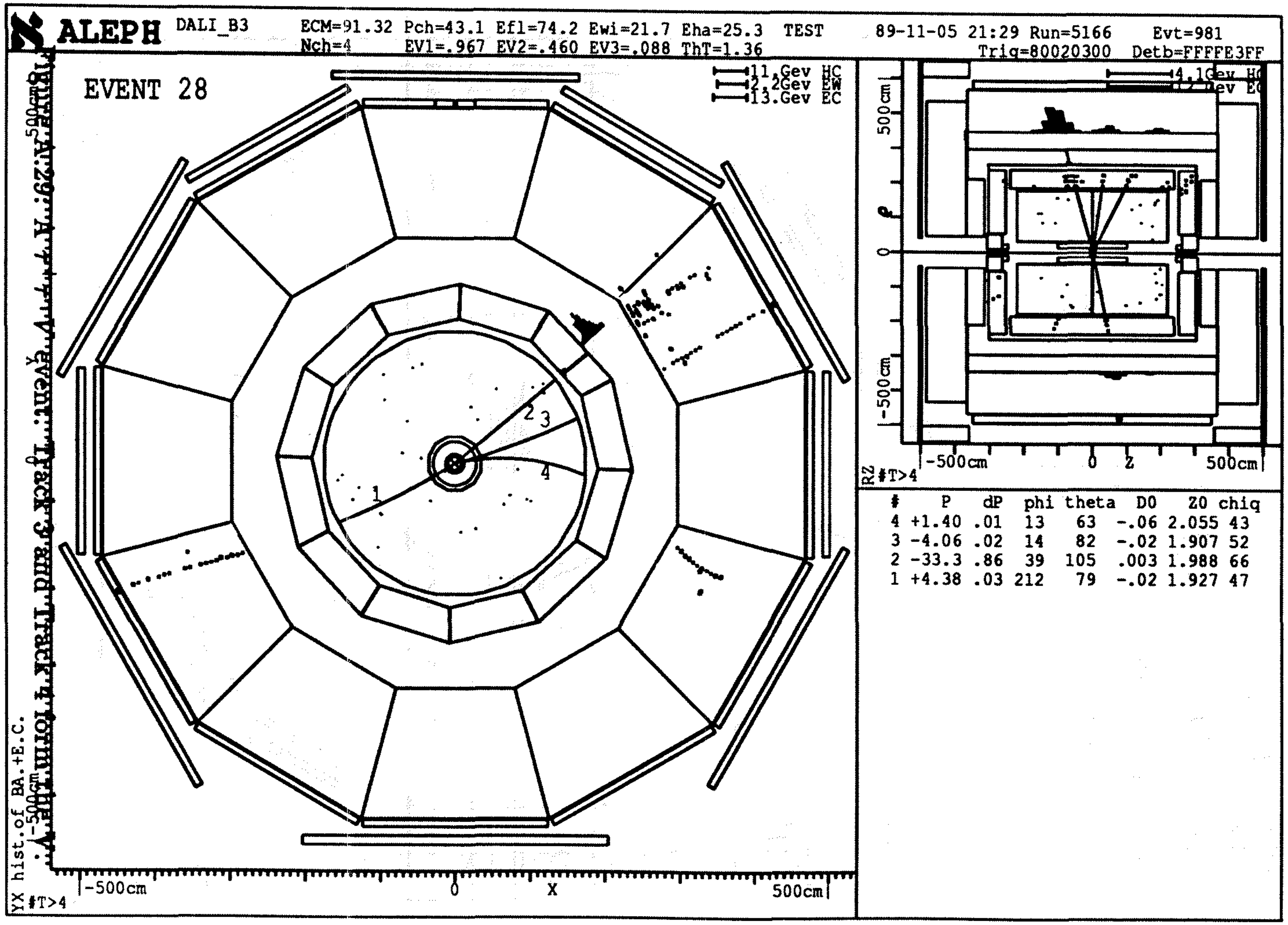
ALEPH
DALI_B3
ECM=91.32 Pch=43.1 Efl=74.2 Ewi=21.7 Eha=25.3 TEST
Nch=4 EV1=.967 EV2=.460 EV3=.088 ThT=1.36
89-11-05 21:29 Run=5166 Evt=981
Trig=80020300 Detb=FFFFE3FF
EVENT 28
11.Gev HC
2.2Gev EW
13.Gev EC
YX hist.of BA.+E.C.
#T>4
-500cm
0
X
500cm
RZ
#T>4
500cm
-500cm
Z
P dP phi theta D0 Z0 chiq
4 +1.40 .01 13 63 -.06 2.055 43
3 -4.06 .02 14 82 -.02 1.907 52
2 -33.3 .86 39 105 .003 1.988 66
1 +4.38 .03 212 79 -.02 1.927 47

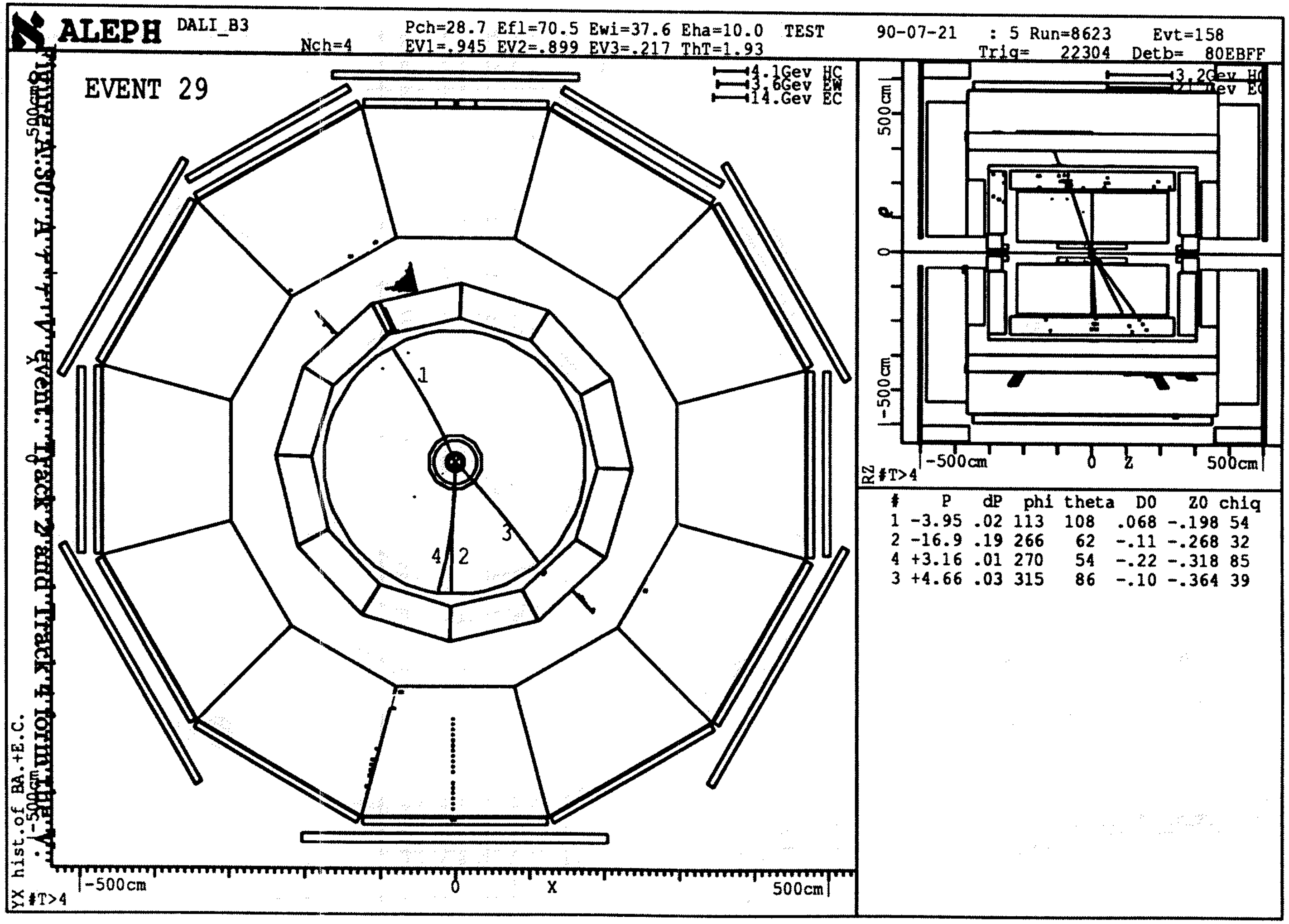

Figure A.30: A [illegible] event: Track 2 and Track 4 form [illegible]

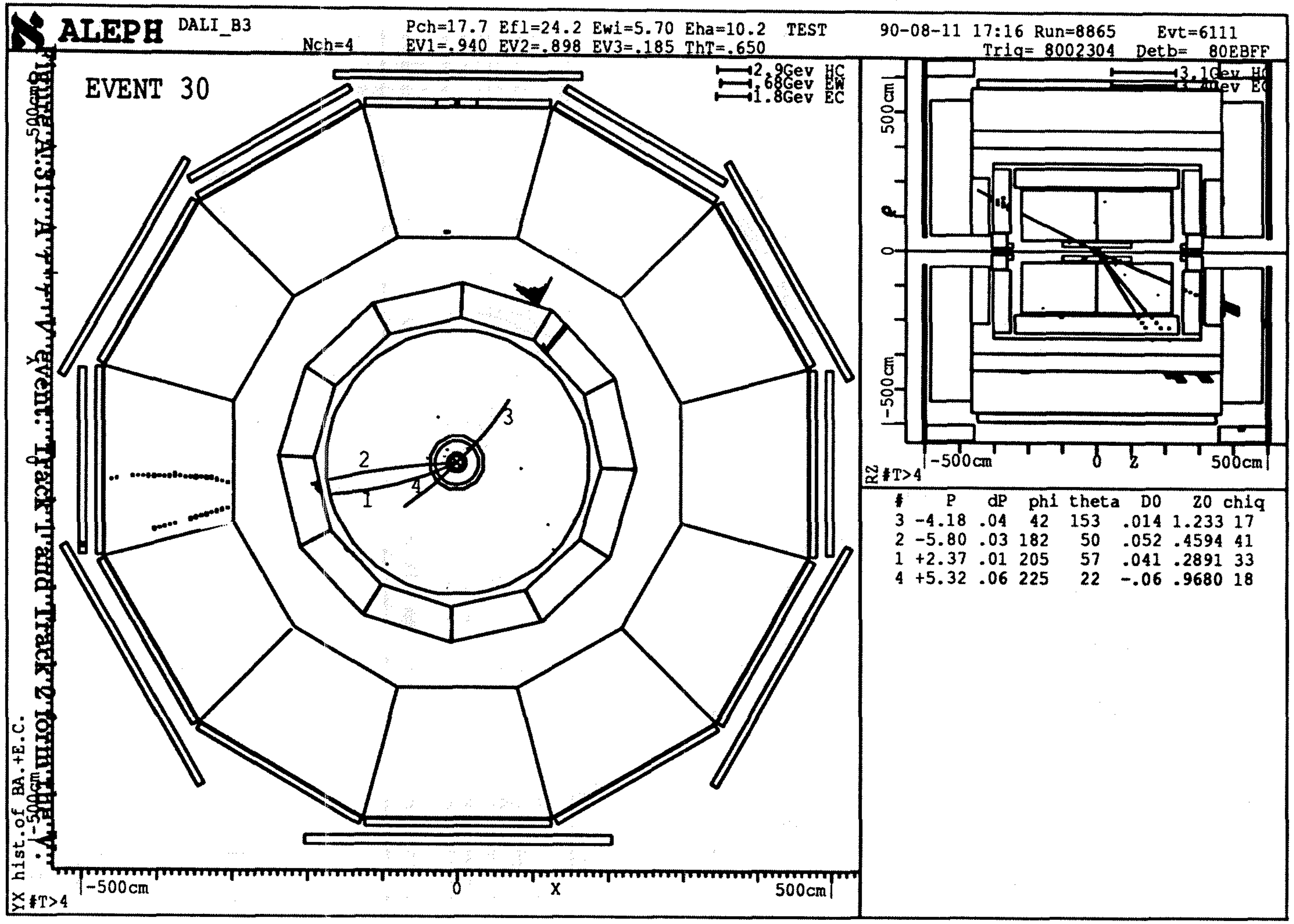
ALEPH DALI_B3
Nch=4
Pch=17.7 Efl=24.2 Ewi=5.70 Eha=10.2 TEST
EV1=.940 EV2=.898 EV3=.185 ThT=.650
90-08-11 17:16 Run=8865 Evt=6111
Trig= 8002304 Detb= 80EBFF
EVENT 30
2.9Gev HC
.68Gev EW
1.8Gev EC
YX #T>4
hist.of BA.+E.C.
-500cm
0
X
500cm
RZ #T>4
3.1Gev HC
Z
P dP phi theta D0 Z0 chiq
3 -4.18 .04 42 153 .014 1.233 17
2 -5.80 .03 182 50 .052 .4594 41
1 +2.37 .01 205 57 .041 .2891 33
4 +5.32 .06 225 22 -.06 .9680 18

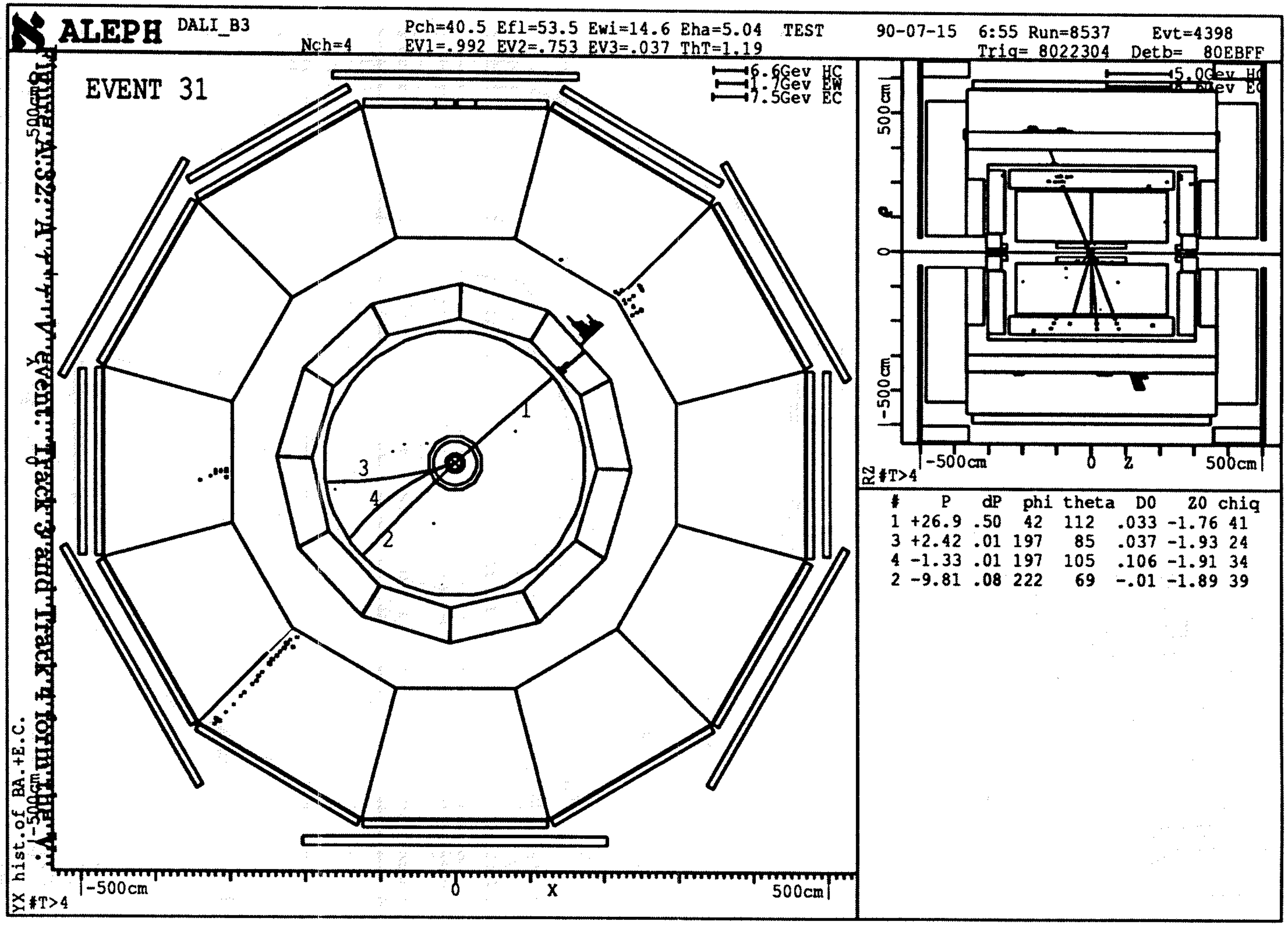

Figure A.32: ... V event. Track 3 and Track 4 form the V.

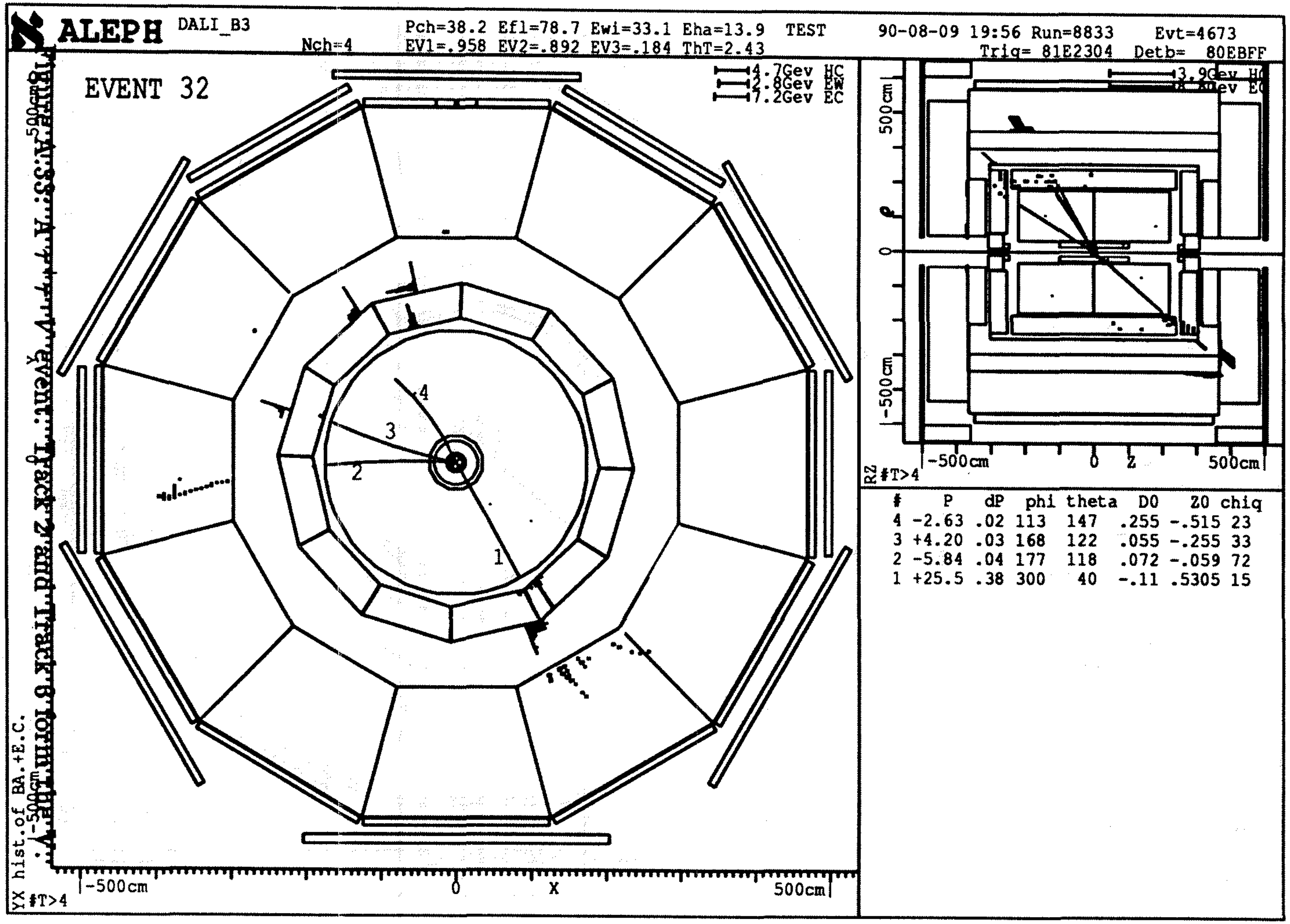
ALEPH
DALI_B3
Nch=4
Pch=38.2 Efl=78.7 Ewi=33.1 Eha=13.9 TEST
EV1=.958 EV2=.892 EV3=.184 ThT=2.43
90-08-09 19:56 Run=8833 Evt=4673
Trig= 81E2304 Detb= 80EBFF
EVENT 32
4.7Gev HC
2.8Gev EW
7.2Gev EC
YX #T>4
-500cm
0
X
500cm
RZ #T>4
500cm
0
-500cm
Z
P dP phi theta D0 Z0 chiq
4 -2.63 .02 113 147 .255 -.515 23
3 +4.20 .03 168 122 .055 -.255 33
2 -5.84 .04 177 118 .072 -.059 72
1 +25.5 .38 300 40 -.11 .5305 15

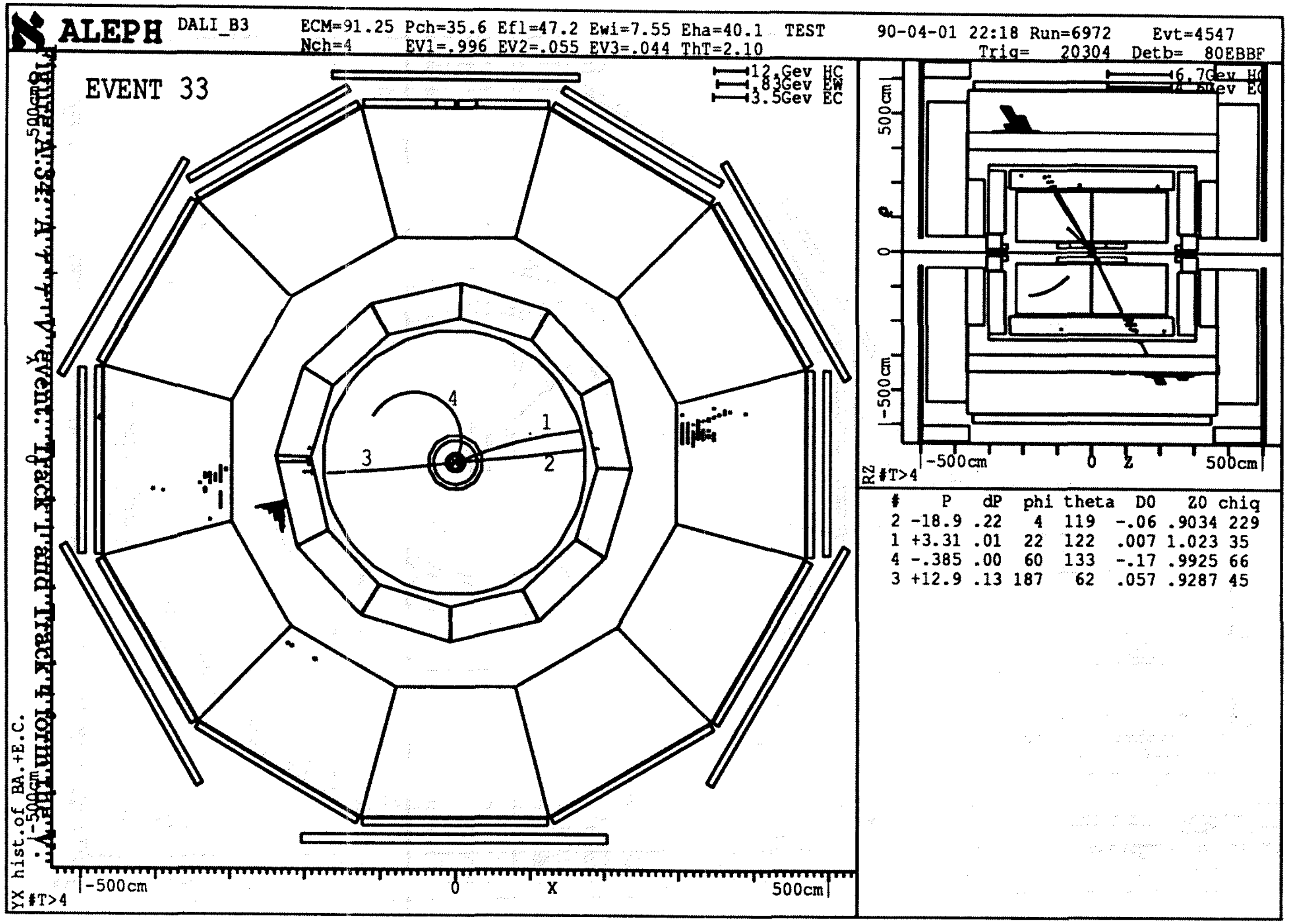

Figure A.34: A ... event. Track 1 and Track 4 form the

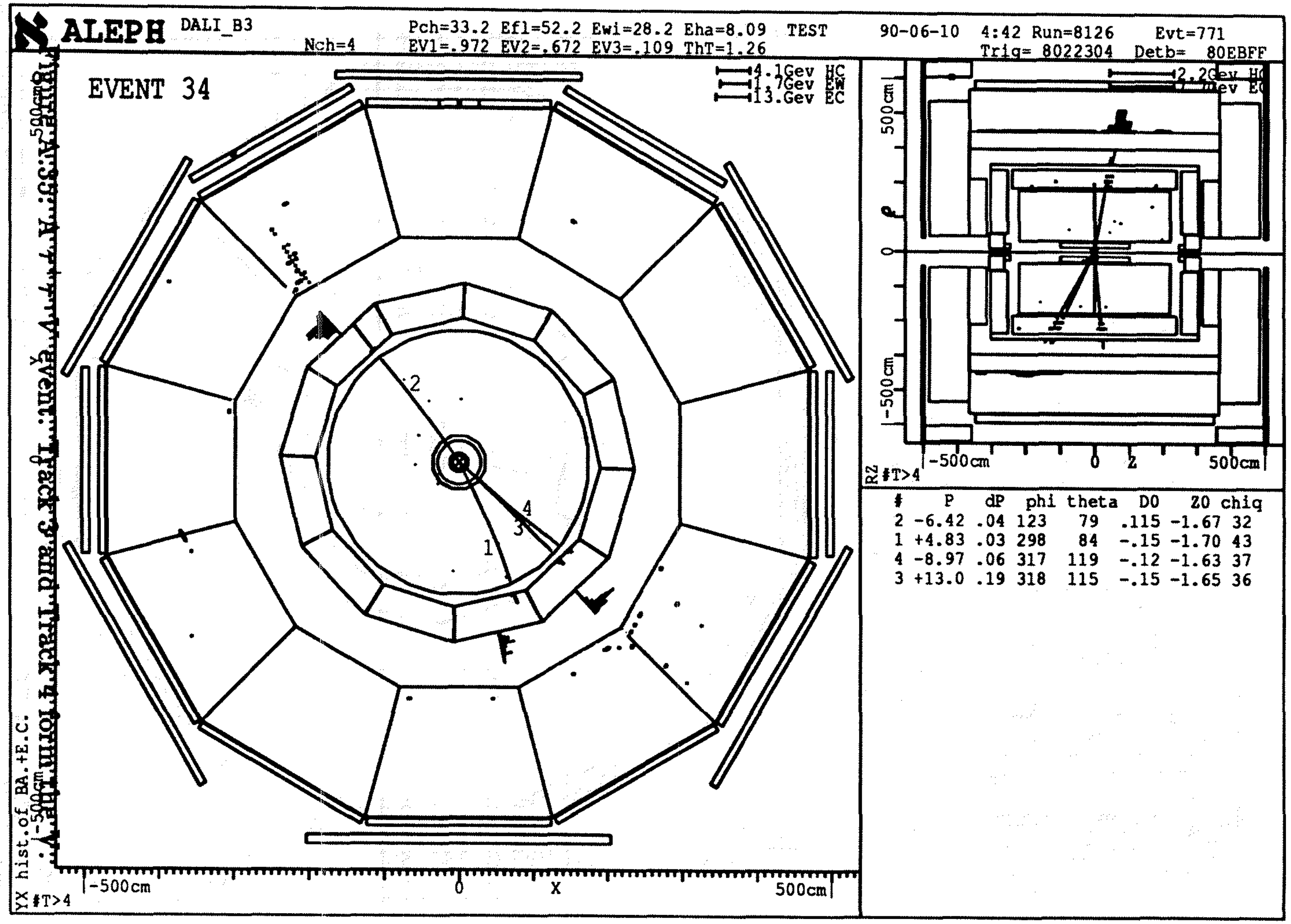

Figure A.33: A [illegible] event. Track 3 and track 4 form the [illegible]

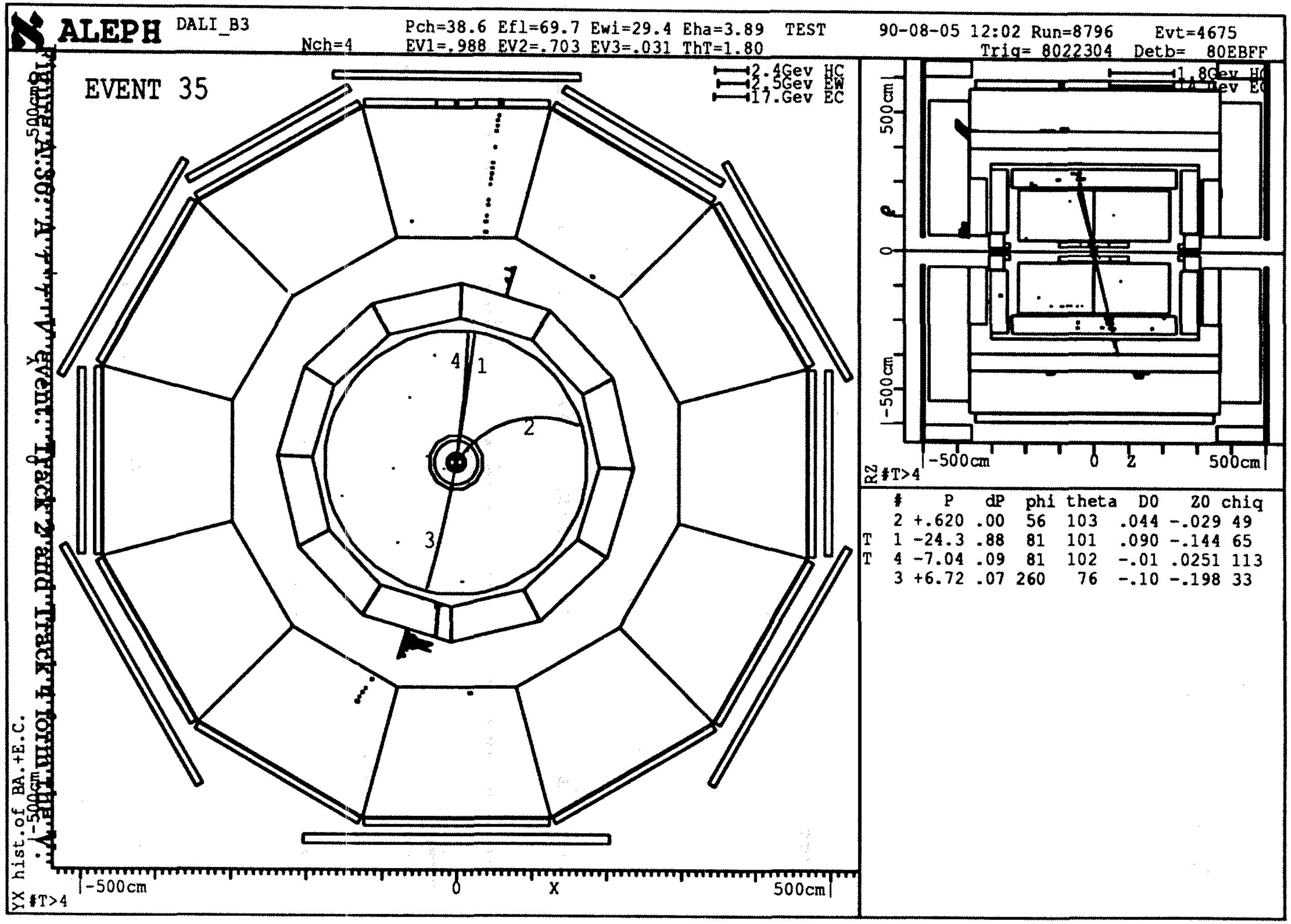

Figure A.50: A [illegible] V event. Track 2 and Track 4 form a V.

Bibliography

[1] S.L. Glashow. *Nucl. Phys. 22 (1961) 579.*

[2] S. Weinberg. *Phys. Rev. Lett. 19 (1967) 1264*

[3] A. Salam. *Proc. Eithth Nobel Symp., May 1968, ed. N. Svartholm (wiley, 1968) p. 367*

[4] S.L. Glashow, J. Iliopoulos and L Maiani. *Phys. Rev. D2 (1970) 1285*

[5] F Englert and R. Brout. *Phys. Rev. Lett. 13 (1964) 508;*

P.W. Higgs. *Phys. Lett. 12 (1964) 132; Phys Rev Lett. 13 (1964) 508;*

G.S. Guralnlnik, C.R. Hagen and T.W.B. Kibble. *Phys Rev Lett 13 (1964) 585;*

T.W.B. Kibble. *Phys. Rev. 155 (1967) 1554.*

J. Hilgart. *Thesis. Geneva, Switzerland*

[6] ALEPH Collaboration. *Nucl. Instr. & Meth. A294 (1990) 21*

[7] J. Knobloch and P. Norton, eds. *Status of Reconstruction in ALEPH, ALEPH note 90-170 (1990)*

[8] R. Brun, *et al. GEANT3, CERN-DD/EE/84-1*

J. Wear. *Thesis, P46. Geneva, Switzerland*

J. Hilgart. *Thesis, P44-45. Geneva, Switzerland*

[9] M.E.Nelson. *PhD Thesis, University of California, Berkely (1983), pages 71-80.*

D. Cinabro. Private communication.

[10] ALEPH Collaboration. *Phys. Lett. 246B (1990) 306*

[11] ALEPH Collaboration. "Measurement of Tau Branching ratios", to be published.

Z.Q. Zhang, Orsay France. Private Communication.

[12] T.T. Wu. Havard University. Cambridge, USA. Private communication.

[13] F.A. Berends, P. Daverdveldt, and R. Kleiss. *Comp. Phys. Comm. 40 (1986) 271.*

[14] The details of the Z contributions can be found in P. Daverveldt. Thesis. Rijksuniversiteit Leiden (1985).

[15] ALEPH Collaboration. *Polarization at LEP, unpublished P149.*

A. Quenzer *et al. Phys. Lett. 46B (1978) 512;*

I.B. Vasserman *et al. Sov. J. Nucl. Phys. 30 (1979) 519;*

I.B. Vasserman *et al. Sov. J. Nucl. Phys. 33 (1981) 519;*

L.M. Kurdadze *et al.* (OLYA) *JETP. Lett. 37 (1983) 733;*

S.R. Amendolia *et al.* (NA7) *Phys. Lett. 138b (1984) 454;*

L.M. Barkov *et al.* (OLYA,CMD) *Nucl. Phys. B256 (1985) 365*

[16] K.J. Abraham and J.J. van der Bij. *Phys. Lett. 248B (1990) 199.*

[17] L. Bergström and R.W. Robinett. *Phys. Lett. 245B (1990) 249.*

[18] Several analyses were performed to compare with this analysis. These include an independent analysis and analysises based on a variation of this one. All these analyses find the same samle of the l^+l^-V events, but the efficiencies are different. In some cases the differencies are as much as 20%.

[19] J. Wear. Thesis. University of California. USA.

J. Harton. Private communication